Institut für Physik
Arbeitsgruppe Nichtlineare Dynamik

Synchronization via correlated noise and automatic control in ecological systems

Dissertation
zur Erlangung des akademischen Grades
doctor rerum naturalium (Dr. rer. nat.)
im Fach Physik / Nichtlineare Dynamik

eingereicht an der
Mathematisch-Naturwissenschaftlichen Fakultät
der Universität Potsdam

von

Nina Kuckländer

Potsdam, Juni 2006

Zusammenfassung

Gegenstand der Arbeit ist die Möglichkeit der Synchronisierung von nichtlinearen Systemen durch korreliertes Rauschen und automatische Kontrolle. Die Arbeit gliedert sich in zwei Teile. Der erste Teil ist motiviert durch Feldstudien an wilden Schafspopulationen auf zwei Inseln des St. Kilda Archipels, die starke Korrelationen aufgrund von Umwelteinflüssen zeigen. In einem linearen System entspricht die Korrelation der beiden Populationen genau der Rauschkorrelation (Moran-Effekt). Es existiert aber noch keine systematische Untersuchung des Verhaltens nichtlinearer Abbildungen unter dem Einfluss korrelierten Rauschens. Deshalb wird im ersten Teils dieser Arbeit systematisch die rauschinduzierte Korrelation zweier logistischer Abbildungen in den verschiedenen dynamischen Bereichen untersucht. Für kleine Rauschintensitäten wird analytisch gezeigt, dass die Korrelation von quadratischen Abbildungen im Fixpunktbereich immer kleiner oder gleich der Rauschkorrelation ist. Im Periode-2 Bereich beschreibt ein Markov-Modell qualitativ die wichtigsten dynamischen Eigenschaften. Weiterhin werden zwei unterschiedliche Mechanismen vorgestellt, die dazu führen, dass die beiden ungekoppelten Systeme stärker als ihre Umwelt korreliert sein können. Dabei wird der neue Effekt der "correlation resonance" aufgezeigt, d. h. es ergibt sich eine Resonanzkurve der Korrelation in Abbhängkeit von der Rauschstärke. Im zweiten Teil der Arbeit wird eine automatische Kontroll-Methode präsentiert, die es ermöglicht sehr unterschiedliche Systeme auf robuste Weise in Phase zu synchronisieren. Die Methode ist angelehnt an Phase-locked-Loops und basiert auf einer Rückkopplungsschleife durch einen speziellen Regler, der es erlaubt die Phasen der kontrollierten Systeme zu ändern. Die Effektivität dieser Methode zur Kontrolle der Phasensynchronisierung wird an regulären Oszillatoren und an Nahrungskettenmodellen demonstriert.

Abstract

Subject of this work is the possibility to synchronize nonlinear systems via correlated noise and automatic control. The thesis is divided into two parts. The first part is motivated by field studies on feral sheep populations on two islands of the St. Kilda archipelago, which revealed strong correlations due to environmental noise. For a linear system the population correlation equals the noise correlation (Moran effect). But there exists no systematic examination of the properties of nonlinear maps under the influence of correlated noise. Therefore, in the first part of this thesis the noise-induced correlation of logistic maps is systematically examined. For small noise intensities it can be shown analytically that the correlation of quadratic maps in the fixed-point regime is always smaller than or equal to the noise correlation. In the period-2 regime a Markov model explains qualitatively the main dynamical characteristics. Furthermore, two different mechanisms are introduced which lead to a higher correlation of the systems than the environmental correlation. The new effect of "correlation resonance" is described, i. e. the correlation yields a maximum depending on the noise intensity. In the second part of the thesis an automatic control method is presented which synchronizes different systems in a robust way. This method is inspired by phase-locked loops and is based on a feedback loop with a differential control scheme, which allows to change the phases of the controlled systems. The effectiveness of the approach is demonstrated for controlled phase synchronization of regular oscillators and foodweb models.

Contents

Introduction

The spontaneous onset of synchronization is one of the most remarkable phenomena found in biological systems and relies on the coordination and interaction among two or more scattered organisms [93]. Synchronization arises in a large class of systems of various origins, ranging from physics and chemistry to biology and social sciences. Examples include swarms of fireflies that flash in unison [119, 130], synchronization in arrays of Josephson junctions [47], the excitation of the Millenium bridge by pedestrians [120] and synchronous firing cardiac pacemaker cells [130]. In ecology, fluctuations of population numbers, such as the classical 10-year Canadian hare-lynx cycle [31], are known to synchronize to a collective rhythm that manifests over millions of square kilometers. The presence, absence or degree of synchronization can be an important part of the function or malfunction of a biological system. For example, epileptic seizures are associated with a state of the brain in which too many neurons are synchronized for the brain to function correctly [83]. In ecology, the synchronization of populations is often seen as detrimental to spatially structured populations [29, 53]. This is because asynchrony enhances the global persistence of a population through rescue effects, even when there are local extinctions.

Synchronization of population dynamics is a very active field of research and there are still open questions. Important questions concern the mechanisms which induce or control synchronization. The central aim of this study is to show new possibilities to synchronize nonlinear systems. This work is divided into two parts.

Synchrony in population fluctuations may arise from three primary mechanisms: migration, interspecies interaction and climatic factors [72]. In general a mixture of two or three of the mechanisms may be the synchronizing factor. In isolated habitats such as islands the climatic fluctuations might be the main reason to synchronize spatially distinct populations, because migration is not possible. Field studies on feral sheep populations on two islands of the St. Kilda archipelago revealed strong correlations due to environmental noise. For a linear system the population correlation equals the noise correlation (Moran effect). The Moran effect played an important role in ecology in the recent years. But there exists no systematic examination of the properties of nonlinear maps under the influence of correlated noise. Therefore, in the first part of this thesis we investigate systematically the sole influence of correlated noise on nonlinear systems.

In the second part of the thesis an automatic control method is presented which synchronizes different systems in a robust way. This method is inspired by phase-locked loops and is based on a feedback loop with a differential control scheme, which allows to change the phases of the controlled systems. The effectiveness of the approach is demonstrated for phase synchronization of regular oscillators and predator-prey systems. For the predator-prey systems, the coupling might be interpreted as a third species which is in symbiosis with the predator.

At the end of each part a summary of our results is given and possible directions of further research are shown.

Part I

The Moran effect in nonlinear maps

Chapter 1

Noise-correlated dynamical systems: The Moran effect

This chapter gives an introduction into synchronization of population dynamics. It reports the experimental and theoretical evidence of synchronization processes in ecology. Especially it focuses on the role of environmental fluctuations in synchronization and summarizes a number of studies that have been published in this context. Finally, the chapter states the specific aims of this work and gives an outline of part I of this thesis.

1.1 Synchronization in ecology

For a century or more ecologists have been greatly interested in studying long-term population cycles. Some of the more remarkable population cycles have periods extending over many years and are thus difficult to explain in terms of simple seasonal patterns. Furthermore, many populations are able to synchronize their oscillations over wide geographical areas. Thus populations that may appear spatially separated are able to rise and fall in abundance (population size) in an unusually synchrony. The 10-year Canadian hare-lynx cycle is one of the better known examples [31], but similar synchronization phenomena are also known for a large number of taxa in different locations: such as fish [123], trees [59], mammals [19, 36, 43, 52, 58, 95, 100], birds [20, 60] and insects [88]. As the geographical distance separating the habitats of the populations increases, synchrony typically decreases.

The study of synchronization in ecology is of considerable importance since it helps to explain interactions between population dynamics and extrinsic environmental variation [57]. This addresses the long debate in ecology if population growth is bounded by endogenous density-dependent processes and/or extrinsic environmental factors [25, 35, 36]. Synchrony between fluctuations in population numbers in different regions has important implications for the persistence of populations. Asynchrony is said to allow for global persistence of a population through

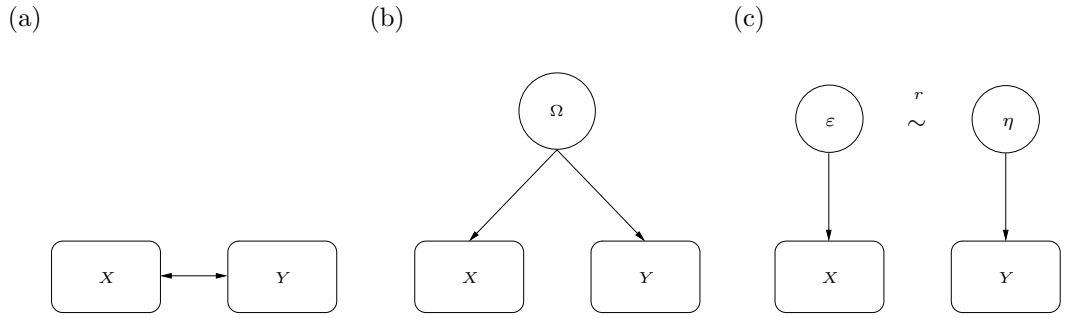

Figure 1.1: Interaction scheme of two systems X, Y with (a) direct or diffusive coupling, e. g. by migration, (b) external forcing with frequency Ω, e. g. a mobile top predator or an external seasonal influence, and (c) noise ε, η which has a correlation coefficient of r.

rescue effects due to migration, even when there are local extinctions. On the other hand, migration may increase the synchrony between populations which increases the global extinction risk [29, 53]. A natural way of examining synchronization in periodic systems is by analyzing the relationship between the phases of oscillators [93, 107]. But phase synchronization need not be dendrimental to population persistence, the complex spatio-temporal structures that can arise might be important for maintaining species persistence [13]. So the synchrony of populations is not only of concern in ecology but also in conservation biology.

In principle, one may differentiate between three main mechanisms, which are able to cause synchrony in population numbers [72], compare Fig. 1.1. Namely these are: (a) Dispersal among (spatially disjunct) populations, (b) interactions with other species that are themselves either synchronized or mobile and (c) environmental stochasticity, often referred to as the Moran effect or the Moran theorem.

The role of dispersal in synchronizing populations has been studied using both autoregressive (linear) models and a variety of nonlinear population models [61]. These studies indicate that fluctuations of any two populations that are governed by the same density-dependent process can be synchronized via the exchange of a small number of individuals each generation. There are further studies addressing the interplay between dispersal and environmental stochasticity [12, 51, 88, 104].

On the other hand, there are also exogenous factors that are able to synchronize populations. Some species may be synchronized by synchronous fluctuations of population species at either higher or lower trophic levels. For example mobile predators may synchronize oscillations in spatially disjunct populations [58]. Synchronous dynamics of herbivorous insects due to El Niño/La Niña climate patterns have been suggested to cause partial synchrony in insectivorous birds [60]. Also parasites are known to synchronize populations [19, 55].

Finally, the Moran effect [82, 108] suggests that if two populations have the same density-dependent structure, they will be correlated due to the influence of common environmental variation. Discussed examples are spatial synchrony in West-African fishes [123], cross species

synchronization of ungulates in Greenland [95, 125] and probably the best known example, the Soay sheep on St. Kilda [16, 22, 43, 122]. Experiments have been conducted with soil mites [9, 8] and rotifers [34]. This environmental variation may include high levels of spatially correlated fluctuations in the physical environment such as temperature, rainfall and wind speed as well as food or some other resource. Population synchrony typically declines with the distance between the populations and most climatic variables exhibit comparable patterns of synchrony as a function of distance [64]. Determining which climate variable may be a driving factor in producing population synchrony is nonetheless complicated and certainly different for various populations. Even different weather variables appear to influence different vital rates of a population [24, 25]. There is evidence that changes in large scale global climate patterns in a multidecadal time scale, such as the North Atlantic Oscillation (NAO) or El Niño Southern Oscillation (ENSO), may affect the levels of observed spatial synchrony in animal populations [21, 49, 95, 117].

In recent years, temporally autocorrelated ('colored') noise has received a lot of attention, because it is believed to be a more accurate description of the actual environmental variability [124, 105, 115]. There are two different approaches to temporally correlated noise: autoregressive (AR) models and $1/f^{\beta}$ noise [28, 41]. In 1985 Steele suggested that terrestrial noise should be white, while marine noise should be reddened, based upon a few empirical records and simple forcing models [115]. Reddened noise has positive temporal autocorrelation, that is successive values are more similar than expected by chance. The population subjected to noise can be regarded as a filter of the noise signal [70]. The exact nature of the environmental noise can be crucial for population persistence [28, 90, 126]. Experimental investigations showed that ciliate populations growing in aquatic microcosms are sensitive to the 'color' of their environmental noise [89]. Concluding, the extinction risk is a subtle interplay between the nature of the noise, the density-dependent structure of the population and the spatial structure of the environment.

In the physical literature synchronization means adjustment of the rhythm of two self-sustained oscillators, i. e. systems capable of generating their own rhythm, due to coupling [93]. That is not true at all for the Moran effect of noise induced correlation, because there is no coupling. However, one can talk of synchronization of two (or many) population cycles which are weakly interacting via migrating animals, e. g. the snowshoe hare-Canada lynx cycle [31]. In ecology, synchronization is often used as a synonym for strong (cross-)correlation of population abundance (or changes in abundance), e. g. in [39, 43]. We use both phrases interchangeably.

There exist various measures of synchrony in ecology. An obvious measure is the correlation between two time series of abundance. Correlation is here usually measured by Pearson's correlation coefficient. Several investigations use the coefficient of variation in density as indicators of synchrony [10, 51]. An overview is given in [18]. Other measures of correlation have also been employed: Blasius and Stone [13] introduced the methods of phase analysis [93] to study spatio-temporal fluctuations of animal populations and to detect synchrony. Cazelles and Stone [21] confirmed with phase analysis the results of Forchhammer et al. [35] and captured more details on the cause of synchrony of the mentioned Soay sheep populations. Buonaccorsi et al. give a nice comparison [18] of several measures of and tests for correlation. They compare the

linear correlation coefficient with a modified Kendall's tau and Spearman's rank correlation. In contrast to the linear correlation these measures are invariant under monotonic transformations of the data such as taking logarithms. The correlation coefficient of the logarithms is somewhat higher than the correlation coefficient of the untransformed variables. Buonaccorsi et al. summarize that the linear correlation may not capture the concept of synchrony of two populations in an ecologically meaningful way nor easily provide the cause of synchrony: For example, the linear correlation can be low while measures of movement together are high, in particular for cyclic populations. But for most cases in the tested data, the linear correlation coefficient proves to be a sufficient measure for capturing synchrony. Furthermore, the common standard statistical tests for zero correlation, assuming N independent different pairs (x_i, y_i), $(i = 1, \ldots, N)$ is invalid, because often population time series x_i and y_i are serially correlated. That means, the value x_{t+1} is much more likely to be near x_t than any other x_{t+j} of the series, as Moran noted in 1949 [80]. So other tests like bootstrapping should be used, see [18] for details.

1.2 The Moran effect

In 1953 Patrick Moran wrote two articles [81, 82] about the statistical analysis of the well known trapping records of the Canadian lynx [31]. In [82] he investigated the relation of the lynx population cycles to weather conditions. Suppose we can describe the dynamics of two populations in different regions with autoregressive (AR) processes

$$\begin{aligned} x_{t+1} &= a x_t + b x_{t-1} + \varepsilon_t \\ y_{t+1} &= a y_t + b y_{t-1} + \eta_t, \end{aligned} \tag{1.1}$$

with different, but correlated random noise sources ε_t, η_t and where x_t, y_t represent the logarithm of the annual abundance of the two populations. In this seminal article Moran stated that the "two processes, $\{x_t\}, \{y_t\}$, generated by the same relationship of form Eq. (1.1) with the random elements ε_t and η_t, the expected correlation between x_t and y_t will be equal to the correlation between ε_t and η_t" [82]. Further supposing that the terms ε_t and η_t are caused by or correlated with the local meteorological conditions at the sites of the two populations (and the latter in the two regions are correlated) we have a plausible explanation for the correlation between the two populations. Later this phenomenon was highlighted by Royama in his synthesis of population dynamics [108] and coined the term 'Moran effect'. Note that this effect holds only for identical systems: If the coefficients a, b of the two populations in Eq. (1.1) are not identical, then this result does no longer hold exactly [18, 106, 109]. Instead, the population correlation will always be smaller than the environmental correlation.

The most common measure of correlation used in ecology is the linear Pearson's correlation coefficient [96]

$$C(X, Y) = \frac{\langle XY \rangle - \langle X \rangle \langle Y \rangle}{\sqrt{\langle X^2 \rangle - \langle X \rangle^2} \sqrt{\langle Y^2 \rangle - \langle Y \rangle^2}}. \tag{1.2}$$

Using this coefficient Moran's statement can be expressed as

$$r_p \equiv C(X, Y) = C(\varepsilon, \eta) \equiv r. \tag{1.3}$$

In a linear model the population correlation, r_p, equals the correlation of the noisy environment, r.

1.3 Case study of feral sheep populations

In order to verify different ecological hypotheses, case studies play an important role. Therefore, ecologists set out to find examples, where the Moran effect could be shown to play a dominant role. Maybe, the most important case for the Moran effect was found the Soay sheep populations of St. Kilda. Feral sheep populations on islands in the uninhabited St. Kilda archipelago in the Outer Hebrids have been monitored since 1955. The Outer Hebrids are a region with high humidity and harsh winds. The most complete series of annual records exist for Soay sheep on the main island Hirta and for Blackface sheep on Boreray, which are depicted in Fig. 1.2(a). Both time series show irregular population fluctuations reflecting population crashes due to starvation in the winter [22]. The data were analyzed and fitted to a self-exciting threshold autoregressive model (SETAR) by Grenfell et al. [43] in 1998. The TAR models are based on the principle of decomposing the state space (in this case the density of animals) into two (or more) regimes. Linear autoregressive models are then fitted to each regime

$$x_{t+1} = \begin{cases} a_{1,0} + a_{1,1}x_t + \varepsilon_{1,t} & x_t \geq C \\ a_{2,0} + a_{2,1}x_t + \varepsilon_{2,t} & x_t < C \end{cases} . \tag{1.4}$$

The variable x_t denotes the logarithm of the sheep numbers and $\varepsilon_{1,t}, \varepsilon_{2,t}$ are normally distributed noises in the two regimes and account for the environmental noise. The constants $a_{i,j}$ are determined by the data. The threshold C can be imagined as a carrying capacity. A short introduction to TAR models is given in [116], this piecewise linear model is compared with a fully linear model in [30].

Another long-standing debate in ecology, whether the regulation of a population happens density-dependent or density-independent, can be addressed with the Soay sheep data. A TAR model can capture the nonlinearity in density-dependence in contrast to linear models: Below the threshold C there is no density-dependence in Fig. 1.2(c), above the threshold any increase in the population density x_t in the last year leads to a decrease in the population growth rate r_t. Fig. 1.2(d) shows the logarithm of the sheep numbers on Hirta in two consecutive years and the fitted SETAR model. The population threshold C lies at $x_t = 7.06$, corresponding to 1171 sheep. The displayed population dynamics is nonlinear with stochastic impacts.

The numbers of sheep on the two islands are highly correlated, as seen in Fig. 1.2(b). However, the question remains what causes these synchronized fluctuations. The sheep are located on close but separate (3.5 km apart) islands, thus the role of dispersal as a synchronization mechanism can be dismissed. Parasites only contribute to winter mortality in malnourished hosts

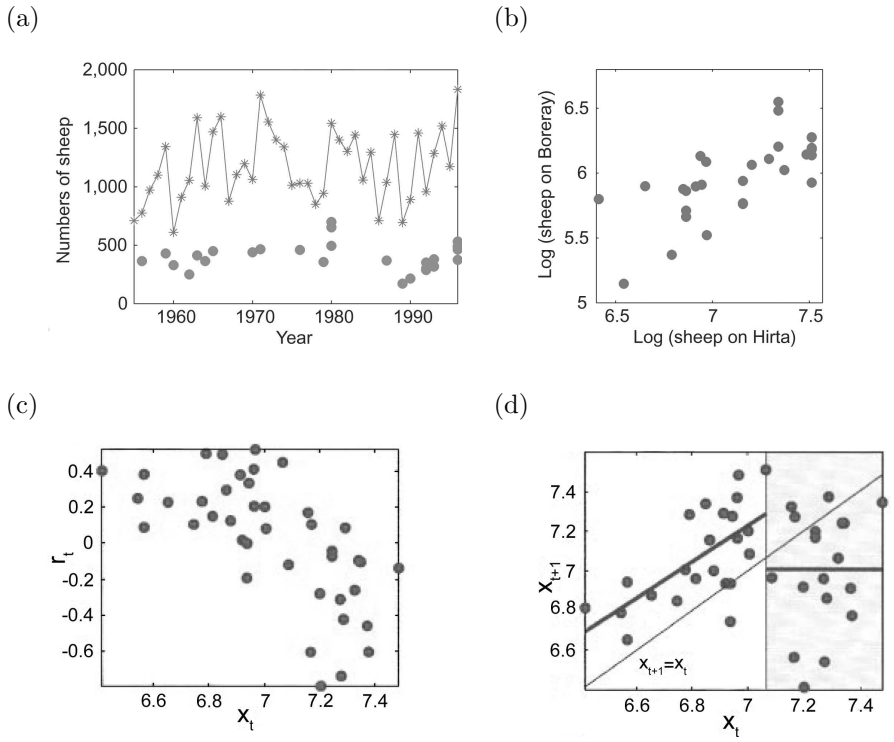

Figure 1.2: Temporal dynamics of feral sheep populations on the St. Kilda archipelago
(a) Time series of total sheep counts from Hirta (∗) and Boreray (•) island. (b) Scatter plot of the logarithm of the population sizes. (c) Plot of the logarithm of the annual population growth rate $r_t = x_{t+1} - x_t$ versus x_t, the logarithm of the population size. The data is taken from the Hirta island. (d) Scatter plot of the logarithm of the Hirta population size (•) and the fitted SETAR model (-), Eq. (1.4). Reprinted by permission from Macmillan Publishers Ltd: Nature [43] ©(1998)

[44, 46]. So it seems that a combination of food-shortage, aggravated through parasitism, and the timing of harsh weather conditions, e. g. March gales, stresses the sheep and causes crashes. This happens more or less synchronously and demonstrates the Moran effect.

Grenfell et al. argued with the aid of simulations that a correlation as high as $r = 0.9$ in the environmental noise between these islands would be required to correlate the two populations as much as the observed value of $r_p = 0.68$, compare Fig. 1.2(b). This has been controversially discussed [16, 42, 109]. Blasius et al. [16] argued that this finding could have been an artifact of the way in which Grenfell et al. analyzed their data. Nonetheless, the observed population correlation is a sample value estimated from a pair of short data series with many missing years, and is probably subject to a large estimation error.

A more detailed model [24], including the demographic structure (age, sex) of the population, indicated that the influence of population structure is strongest at high and intermediate initial population sizes. Another study considered the reproductive cost in female Soay sheep [122]. In

the mentioned article by Grenfell et al. [43], the environmental noise taken into account was the April temperature and the duration of March gales. However, a large-scale climate index covers several months and incorporates the variation of several climate variables. So Forchhammer et al. [35] used the North Atlantic Oscillation (NAO) winter index and revealed that warm, wet and windy winters (high NAO) that precede birth depressed juvenile survival. However, these weather conditions increased adult survival and fecundity due to increased spring/summer grass availability. So real systems with nonlinear dynamics display the Moran effect.

1.4 A primer of the logistic map

In the following we investigate the Moran effect in nonlinear maps. For this we make extensive use of the logistic map, because it is simple and well-studied. Therefore, we start with a short review of its basic properties.

In 1976 May wrote an article [77] about simple mathematical models of animal populations and their complicated dynamical properties. To analyze the simplest case of temporal non-overlapping generations he used unimodal maps of the kind: $x_{n+1} = g(x_n)$. Most importantly he studied the *logistic map*,

$$x_{n+1} = a x_n (1 - x_n), \tag{1.5}$$

which had already been introduced by Verhulst (1845). This study of May became famous, because he showed that a simple map as Eq. (1.5) can show very complicated dynamics. This article inspired many studies. Nowadays the logistic map is a toy-model to study properties of dynamical systems. The variable a is the bifurcation or control parameter. For $a \in [0, 4]$ the iterates of the map stay in the interval [0,1]. The logistic map is a model for the reproduction of biological populations with discrete, non-overlapping generations as it is the case for many temperate zone insects, e. g. cockchafers. The linear term describes the growth of the population and the second, nonlinear term represents the saturation effect due to the limitation of resources like food or space. Fig. 1.3(a) shows the bifurcation diagram of the logistic map without noise. For a small growth rate $a = a_0 < 1$ the population always goes extinct: $x_n \to 0$ as $n \to \infty$. For $a = a_1 \in [1, 3]$, the population grows and reaches a non-zero steady state. This steady state x_* is a *fixed point*, that means it does not change upon further iteration of the map g, $g(x_*) = x_*$. A fixed point is *stable* if $|g'(x_*)| < 1$. For even larger $a = a_2 \in [3, 1+\sqrt{6}]$, the steady state becomes unstable and the population oscillates about the former steady state alternating between two definite population sizes. This type of oscillation, in which x_n repeats every two iterations, is called a *period-2 cycle*. As a increases, the period-2 orbit doubles at $a = a_4$ to a period-4 orbit. The population approaches a cycle which repeats every four generations. Further period-doublings occur as a increases and a_n finally converges to a limiting critical parameter value of $a_\infty = 3,569946\ldots$ [45]. This way into chaos is called the Feigenbaum route to chaos that all quadratic maps of the unit interval with a single maximum undergo. This gives rise to the universality class of the logistic map with characteristic scaling functions and universal exponents [32]. Note that the Ricker map is in the same class [3].

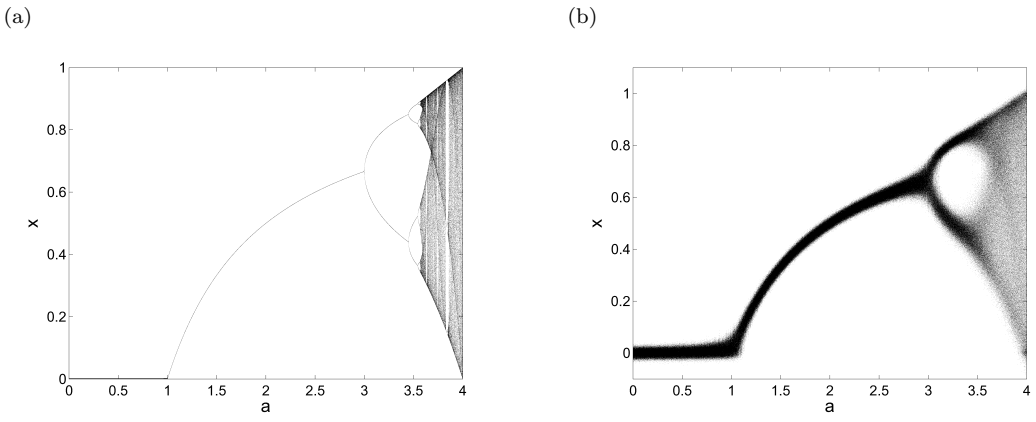

Figure 1.3: Bifurcation diagram of the logistic map (a) without noise and (b) in presence of external additive Gaussian noise with amplitude $\sigma = 0.01$.

In this study we are mostly concerned not with the chaotic but the fixed-point and periodic regimes. In these regimes dynamics are furthermore interesting in the presence of external additive noise

$$x_{n+1} = g(x_n) + \varepsilon_n. \tag{1.6}$$

With external noise the fine structure of the bifurcation diagram is washed out as is demonstrated in Fig. 1.3(b). Moreover, with noise the bifurcation is detected earlier, which can be seen in Fig. 1.3(b) by the broadening of the variance of the fluctuations. This effect was discovered by Wiesenfeld [127, 128], who termed the phenomenon noisy precursor. For the logistic map this has been analyzed in detail by [67]. The higher the noise intensity is, the stronger the higher period cycles are suppressed.

The main order parameter which is used to detect if the system is in the chaotic regime or not is the largest Lyapunov exponent. For a map $g(x)$ the *Lyapunov exponent* is defined as

$$\lambda = \lim_{N\to\infty} \frac{1}{N} \sum_{i=1}^{N} \ln \|g'(x_i)\|. \tag{1.7}$$

The Lyapunov exponent describes how trajectories in phase space that were initially close to each other evolve after long time. It is an average quantity that describes the shrinking or stretching of phase space volumes: A large negative value implies great insensitivity to the initial difference of the trajectories and a vanishing value leads to neither growth nor decay of the initial difference as it is the case for conservative systems. Whereas a large positive value implies rapid separation and great sensitivity of the system to the initial conditions, which is the character of chaos. The scaling of λ in the presence of noise in the vincinity of the critical point has been reported in 1981 numerically by Crutchfield et al. [26] and theoretically by Shraiman et al. [112]

$$\lambda = (a_\infty - a)^\beta L((a_\infty - a)^{-\frac{1}{\gamma}}\sigma), \tag{1.8}$$

where σ is the intensity of the noise, $\beta = \ln 2/\ln \delta$ and $\gamma = \ln \delta/\ln \mu \approx 0.819$. The scaling function L describes the change of the scaling variable, here the Lyapunov exponent λ, under the discrete change of the scale, that is the distance of the system to the critical point. Here, the variables δ and μ are universal exponents which were introduced and calculated by Feigenbaum [32]

$$\delta = \lim_{k\to\infty} \frac{a_{k+1} - a_k}{a_{k+2} - a_{k+1}} = 4.669\ldots, \qquad \mu^{-1} = 0.1525. \tag{1.9}$$

The exponent δ is a kind of a scaling constant. The variable μ^{-1} can be interpreted as the factor by which the noise should be increased to wipe out one bifurcation. That means that at the critical parameter value a_∞ where chaos sets in we have $\lambda = 0$ and thus

$$(a_\infty - a) \sim \sigma^\gamma. \tag{1.10}$$

For vanishing noise one obtains a scaling law which is well known from the theory of critical phenomena [102]

$$\lambda \sim (a_\infty - a)^\beta. \tag{1.11}$$

This connection has been worked out by Shraiman, Wayne and Martin [112] and in [33]. An overview of older work is given in [27].

1.5 Review of noise-correlated maps

These findings in the field were and still are a challenge for theory. Many approaches have been pursued to study noise-induced correlation in nonlinear systems.

In several publications [2, 10, 39, 100, 101] the role of nonlinearity and correlated noise has been analyzed by means of the *Ricker map* [103],

$$x_{n+1} = x_n \exp(a(1 - x_n)), \tag{1.12}$$

where a is the growth parameter of the population. The exponential takes into account the negative role of competition at high population densities. Introduced in 1954 by W. E. Ricker, the map is a model of density-dependence which is widely used in fisheries biology. While the noisy Ricker map is defined as

$$x_{n+1} \quad = \quad x_n \varepsilon_n \exp(a - x_n + \xi_n) \tag{1.13}$$

in [10, 100, 101], the authors of [39] use the form

$$x_{n+1} \quad = \quad x_n \exp(a - x_n + \varepsilon_n). \tag{1.14}$$

In the context of analyzing spatial synchronization [2, 10] the noise ξ_n in Eq. (1.13) accounts for local stochasticity in each patch and the noise term ε_n is a global random mortality factor. Both approaches share the disadvantage that the fixed point $x_* = 1$ of the undisturbed Ricker

map Eq. (1.12) is not preserved and that the fixed point $x_* = 0$ (extinction of the population) can become stable. This can be resolved using parametric noise [75]

$$x_{n+1} = x_n \exp\left(a(1+\varepsilon_n)(1-x_n)\right). \tag{1.15}$$

All mentioned studies employ multiplicative noise. Arguments concerning the scaling of the noise intensity σ between additive and multiplicative noise for the logistic map are put forward by Linz in [75]: If $a > a_1(\sigma)$ is sufficiently larger than 1, so that the fixed point is away from the basin of attraction of $-\infty$, then for small noise intensities multiplicative and additive noise cause similar response behavior

$$\sigma_{\text{additive}} \leftrightarrow \frac{a-1}{a}\sigma_{\text{multiplicative}}, \tag{1.16}$$

where the scaling factor is the nonzero fixed point of the logistic map. The validity of this relationship has been checked for $a < 3$ and $a \geq 3$. It can be derived from the requirement that the moment generating functions of the additive and the multiplicative noise are the same.

The above studies show figures illustrating the interplay between noise correlation, noise intensity and the bifurcation parameter contributing to the correlation of the two systems. Higher noise correlation, r, provided higher population correlation, r_p. Certainly respecting Moran's theorem that is $r_p \leq r$. For an increasing bifurcation parameter (increasing nonlinearity) the correlation was lost [39, 100]. Depending if the investigated system is in the fixed-point or period-2 regime, decreasing [39] or increasing [100, 101] noise intensity accounts for high population correlation.

In the physical context, the synchronization of identical maps with different initial conditions governed by the same noise has been studied. As argued by Pikovsky [91], the sychronization can be explained and quantitatively predicted by observing that, at some value of the noise amplitude, the Lyapunov exponent associated with the dynamics changes from positive to negative. A necessary condition for the occurrence of synchronization is that the dynamical system has expanding and contracting regions, so that noise may amplify the role of the latter against the former. Pikovsky [91] introduced the concept of a distribution exponent, which describes the distribution of the separations in phase space between the two systems subject to noise. This idea was elaborated further by Khoury et al. [62, 63].

We do not want to address which particular noise is appropriate for a particular dynamical system in nature that is represented by such simplified models. We rather present in this thesis the effects of additive noise.

1.6 Noise-correlated nonlinear maps

After the previous introductory sections an outline of part I of this thesis is given in this section. We use two noise-correlated logistic maps to study the nonlinear Moran effect systematically.

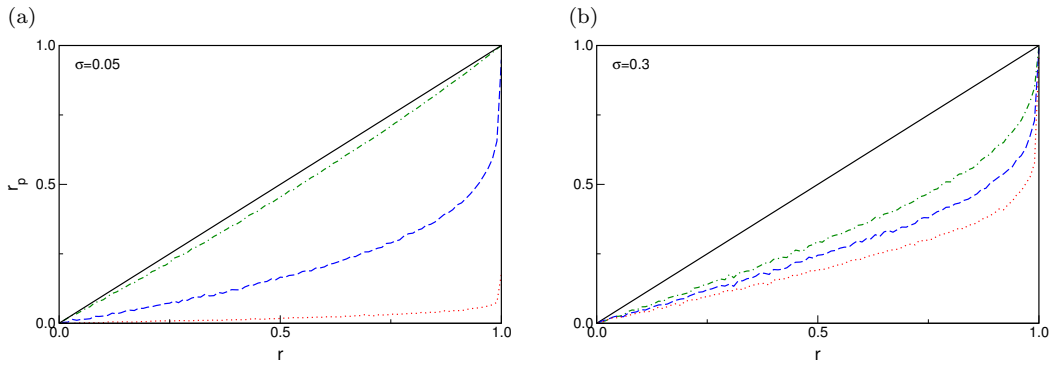

Figure 1.4: Correlation r_p of two identical logistic maps against the correlation r of the added Gaussian noise for two different noise intensities: (a) $\sigma = 0.05$, (b) $\sigma = 0.3$. The bifurcation parameter has the values $a = 2.9\,(- \cdot -), a = 3.3\,(--)$ and $a = 3.9\,(\cdots)$.

Following [16, 39], where other maps are used, we show a diagram relating the noise correlation r and the population correlation r_p. In Fig. 1.4 the selected parameter values $a = 2.9, a = 3.3$ and $a = 3.9$ are located in the fixed-point, period-2 and chaotic regime of the logistic map, respectively. In the limit of increasing noise intensities or decreasing the bifurcation parameter the system reflects the linear Moran effect, $r_p = r$. This is plausible, because in the fixed-point regime the map is almost linear. Because of this monotonic behavior of the population correlation, the noise correlation is fixed in the following in order to analyze the dependency on the other variables.

In [39, 100, 101] curves of the population correlation in dependence on the bifurcation parameter of the Ricker map have lead to the conclusion that desynchronization takes place if the chaotic regime is approached. This can be explained by the fact that for relatively small noise (compared to the amplitude of the period-2 cycle), the presence of the 2-cycle dynamics remains intact and the fluctuations for both maps are either highly correlated, $r \approx 1$, or almost completely anticorrelated, $r \approx -1$. However, under the influence of noise rare jumps are possible between these in-phase and out-of-phase states. This leads to contributions of the total correlation which cancel each other out, and on average lead to a vanishing value of r_p. In the period-n ($n \geq 2$) regime, the correlation drops drastically, compare Fig. 1.5(a). This can be explained by the fact, that the systems have many different possible states. Therefore, the average correlation is close to zero. For high noise intensities the nonlinearity of the map does not play a role compared to the dominant noise dynamics, see Fig. 1.5(b). Furthermore Fig. 1.5(b) confirms the finding that depending on the dynamical regime of the system, decreasing [39] or increasing [100, 101] noise intensity leads to high population correlation (for smaller noise intensities).

These figures demonstrate a rich behavior in nonlinear maps with additive correlated noise. In this part of the thesis we perform therefore a systematic study of noise induced correlation of nonlinear maps. The following chapters are structured according to the regimes of the bifurcation diagram of the logistic map. In chapter 2 we present ways of constructing correlated

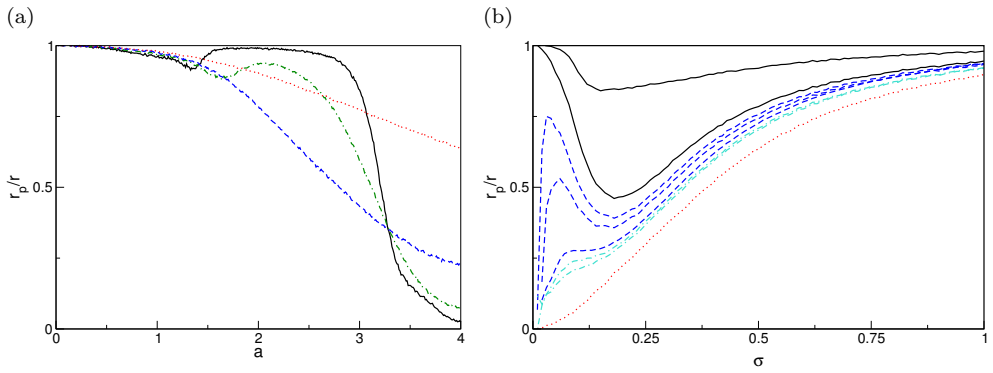

Figure 1.5: Plot of the relative correlation coefficient r_p/r of two logistic maps with additive correlated Gaussian noise versus (a) the bifurcation parameter a for different noise intensities: $\sigma = 0.05\,(-), \sigma = 0.1\,(- \cdot -), \sigma = 0.2\,(--)$ and $\sigma = 0.5\,(\cdots)$ and (b) the noise intensity σ in different regimes of the logistic map: fixed-point $(-)$, period-2 $(--)$, period-4 $(- \cdot -)$ and chaotic $(\cdots)$. The noise correlation is $r = 0.5$.

noise and introduce correlation measures. As a starter in chapter 3 we reproduce Moran's statement for linear systems. Then we investigate identical quadratic maps with additive noise in the fixed-point regime analytically and numerically. We obtain as a new result a second order approximation of the Moran theorem. Furthermore the impact of the boundary conditions applied to the noisy logistic map is analyzed. In chapter 4 the period-2 regime of the logistic map and the desynchronization is investigated in detail. Calculating numerically transition rates we confirm the validity of the Kramers' rule in our case. Additionally, the approach of a Markov model is tested and we elaborate on the idea of correlated Markov processes. A more detailed realization of the previously described correlated Markov processes is studied by courtesy of piecewise constant maps with additive correlated noise. In chapter 5 we turn our attention to different methods to achieve an amplification of the linear correlation, that is the correlation of the processes is higher than the correlation of the added noises. We present numerically a method for nonlinear maps using a structured joint noise distribution, which to our knowledge has not been reported before. As a second approach we incorporate temporally correlation of the noise, which enhances the correlation-coefficient even for linear maps. Ending part I of the thesis, we summarize our findings and give an outlook on possible directions of further research. At the end of the thesis, the first two appendices review the basic Frobenius-Perron equation for the calculation of the invariant distribution and the construction of correlated noise distributions. In the last two appendices solutions of the bivariate Normal probability function are reviewed and the transition probabilities of the piecewise constant maps are calculated.

Chapter 2

Construction of correlated noise

In this chapter we discuss the different possibilities of correlating additive noise and introduce measures for correlation.

Suppose we ask for the correlation in the scatter plot of two time-series like in Fig. 1.2(b) or of two random processes, see Fig. 2.1. The linear (Pearson's) *correlation coefficient* [96] of two random variables X, Y is defined by

$$C(X,Y) = \frac{\langle XY\rangle - \langle X\rangle\langle Y\rangle}{\sqrt{\langle X^2\rangle - \langle X\rangle^2}\sqrt{\langle Y^2\rangle - \langle Y\rangle^2}}. \tag{2.1}$$

The value of the correlation coefficient varies between -1 and $+1$. A positive value of $C(X,Y) = +1$ corresponds to the case in which the data points or realizations lie on a perfect straight line with positive slope. This would be the case if for example all realizations in Fig. 2.1 would lie on the diagonal. The value $+1$ holds independent of the magnitude of the slope. The correlation coefficient takes on a value of -1 when the data points lie on a perfect straight line with negative slope, Y decreasing as X increases. This is called *anti-correlation* or complete negative correlation. A value of $C(X,Y)$ near zero indicates that the variables X and Y are uncorrelated. However, this does *not* imply that these variables are independent, because the correlation coefficient takes only the first and second moments of the variables into account. So there can be still correlations in the higher (greater than two) moments, even if $C(X,Y) = 0$. Only for Gaussian noise the conclusion 'independent follows from uncorrelated' holds. In general, if X and Y are *independent*, their joint distribution factorizes $\rho(X,Y) = \rho(X)\rho(Y)$ and it follows that $C(X,Y) = 0$ but not inversely. A measure for independence, the mutual information, will be discussed in the Sec. 2.3.

As mentioned in Chap. 1, environmental noise can be composed of two (or more) components. Following this idea, we consider two pairs of correlated noise sources which are added. The system of equations for this setup reads as follows:

$$\begin{aligned} \varepsilon &= \xi_1 + \xi_2, \\ \eta &= \zeta_1 + \zeta_2. \end{aligned} \tag{2.2}$$

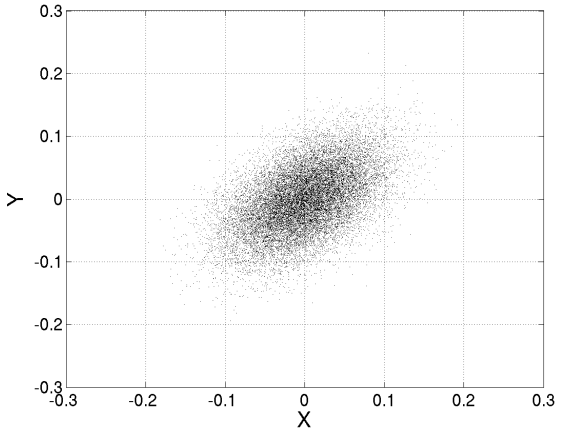

Figure 2.1: Joint probability distribution of two bivariate Gaussian random variables, Eq. (2.10), $\sigma = 0.05$. The linear correlation coefficient, Eq. (2.1), is $C(X, Y) = 0.5$.

The assumptions for the particular noises are: $\langle \xi_i \rangle = \langle \zeta_i \rangle = 0$, $\langle \xi_i^2 \rangle = \langle \zeta_i^2 \rangle = \sigma_i^2$, $C(\xi_i, \zeta_i) = r_i$, $C(\xi_i, \zeta_j) = 0$, with $i, j \in \{1, 2\}$ and $i \neq j$.
Now the first moments read as:

$$\langle \varepsilon \rangle = \langle \eta \rangle = 0, \tag{2.3}$$

$$\langle \varepsilon \eta \rangle = r_1 \sigma_1^2 + r_2 \sigma_2^2, \tag{2.4}$$

$$\langle \varepsilon^2 \rangle = \langle \eta^2 \rangle = \sigma_1^2 + \sigma_2^2. \tag{2.5}$$

This results in a linear correlation coefficient of

$$C(\varepsilon, \eta) = \frac{r_1 \sigma_1^2 + r_2 \sigma_2^2}{\sigma_1^2 + \sigma_2^2}. \tag{2.6}$$

The result can be easily extended to a sum of N pairs of correlated noises

$$C(\varepsilon, \eta) = \sum_{n=1}^{N} r_n \sigma_n^2 \Big/ \sum_{n=1}^{N} \sigma_n^2. \tag{2.7}$$

Note, that this leads to a convenient method to generate correlated noise which will be used in the following sections. A noise corresponding to this structure with a common part $r_1 = 1\,(\xi_1 = \zeta_1)$ and an independent part $r_2 = 0$ was used for example in [110, 131].

The probability density function $f(\varepsilon, \eta)$ of this noise can be calculated from the Frobenius-Perron equation, see appendix A, with $x \simeq \varepsilon$. It is generated by a convolution of the two noise distributions $f_1(\xi_1, \zeta_1), f_2(\xi_2, \zeta_2)$

$$f = f_1 \star f_2, \tag{2.8}$$

$$= \iint_{-\infty}^{\infty} d\xi_1 d\zeta_1 \, f_1(\xi_1, \zeta_1) \, f_2(\varepsilon - \xi_1, \eta - \zeta_1), \tag{2.9}$$

where $\star$ is the convolution operator. For example, for bivariate Gaussian noise $f_{1,2}$ this produces bivariate Gaussian noise again

$$f(\varepsilon,\eta) = \frac{1}{2\pi\sqrt{1-r^2\sigma^2}} \exp\left(-\frac{\varepsilon^2+\eta^2-2r\varepsilon\eta}{2\sqrt{1-r^2\sigma^2}}\right), \tag{2.10}$$

with $r = C(\varepsilon,\eta)$ of Eq. (2.6) and $\sigma^2 = \langle\varepsilon^2\rangle = \langle\eta^2\rangle$ of Eq. (2.5).

2.1 (A)symmetrically correlated noise

Correlated noise can be created in different ways. In the literature correlated noise is often composed of a common part and a different part [113, 62]. A special case of Eq.(2.2) is

$$\begin{aligned} \varepsilon &= a\xi + b\xi', \\ \eta &= a\xi - b\xi', \end{aligned} \tag{2.11}$$

where ξ, ξ' are random numbers either drawn uniformly from the interval $[-\sqrt{3}, \sqrt{3}]$ or Gaussian distributed with a standard deviation of 1 and $a, b \in \mathbb{R}_+$. This compares to Eq. (2.2) with $r_1 = 1, r_2 = -1$. In [62] the parameters a, b are chosen as $a = 1, b = 1/2$ with Gaussian and uniform noise. In this thesis we have chosen a noise satisfying $\langle\varepsilon\rangle = \langle\eta\rangle = 0$, $\langle\varepsilon^2\rangle = \langle\eta^2\rangle = \sigma^2$, $\langle\varepsilon\eta\rangle = r\sigma^2$, so that $C(\varepsilon,\eta) = r$. This results in $a = \sigma\sqrt{(1+r)/2}, b = \sigma\sqrt{(1-r)/2}$. Thus the symmetrically correlated noise reads as:

$$\begin{aligned} \varepsilon &= \sigma\sqrt{\frac{1+r}{2}}\xi + \sigma\sqrt{\frac{1-r}{2}}\xi', \\ \eta &= \sigma\sqrt{\frac{1+r}{2}}\xi - \sigma\sqrt{\frac{1-r}{2}}\xi', \end{aligned} \tag{2.12}$$

where the random variables are indistinguishable, that means the joint probability distribution is symmetric to the diagonal. The asymmetric version, where the random variables are distinguishable, is

$$\begin{aligned} \varepsilon &= \sigma\xi, \\ \eta &= r\varepsilon + \sqrt{1-r^2}\sigma\xi'. \end{aligned} \tag{2.13}$$

This kind of noise is used in [113]. For Gaussian noise ξ, ξ' these definitions of correlated noise, Eq. (2.12) and Eq. (2.13), make no difference, but for uniform noise the derived joint probability density functions $p(\varepsilon,\eta)$ are not identical. This results also in differences in the correlation of two populations with these noises added, as shown in Fig. (2.2). Especially for high noise intensities there are pronounced differences in the relative correlation coefficient of the populations. In this thesis we use the symmetrically constructed noise. But this correlated noise is nevertheless only uniform in the joint distribution, while the projections $p(\varepsilon), p(\eta)$ are not uniformly distributed. This is demonstrated in Fig. 2.3(a), where both projections are not uniform. The asymmetrically generated noise has automatically a uniform distribution $p(\varepsilon)$, but $p(\eta)$ is still not uniform.

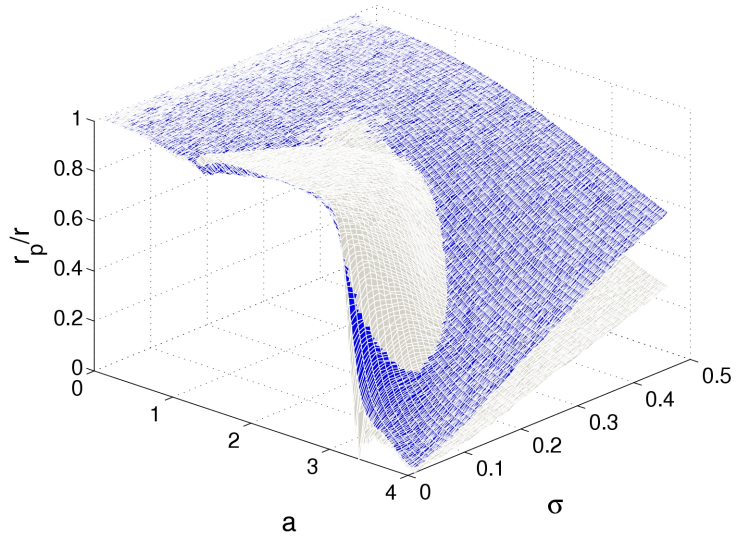

Figure 2.2: Comparing the relative correlation coefficient r_p/r of two logistic maps Eq. (1.5) with additive symmetrically (red), Eq. (2.12), and symmetrically (yellow), Eq. (2.13), correlated uniform noise. The correlation of the noise is $C(\varepsilon, \eta) = r = 0.5$.

2.2 Different correlated uniform noises

In order to achieve uniformly distributed noise also in the projections of each noise, we construct a different noise distribution, which is plotted in Fig. 2.3(c). It is generated as follows:

$$\begin{aligned} \varepsilon &= \sigma\sqrt{3}(2\xi - 1), \\ \eta &= \sigma\sqrt{3}\left(2\left[1 - \left\{1 - \left(\xi + (1-c)(\xi' - \frac{1}{2})\right) \bmod 1\right\} \bmod 1\right] - 1\right), \end{aligned} \tag{2.14}$$

where ξ, ξ' are random numbers drawn from the interval $[0, 1]$ with a standard deviation of 1 and $c \in [0, 1]$. The factor $\sqrt{3}$ is incorporated so that $\langle \varepsilon^2 \rangle = \langle \eta^2 \rangle = \sigma^2$. The modulo function has the following sense: The lacking corners in the triangular distribution in Fig. 2.3(a) to the uniform distribution in Fig. 2.3(b) are added in the corners of the product space $[0, 1] \times [0, 1]$, see Fig. 2.3(c). Computation of the correlation of these two noises shows that $C(\varepsilon, \eta) < c$ for all parameters. The plot of the relative correlation coefficient, see Fig. 2.4(a)-(b), does not look qualitatively different for this uniform noise. The only small difference, an amplification of the correlation coefficient, will be discussed in section 5.1. Another special, localized correlated uniform noise is described in [39].

2.3 Nonlinear correlation measures

At the end of section 1.2 we mentioned already other correlation measures than Pearson's correlation. Pearson's linear correlation coefficient is not invariant under nonlinear transformations

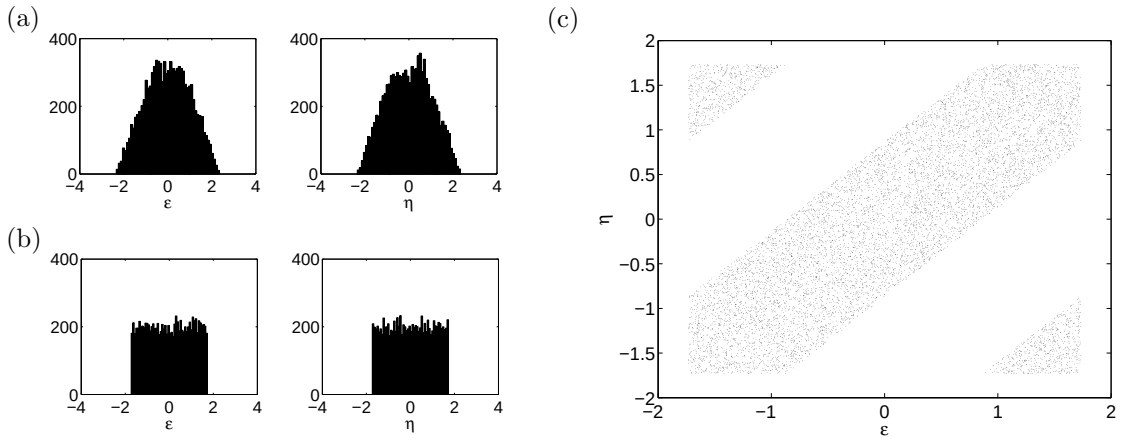

Figure 2.3: Projections $p(\varepsilon)$ and $p(\eta)$ of correlated uniform noise: (a) is symmetrically correlated according to Eq. (2.12), $r = 0.5$ and (b) modulo noise of Eq. (2.14), $c = 0.5$. 10^4 realizations of the noise sorted in 50 histogram bins. (c) Joint probability distribution of modulo uniform noise Eq. (2.14), $c = 0.5$

of the data like taking the logarithm of the data points [96]. But if we sort the data points according to their value and assign to each data point a rank value corresponding to his place in the sorted data, then the correlation coefficient of the rank list will be invariant under monotonic transformations, because they preserve the rank order. This measure is called *Spearman's rank correlation*

$$\rho_S = \frac{\sum_i (R_i - \bar{R})(S_i - \bar{S})}{\sqrt{\sum_i (R_i - \bar{R})^2}\sqrt{\sum_i (S_i - \bar{S})^2}}, \tag{2.15}$$

where R_i and S_i denote the rank values of data points from the two data sets X and Y.

Another related nonlinear correlation measure is *Kendall's Tau*. Basically it measures the tendency of the time series to move in the same direction. For any sample of N observations, there are $N(N-1)/2$ possible comparisons of pairs of data points (x_i, y_i) and (x_j, y_j) with $i \neq j$. We call a pair concordant (discordant), if the relative rank order of the two x's is the same (opposite) as that of the y's. If the two x's (y's) have identical values (a so called 'tie'), this pair will be called an extra y-pair (extra x-pair). Let $N_C(N_D)$ be the number of concordant (discordant) pairs and $N_{ty}(N_{tx})$ the number of extra y-pairs (x-pairs). Kendall's Tau is now defined as following

$$\tau = \frac{N_C - N_D}{\sqrt{N_C + N_D + N_{tx}}\sqrt{N_C + N_D + N_{ty}}}. \tag{2.16}$$

To be precise, this is Kendall's Tau b.

If both above described measures are zero, one cannot conclude that the data sets X and Y are independent. A test for dependence is the mutual information which is based on entropies: For a random variable X with a finite set of M possible states $\{x_1, x_2, \ldots, x_M\}$, the Shannon

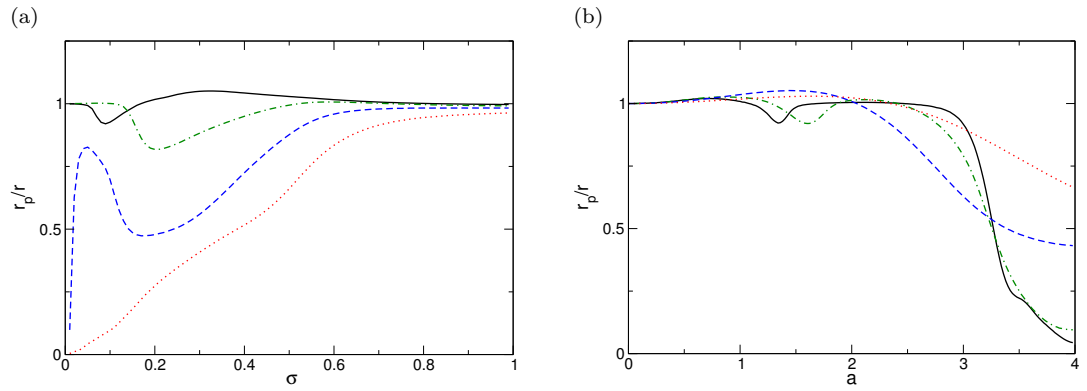

Figure 2.4: Relative correlation coefficient for two logistic maps with additive correlated modulo noise, Eq. (2.14), $c = 0.5 : C(\varepsilon, \eta) = r = 0.375$, versus (a) the noise intensity σ for $a = 1.55\,(-), a = 2.4\,(- \cdot -), a = 3.1\,(--)$ and $a = 4\,(\cdots)$ and (b) the bifurcation parameter a for $\sigma = 0.05\,(-), \sigma = 0.1\,(- \cdot -), \sigma = 0.32\,(--)$ and $\sigma = 0.5\,(\cdots)$. Transient and runtime are 10^6 iteration steps and the plot is averaged over 100 realizations.

entropy $H(X)$ is defined as [96, 111]

$$H(X) = -\sum_{i=1}^{M} p(x_i) \log p(x_i), \tag{2.17}$$

where $p(x_i)$ denotes the probability of the state x_i. For equiprobable events the Shannon entropy is maximal. If the outcome of the measurement is completely determined to be x_k ($p(x_k) = 1$), then the Shannon entropy is zero. For two variables X and Y the joint entropy $H(X, Y)$ is defined analogously

$$H(X, Y) = -\sum_{i=1}^{M} \sum_{j=1}^{M} p(x_i, y_j) \log p(x_i, y_j). \tag{2.18}$$

The *mutual information* or transinformation $I(X, Y)$ between the two variables X and Y measures the independence of the two random variables

$$I(X, Y) = \sum_{i=1}^{M} \sum_{j=1}^{M} p(x_i, y_j) \log \left(\frac{p(x_i, y_j)}{p(x_i) p(y_j)} \right) = H(X) + H(Y) - H(X, Y). \tag{2.19}$$

If both systems are independent, their joint probability distribution factorizes $p(x, y) = p(x)p(y)$ and the mutual information is zero! Note that the mutual information is symmetric in X and Y, i. e. the mutual information says nothing about the direction of the information flow between X and Y.

In the numerical estimation of the mutual information from data finite-size effects have to be taken into account. For finite number N of data points, the mutual information gets systematically overestimated [118, 54]

$$\langle I_{observed} \rangle = I_{true} + \frac{(M-1)^2}{2N} + \mathcal{O}\left(\frac{1}{N^2} \right). \tag{2.20}$$

As a rule of thumb, each 'bin' should have a chance to appear (at least) three times, thus $N_{min} \geq 3M^2$. For the comparison of all correlation measures presented in this chapter we use two logistic maps, Eq. (1.5), with additive correlated Gaussian noise. The length of the transient and runtime are 10^4 steps and so the number of bins was chosen to be $M = 2^4 = 16$ for each variable. There are no qualitative differences between the measures for this kind of noise, compare Fig. 2.5.

For correlated Gaussian noise the mutual information can be nicely expressed through the linear correlation. Entering the bivariate Gauss distribution Eq. (2.10) into the continuous version of the definition of the mutual information Eq. (2.19) yields

$$I(\varepsilon,\eta) = \int\!\!\int_{-\infty}^{\infty} d\varepsilon d\eta\, p(\varepsilon,\eta) \log_b \left(e^{-\frac{r^2\left(\varepsilon^2+\eta^2\right)-2r\varepsilon\eta}{2\sigma^2(1-r^2)}} \cdot \frac{1}{\sqrt{1-r^2}} \right). \tag{2.21}$$

The integral splits into two parts due to the logarithm identities. The first part with the exponentials sums up to zero after crunching through analytics. The base b of the logarithm is here for two systems chosen as $b = 2$. Changing to the natural logarithm, $\log_b x = \ln x / \ln b$, this leaves us with

$$I(\varepsilon,\eta) = -\frac{\ln\left(\sqrt{1-r^2}\right)}{\ln(b)}. \tag{2.22}$$

This formula also applies to two linear maps or two logistic maps g with correlated additive Gaussian noise in the fixed-point regime with weak noise, because their joint distribution has just another noise intensity $\sigma' = \sigma/\sqrt{1-g'(x_*)^2}$ which cancel out in Eq. (2.21). For very strong noise the dynamics of the maps can be neglected. So we can express the Moran theorem (1.3) in terms of the mutual information of the two systems

$$I(X,Y) = I(\varepsilon,\eta). \tag{2.23}$$

This result is valid exactly for two identical one-dimensional maps in their fixed-point regime with weak or very strong noise.

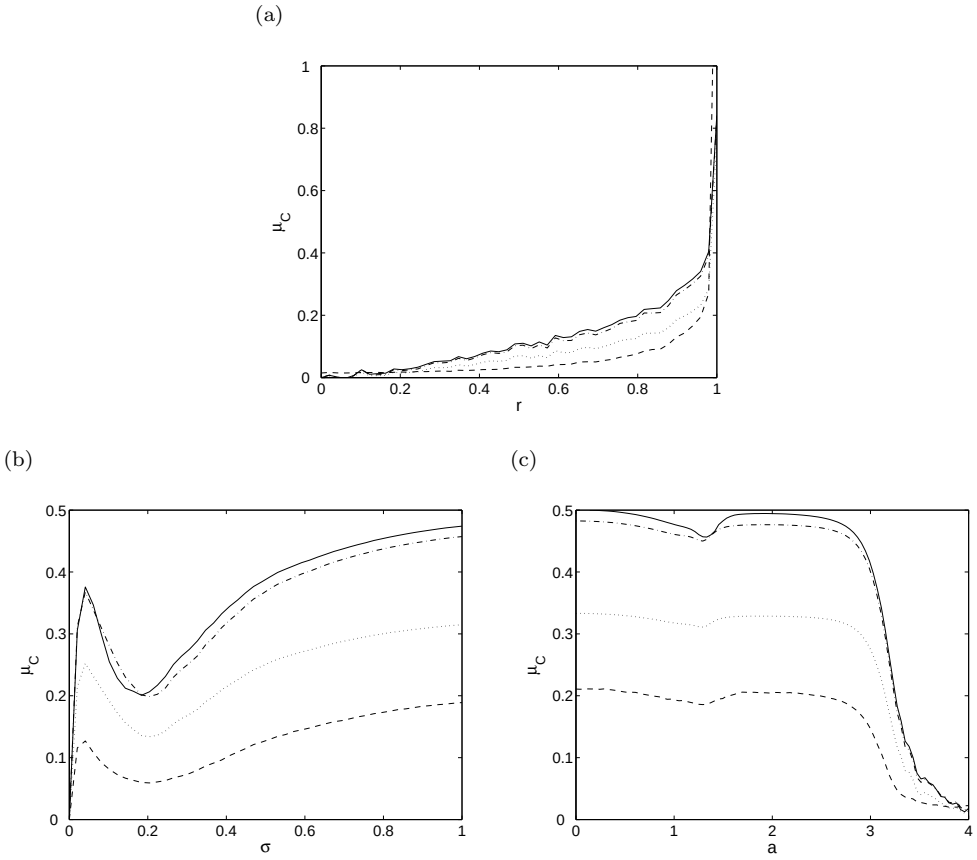

Figure 2.5: Comparison of the presented correlation measures μ_C
Pearson's linear correlation coefficient $(-)$, Spearman's rank correlation $(- \cdot -)$, Kendall's Tau $(\cdots)$ and the mutual information $(--)$ of two logistic maps with additive correlated Gaussian noise versus (a) the linear correlation coefficient r for $a = 3.4, \sigma = 0.05$, (b) the noise intensity σ for $a = 3.1, r = 0.5$ and (c) the bifurcation parameter a for $\sigma = 0.05, r = 0.5$. Transient and runtime are 10^4 iteration steps and the plots are averaged over 10 realizations.

Chapter 3

Dynamics in the fixed-point regime

In this chapter we investigate and extend Moran's statement for nonlinear, identical maps. In particular we focus on the fixed-point regime. First, we reproduce Moran's statement for linear maps. Then we develop a second order correction of Moran's theorem for quadratic maps with weak noise. Further we examine the implications of the boundary conditions applied to the noisy logistic map, as they seem to play a role for the correlation. Finally, an approximation for the logistic map in the trivial fixed-point regime by a piecewise linear map is made.

3.1 Introductory remarks

3.1.1 Two linear maps with correlated additive noise

In this subsection we reproduce the proof of the Moran effect. Let us start by considering two identical linear maps with correlated additive noise

$$\begin{aligned} x_{n+1} &= ax_n + b + \varepsilon_n \\ y_{n+1} &= ay_n + b + \eta_n, \end{aligned} \tag{3.1}$$

with $a, b \in \mathbb{R}$ and $|a| < 1$ to stay in the interval $[0, 1]$. The noise satisfies the following conditions: $\langle \varepsilon^2 \rangle = \langle \eta^2 \rangle = \sigma^2, \langle \varepsilon \rangle = \langle \eta \rangle = 0$, and is correlated:

$$C(\varepsilon_n, \eta_n) = r. \tag{3.2}$$

The mean values of the variable x are the same in the stationary state,

$$\langle x_n \rangle = \langle x_{n+1} \rangle = \langle ax_n + b + \varepsilon_n \rangle. \tag{3.3}$$

This yields an expression for the mean value

$$\langle x_n \rangle = \frac{b}{1-a}. \tag{3.4}$$

The second moment of x is determined by

$$\langle x_n^2 \rangle = a^2 \langle x_n^2 \rangle + b^2 + \langle \varepsilon_n^2 \rangle + 2ab \langle x_n \rangle, \tag{3.5}$$

which yields finally

$$\langle x_n^2 \rangle = \frac{\sigma^2}{1-a^2} + \frac{b^2}{(1-a)^2}. \tag{3.6}$$

The standard deviation of the map is

$$\sigma_x^2 = \langle x_n^2 \rangle - \langle x_n \rangle^2 = \frac{\sigma^2}{1-a^2}. \tag{3.7}$$

The cross correlation reads as follows

$$\langle x_n y_n \rangle = \frac{r\sigma^2}{1-a^2} + \frac{b^2}{(1-a)^2}. \tag{3.8}$$

By inserting the calculated moments in the definition of the linear correlation coefficient Eq. (2.1) we reproduce Moran's statement Eq. (1.3):

$$C(x_{n+1}, y_{n+1}) = \frac{\langle x_n y_n \rangle - \langle x_n \rangle^2}{\sigma_x^2} = C(\varepsilon_n, \eta_n). \tag{3.9}$$

This means the population correlation equals the noise correlation. If we include the preceding term x_{n-1} in Eq. (3.1), i.e. consider an AR(2) process, then Moran's statement still holds [109]. However, the calculations become lengthier. For non-identical linear maps the population correlation is always smaller than the noise correlation [18].

3.1.2 Fixed-point regime of maps

In the following we study two identical, one-dimensional, nonlinear systems with correlated additive noise, which can be described by the equations

$$\begin{aligned} x_{n+1} &= g(x_n) + \varepsilon_n, \\ y_{n+1} &= g(y_n) + \eta_n. \end{aligned} \tag{3.10}$$

The random variables ε, η are correlated as introduced in the last chapter.

As a paradigmatic example for the nonlinear map g we choose the logistic map

$$\begin{aligned} x_{n+1} &= a x_n (1 - x_n) + \varepsilon_n, \\ y_{n+1} &= a y_n (1 - y_n) + \eta_n, \end{aligned} \tag{3.11}$$

where $a \in [0, 4]$. A given point x_* is a *fixed point* if it does not change upon iteration of the map, $g(x_*) = x_*$. A fixed point is *stable* if $|g'(x_*)| < 1$.

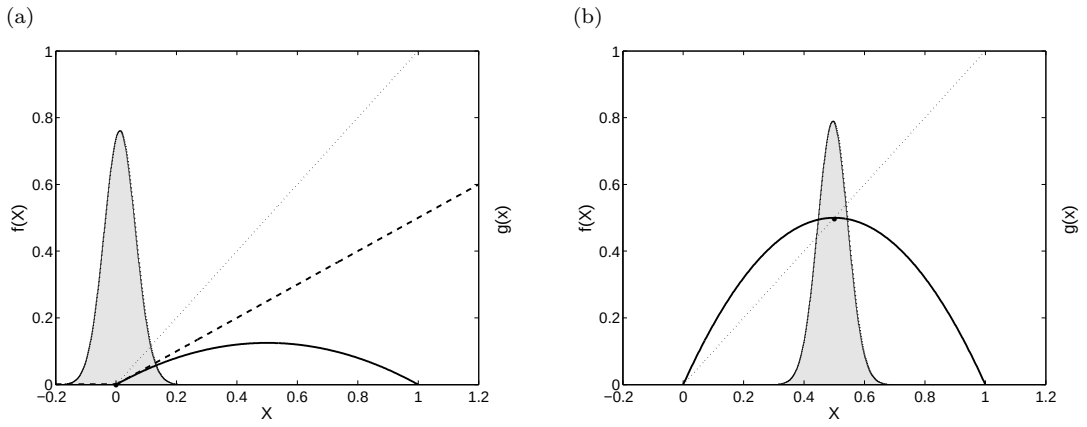

Figure 3.1: Stable fixed-point regimes of the logistic map Eq. 3.11 with additive noise, $\sigma = 0.05$ Plotted is the logistic map $(-)$ (a) in the trivial fixed-point regime, $x_* = 0, a = 0.5$, and (b) in the non-trivial fixed-point regime, $x_* = 0.5, a = 2$. The diagonal line $(\cdots)$ indicates $g(x) = x$. As an approximation in (a) the piecewise linear map $g(x_{n+1} > 0) = ax_n$, $g(x_{n+1} < 0) = 0$ is drawn $(--)$. Additionally the probability distribution $f(x)$ of the logistic map with additive Gaussian noise (gray shaded area) is displayed.

The logistic map has two stable fixed-point regimes which are depicted in Fig. 3.1. The trivial fixed point $x_* = 0$ is stable for $0 < a < 1$. Note that the neighborhood of the trivial fixed point is non-smooth. The other one is the non-trivial fixed point $x_* = 1 - 1/a$, which is stable for $1 < a < 3$ and has a smooth neighborhood. These different neighborhoods of the fixed points require different approaches: In Sec. 3.2 we linearize around the fixed point of a quadratic map, not taking into account the boundary conditions of the map. This is more adequate for the case shown in Fig. 3.1(b). In Sec. 3.4 we investigate the effects of the boundary conditions applied to $x \notin [0, 1]$. Then in section 3.5 we make another approach in the neighborhood of the trivial fixed point with a piecewise linear map displayed in Fig. 3.1(a).

3.2 Linearization around the fixed point

In this section we compute a second order extension of the Moran theorem for identical quadratic maps with weak noise. This correction is proposed by Ripa in [104], where he investigates linear systems with additive noise and dispersal between the populations.

We consider two identical unimodal one-dimensional maps g in the interval $[0, 1]$ with a fixed point x_*. Further we make a Taylor expansion of the map g around the fixed point x_* for small noise intensities up to the fourth order. The map g is assumed to be a function with at least four continuous derivatives. The mean value of the deviation $\delta x_n = x_n - x_*$ from the fixed

point can be written as

$$\begin{aligned}\langle \delta x_{n+1}\rangle &= \langle g(x_n) - x_*\rangle \\ &\approx \langle \varepsilon_n + g'(x_*)\delta x_n + g''(x_*)\frac{\delta x_n^2}{2} + g'''(x_*)\frac{\delta x_n^3}{6} + g''''(x_*)\frac{\delta x_n^4}{24}\rangle.\end{aligned} \tag{3.12}$$

Note that for the logistic function the fixed point is $x_* = 1 - 1/a$ for $1 < a < 3$ and the third and fourth derivative are zero. For the sake of simplicity, we use the notation $g'_* \equiv g'(x_*)$. In the stationary state we obtain the mean value

$$\langle \delta x_n\rangle = g'_* \langle \delta x_n\rangle + \frac{g''_*}{2}\langle \delta x_n^2\rangle + \frac{g'''_*}{6}\langle \delta x_n^3\rangle + \frac{g''''_*}{24}\langle \delta x_n^4\rangle . \tag{3.13}$$

In order to compute the mean value the following higher moments are needed:

$$\langle \delta x_n^2\rangle = \langle \varepsilon_n^2\rangle + (g'_*)^2\langle \delta x_n^2\rangle + g'_* g''_*\langle \delta x_n^3\rangle + \left(\frac{(g''_*)^2}{4} + \frac{g'_* g'''_*}{3}\right)\langle \delta x_n^4\rangle , \tag{3.14}$$

$$\langle \delta x_n^3\rangle = 3g'_*\langle \varepsilon_n^2\rangle\langle \delta_n\rangle + 3\langle \varepsilon_n^2\rangle\frac{g''_*}{2}\langle \delta_n^2\rangle + (g'_*)^3\langle \delta x_n^3\rangle + \frac{(g'_*)^2 g''_*}{2}3\langle \delta x_n^4\rangle , \tag{3.15}$$

$$\langle \delta x_n^4\rangle = \langle \varepsilon_n^4\rangle + (g'_*)^4\langle \delta x_n^4\rangle + 6\langle \varepsilon_n^2\rangle (g'_*)^2\langle \delta x_n^2\rangle , \tag{3.16}$$

$$\langle \delta x_n \delta y_n\rangle = \langle \varepsilon_n\eta_n\rangle + (g'_*)^2\langle \delta x_n\delta y_n\rangle + g*' g''_*\langle \delta x_n^2\delta y_n\rangle + \frac{g'_* g'''_*}{3}\langle \delta x_n^3\delta y_n\rangle + \tag{3.17}$$

$$+ \frac{(g''_*)^2}{4}\langle \delta x_n^2\delta y_n^2\rangle , \tag{3.18}$$

$$\langle \delta x_n^2\delta y_n\rangle = g'_*\left(2\langle \varepsilon_n\eta_n\rangle + \langle \varepsilon_n^2\rangle\right)\langle \delta x_n\rangle + g''_*\left(\langle \varepsilon_n\eta_n\rangle + \frac{1}{2}\langle \varepsilon_n^2\rangle\right)\langle \delta x_n^2\rangle + \tag{3.19}$$

$$+ (g'_*)^3\langle \delta x_n^2\delta y_n\rangle + (g'_*)^2 g''_*\langle \delta x_n^3\delta y_n\rangle + \frac{(g'_*)^2 g''_*}{2}\langle \delta x_n^2\delta y_n^2\rangle , \tag{3.20}$$

$$\langle \delta x_n^3\delta y_n\rangle = \langle \varepsilon_n^3\eta_n\rangle + 3(g'_*)^2\langle \varepsilon_n^2\rangle\langle \delta x_n\delta y_n\rangle + (g'_*)^4\langle \delta x_n^3\delta y_n\rangle , \tag{3.21}$$

$$\langle \delta x_n^2\delta y_n^2\rangle = \langle \varepsilon_n^2\eta_n^2\rangle + 2(g'_*)^2\langle \varepsilon_n^2\rangle\langle \delta x_n^2\rangle + 4(g'_*)^2\langle \varepsilon_n\eta_n\rangle\langle \delta x_n\delta y_n\rangle + (g'_*)^4\langle \delta x_n^2\delta y_n^2\rangle \tag{3.22}$$

The odd higher order moments of Gaussian random variables are zero. The even higher order Gaussian moments of the noise are calculated by summation over all possible combinations of different pairwise averages of the random variables (Wick's Theorem) [102]. Solving this system of linear equations, we can calculate the shift of the mean value due to noise

$$\begin{aligned}\langle \delta x_n\rangle &= \frac{g''_*\sigma^2}{2(1-g'_*)^2(1+g'_*)} + \frac{3\left(1+2g'_*+2(g'_*)^2+5(g'_*)^3\right)(g''_*)^3\sigma^4}{8\left(1-g'_*\right)^5\left(1+g'_*\right)^3\left(1+g'_*+(g'_*)^2\right)} + \\ &+ \frac{\sigma^4\left(2g''_* g'''_*\left(1+3g'_*+2(g'_*)^2-(g'_*)^3-5(g'_*)^4\right)+\left(1-(g'_*)^2-(g'_*)^3+(g'_*)^5\right)g''''_*\right)}{8\left(1-g'_*\right)^5\left(1+g'_*\right)^3\left(1+g'_*+(g'_*)^2\right)},\end{aligned} \tag{3.23}$$

and the variance

$$\langle \delta x_n^2\rangle - \langle \delta x_n\rangle^2 = \frac{\sigma^2}{1-(g'_*)^2} + \frac{\sigma^4\left(\left(1+2g'_*+2(g'_*)^2+7(g'_*)^3\right)(g''_*)^2+2g'_*\left(1-(g'_*)^3\right)g'''_*\right)}{2\left(1-g'_*\right)^4\left(1+g'_*\right)^3\left(1+g'_*+(g'_*)^2\right)}. \tag{3.24}$$

The ratio

$$K = \frac{\left\langle \delta x_n^2 \right\rangle - \left\langle \delta x_n \right\rangle^2}{\sigma^2} = \frac{1}{1-(g'_*)^2} + \sigma^2 \frac{\left(\left(1 + 2g'_* + 2(g'_*)^2 + 7(g'_*)^3\right) (g''_*)^2 + 2g'_* \left(1 - (g'_*)^3\right) g'''_* \right)}{2\left(1-g'_*\right)^4 \left(1+g'_*\right)^3 \left(1+g'_*+(g'_*)^2\right)} \tag{3.25}$$

is a natural measure of the noise amplification in the proximity of a bifurcation threshold of the map. The amplification effect was studied in a physical context by Wiesenfeld [127] and Surovyatkina et al. [67] and in an ecological context in [40]. The term amplification is here used in the sense of a rise in the amplitude of fluctuations due to noise before a bifurcation and thus earlier detection of the bifurcation. This is the noisy precursor mentioned in Sec. 1.4. We confirm the result of Surovyatkina et al. [67] for the logistic map: $K = 1/(2(a_c - a)) \approx 1/\sigma$. Associated with the noisy precursor is a weakening of the amplification effect on quick transitions through the bifurcation point. The duration of the time series must not be less than the fluctuation transient time steps

$$n_{\text{trans}} \geq \frac{1}{\sigma}. \tag{3.26}$$

The covariance of the two maps can be expressed as

$$\langle \delta x_n \delta y_n \rangle - \langle \delta x_n \rangle^2 = \frac{r\sigma^2}{1-(g'_*)^2} + \frac{r\sigma^4 \left(\left(r + 2g'_* + 2(g'_*)^2 + (6+r)(g'_*)^3\right) (g''_*)^2 + 2g'_* \left(1 - (g'_*)^3\right) g'''_* \right)}{2\left(1-g'_*\right)^4 \left(1+g'_*\right)^3 \left(1+g'_*+(g'_*)^2\right)}. \tag{3.27}$$

The correlation coefficient is defined as the quotient of Eq. (3.27) and Eq. (3.24). The denominator is expanded using the approximation

$$(A \pm \sigma^2)^{-1} \approx A^{-1} \left(1 \mp \frac{\sigma^2}{A}\right)$$

for small noise intensities, $|\sigma^2| < A$. This yields for the relative correlation

$$\frac{r_p}{r} = 1 - \frac{(1-r)\left(1 - g'_* + (g'_*)^2\right)(g''_*)^2}{2\left(1-g'_*\right)^3 \left(1+g'_*\right)\left(1+g'_*+(g'_*)^2\right)} \sigma^2 + \mathcal{O}(\sigma^4). \tag{3.28}$$

Note that the coefficient of σ^2 is always positive ($|g'_*| < 1$ in the fixed-point regime). This result is also valid for the fixed point of the nth iterate of g.

For the logistic map in the non-trivial fixed-point regime this new result reads

$$\frac{r_p}{r} = 1 - \frac{2a^2 \left(a - 1 + (2-a)^2\right)(1-r)}{(a-1)^3 (3-a)\left(3 - a + (2-a)^2\right)} \sigma^2. \tag{3.29}$$

Recalling the parameter ranges $1 < a < 3$ and $-1 < r < 1$, the fraction in Eq. (3.29) proofs positive. Therefore, in the fixed-point regime of a one-dimensional quadratic map there is no correlation enhancement, i.e. $r_p > r$, possible for small additive Gaussian noise.

In Fig.3.2 we compare the analytics presented in this subsection with direct numerical simulations. The simulations have been programmed in C, typically with a transient time and a

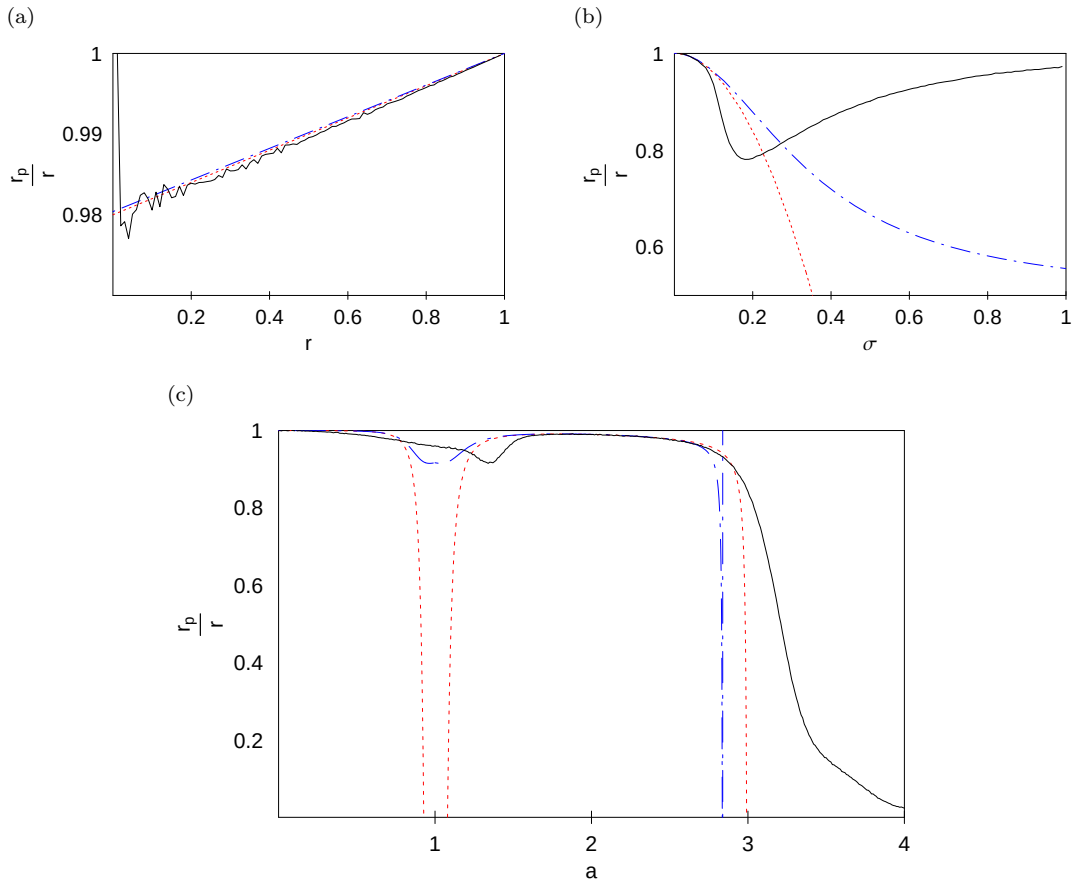

Figure 3.2: Comparison of the small noise expansion and the simulation $(-)$ of two logistic maps with additive correlated Gaussian noise. Plotted is the relative correlation coefficient r_p/r versus (a) the noise correlation r for $a = 2, \sigma = 0.05$, (b) the noise intensity σ for $a = 2, r = 0.5$, and (c) the bifurcation parameter a for $r = 0.5, \sigma = 0.05$. The relative correlation coefficient is plotted up to the second order in σ $(\cdots)$. The not expanded correlation coefficient, that is the quotient of Eq. (3.27) and Eq. (3.24), is additionally shown $(--)$.

runtime of 10^7 iteration steps of the map. The assumptions for the calculations are independent of the noise correlation r and thus the expansion is sufficient for all r for small noise intensities, as shown in Fig. 3.2(a). As can be seen in Fig. 3.2(b), the analytic approach works as expected only for small noise intensities $\sigma \leq 0.1$. At the bifurcation thresholds $a = 1$ and $a = 3$ the denominator in Eq. (3.29) is zero and the expansion breaks down as demonstrated in Fig. 3.2(c). In the simulations the logistic map has been set to zero outside the interval $[0, 1]$ in order to stay in the convergent regime. Whereas the Taylor-expansion around the fixed point for weak noise does not take the boundary conditions into account. The correlation is overestimated for $0 < a < 1$, as can be seen in Fig. 3.2(c). The effect of the boundary condition will be discussed in Sec. 3.4.

3.3 Lowest order calculations of stationary probability density functions

In the following we use another approach to calculate the correlation of two logistic maps in the fixed-point regime. Solving the Frobenius-Perron integral equation we compute the (joint) probability density function of the maps with additive noise.

3.3.1 Invariant density of one noisy system in the fixed-point regime

The integral equation for the invariant density f of a one-dimensional map, often called Frobenius-Perron equation, is introduced in detail in App. A. For a map g with additive Gaussian noise it reads as follows

$$f(x) = \iint_{-\infty}^{\infty} p_\sigma(\varepsilon)\, f(x')\delta(x - g(x') - \varepsilon)dx'd\varepsilon \tag{3.30}$$

$$= \int_{-\infty}^{\infty} p_\sigma(x - g(x'))\, f(x')dx', \tag{3.31}$$

where $p_\sigma(x)$ is the Gaussian distribution. The solution in the fixed-point regime of the map g, $g(x_*) = x_*$, can be approximated in first order by a Gaussian distribution

$$f(x) \approx p_w(x - x_*), \tag{3.32}$$

with unknown variance w.

Expanding the kernel of Eq. (3.31) at the fixed point to first order, with $\delta x = x - x_*$,

$$p_\sigma(x - g(x')) \approx p_\sigma(\delta x - \delta x'\, g'_*) \tag{3.33}$$

$$= \frac{1}{g'_*}\, p_{\sigma/g'_*}\left(\frac{\delta x}{g'_*} - \delta x'\right), \tag{3.34}$$

we arrive at a conditional equation for the stationary probability density function

$$\int_{-\infty}^{\infty} p_\sigma(x - g(x'))\, f(x')dx' = \frac{1}{g'_*}\int_{-\infty}^{\infty} p_{\sigma/g'_*}\left(\frac{\delta x}{g'_*} - \delta x'\right) p_w(\delta x')\, d\delta x' \tag{3.35}$$

$$= \frac{1}{g'_*}\, p_{\sqrt{(\sigma/g'_*)^2 + w^2}}\left(\frac{\delta x}{g'_*}\right) \tag{3.36}$$

$$= p_{\sqrt{\sigma^2 + (wg'_*)^2}}(\delta x). \tag{3.37}$$

The convolution of two Gaussian functions is a Gaussian function again. We remind the reader of the abbreviation $g'_* \equiv g'(x_*)$. This reproduces the ansatz Eq. (3.32), which leads to the following condition for the variance w

$$w \stackrel{!}{=} \sqrt{\sigma^2 + (wg'_*)^2} = \frac{\sigma}{\sqrt{1 - g'^2_*}}. \tag{3.38}$$

This yields the final result

$$f(x) = p_{\sigma/\sqrt{1-g'^2_*}}(x - x_*) = \frac{\exp\left(-(1 - g'^2_*)(x - x_*)^2/2\sigma^2\right)}{\sqrt{2\pi\sigma^2/(1 - g'^2_*)}}. \tag{3.39}$$

3.3.2 Stationary joint probability density function in the fixed-point regime

For two identical one-dimensional maps with additive noise the stationary joint probability distribution can be calculated likewise. The corresponding integral equation is

$$f(x,y) \quad = \quad \iint_{-\infty}^{\infty} dx'dy' \; f(x',y')\, p_{r,\sigma}\left(x-g(x'), y-g(y')\right). \tag{3.40}$$

The probability density function is approximated by a bivariate Gaussian centered at the fixed-point

$$f(x,y) \approx p_{\rho,w}(x-x_*, y-x_*), \tag{3.41}$$

with unknown correlation ρ and variance w.

Again we expand the kernel of the integral at the fixed point to first order, with $\delta x = x - x_*$,

$$p_{r,\sigma}(x-g(x'), y-g(y')) \quad \approx \quad \frac{1}{g_*'^2}\, p_{r,\sigma/g_*'}\left(\frac{\delta x}{g_*'} - \delta x', \frac{\delta y}{g_*'} - \delta y'\right). \tag{3.42}$$

For bivariate Gaussian distributions, the argument of the last subsection can be used for the difference and sum of the variables separately. In terms of $x'_\pm := (x' \pm y')/\sqrt{2}$, the joint probability density functions f, p factorize in the transformed coordinate system (x'_+, x'_-) as

$$p_{r,\sigma}(x'-a, y'-b) \quad = \quad \frac{\exp\left(-\frac{(x'-a)^2+(y'-b)^2-2r(x'-a)(y'-b)}{2\sigma^2(1-r^2)}\right)}{2\pi\sigma^2\sqrt{1-r^2}} \tag{3.43}$$

$$= \quad p_{\sigma\sqrt{1+r}}\left(x'_+ - \frac{a+b}{\sqrt{2}}\right) p_{\sigma\sqrt{1-r}}\left(x'_- - \frac{a-b}{\sqrt{2}}\right), \tag{3.44}$$

where $a, b \in \mathbb{R}$. Applying this transformation to the expanded kernel of Eq. (3.40) we obtain equivalently to the last subsection

$$\rho = r, \qquad w = \frac{\sigma^2}{\sqrt{1-g_*'^2}}. \tag{3.45}$$

This means, the correlation ρ of the two maps is the same as the correlation r of the noise (Moran). Whereas the variance of the maps is corrected compared to the noise variance by a factor containing the slope of the nonlinear map at the fixed point. This yields the following stationary joint probability distribution

$$f(x,y) \quad = \quad p_{\sigma\sqrt{\frac{(1+r)}{1-g_*'^2}}}\left(\frac{\delta x+\delta y}{\sqrt{2}}\right) p_{\sigma\sqrt{\frac{(1-r)}{1-g_*'^2}}}\left(\frac{\delta x-\delta y}{\sqrt{2}}\right) \tag{3.46}$$

$$= \quad \frac{\left(1-g_*'^2\right)\exp\left(-(1-g_*'^2)\frac{(x-x_*)^2+(y-x_*)^2-2r(x-x_*)(y-x_*)}{2\sigma^2(1-r^2)}\right)}{2\pi\sigma^2\sqrt{1-r^2}}, \tag{3.47}$$

which can be used for example to calculate moments or the correlation.

3.4 Comparison of different boundary conditions

In the introductory section of this chapter we noted that the neighborhood of the trivial fixed point is non-smooth. This is due to a well known problem for logistic maps with additive noise: The logistic map $x_{n+1} = ax_n(1 - x_n),\ a \in [0, 4]$, escapes to $-\infty$ if $x_n \notin [0, 1]$. So if we add a noise term, we can leave this interval. One can assume several boundary conditions to avoid this problem:

(a) setting the map to zero outside the interval $[0, 1]$

$$x_{n+1} = \begin{cases} g(x_n) + \varepsilon_n & 1 \geq x_n \geq 0 \\ \varepsilon_n & \text{else} \end{cases}$$

(b) periodic continuation of the map:

$$g(x_n + 1) = g(x_n)$$

(c) strictly positive: $x_{n+1} = \min(1, \max(0, g(x_n)+\varepsilon_n))$ This has the advantage that in ecology population numbers must be always positive.

(d) no boundary conditions at all but using only a limited range of parameters, $-\frac{a}{4} < \sigma < 1 - \frac{a}{4}$, to stay in the interval $[0, 1]$

In Fig. 3.3 the consequences of the different possibilities can be seen. The first variant, setting the function to zero if we leave the interval $[0, 1]$, comes closest to the original logistic map without boundary conditions. As the first variant is also ecologically sensible, we focus on this in the following.

The local minimum in the relative correlation coefficient at the first transcritical bifurcation for $a = 1$ is due to the boundary conditions. As Linz et al. explains in [75], the basin of attraction of $-\infty$ touches the fixed point just at $a = 1$. Any additive noise, no matter how small, drives the system towards $-\infty$, independent of its initial condition. In the fixed-point regime for $1 < a < 3$ the trivial fixed point $x_* = 0$ is unstable, but the boundary conditions map all diverging states to this unstable fixed point. Therefore, each system can stay in two states and on average the correlation coefficient decreases after the first bifurcation. This desynchronization of bistable systems will be explained in detail in Chap. 4.1.

In Fig. 3.4 the joint probability distribution of the different boundary conditions are shown. The maximum of the distribution is shifted toward positive values of the variables if boundary conditions are applied.

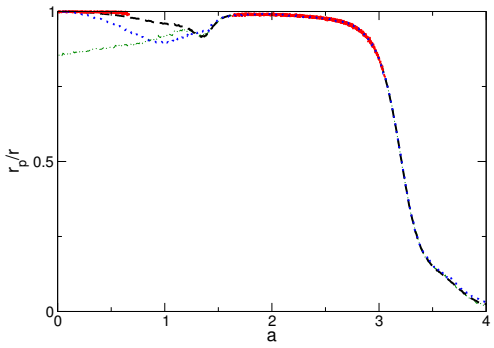

Figure 3.3: Comparison of various boundary conditions for two logistic maps with additive correlated Gaussian noise: $(--)$ setting to zero, $(\cdots)$ periodic, $(- \cdot -)$ strictly positive, $(\times)$ no boundary conditions. The parameters are $r = 0.5$, $\sigma = 0.05$, both transient time and runtime are 10^5 iteration steps.

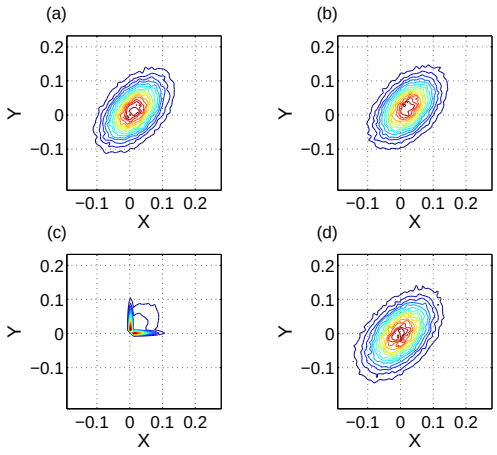

Figure 3.4: Joint probability distribution of two logistic maps with additive correlated Gaussian noise $\sigma = 0.05, r = 0.5, a = 0.5$, gridsize 0.009, 10^5 realizations, with various boundary conditions: (a) setting to zero, (b) periodic, (c) strictly positive, (d) no boundary conditions.

3.5 Piecewise linear maps

As an approximation of the logistic map in the trivial fixed-point regime ($a = 0 \ldots 1$), depicted in Fig. 3.1(a), we use the following piecewise linear map with Gaussian distributed noise ε:

$$x_{n+1} = \begin{cases} ax_n + \varepsilon_n & x_n \geq 0 \\ 0 + \varepsilon_n & x_n < 0 \end{cases}, \tag{3.48}$$

with $a \leq 1$; for the boundary condition 'setting to zero'.

To test the approximation with this piecewise linear map in the trivial fixed-point regime of the logistic map, the relative correlation coefficient of both systems is shown in Fig. 3.5. The piecewise linear map is a good approximation for $a < 0.5$. The correlation of the two maps is independent of the noise intensity σ like it is the case for two linear maps. But in contrast to the latter, the correlation coefficient of piecewise linear maps is not independent of the bifurcation parameter a. In Fig. 3.5 the effect of different boundary conditions on the correlation coefficient of two piecewise linear maps is demonstrated. No boundary conditions means that we have also $x_{n+1} = ax_n + \varepsilon_n$ for $x_n < 0$, i.e. the linear map producing the Moran effect. So the strong nonlinearity at zero leads to a weakening of the linear Moran effect. In the following we make an estimation of the linear correlation of these piecewise linear maps and approximate further the probability density function of this piecewise linear map.

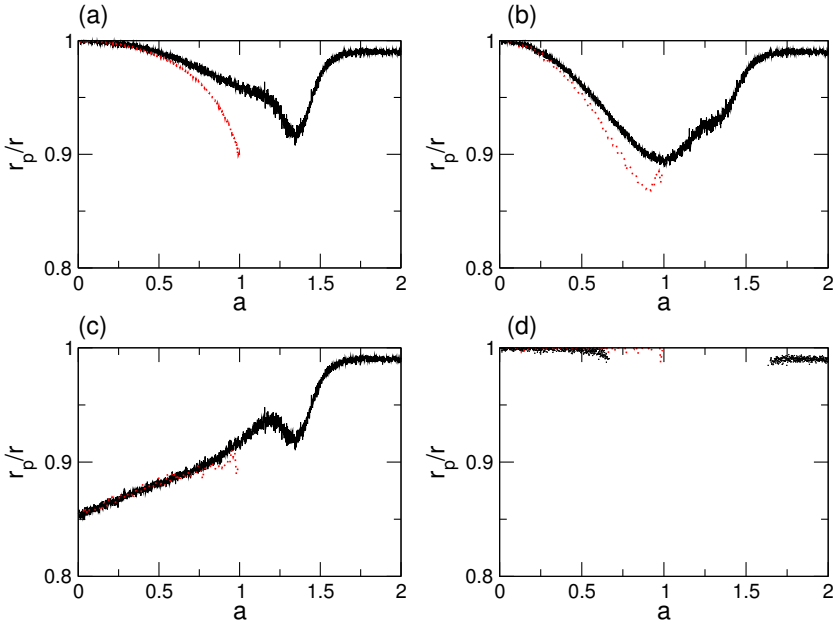

Figure 3.5: Comparison of the piecewise linear map, Eq. 3.48, $(\cdots)$ and the logistic map, Eq. 3.11 (-) map for Gaussian correlated noise with various boundary conditions: (a) setting to zero, (b) periodic, (c) ecological, (d) no boundary conditions; $r = 0.5$, $\sigma = 0.05$. Both runtime and transient time are 10^5 iteration steps.

3.5.1 Estimation of the correlation

The calculation of moments to compute the correlation is a bit trickier compared to Sec. 3.1.1, because there is one more variable. Thus, it leads to an under-determined system of equations

$$\langle x_n \rangle = \langle x_{n+1} \rangle = a \langle \Theta(x_n) x_n \rangle, \tag{3.49}$$

where $\Theta(x)$ denotes the Heaviside function with $\Theta(x < 0) = 0, \Theta(x > 0) = 1$. But one can estimate the moments,

$$\langle x_{n+1} \rangle = a \langle \Theta(x_n) x_n \rangle \geq a \langle x_n \rangle. \tag{3.50}$$

The second moment can be estimated by

$$\langle x_{n+1}^2 \rangle = a^2 \langle \Theta(x_n) x_n^2 \rangle + \sigma^2 \leq a^2 \langle x_n^2 \rangle + \sigma^2. \tag{3.51}$$

The cross correlation term yields

$$\langle x_{n+1} y_{n+1} \rangle = a^2 \langle \Theta(x_n) x_n \theta(y_n) y_n \rangle + r\sigma^2. \tag{3.52}$$

For $r \approx 1$ the signum of x_n and y_n are the same and the following estimation

$$\langle \Theta(x_n) x_n \Theta(y_n) y_n \rangle \leq \langle x_n y_n \rangle \tag{3.53}$$

holds. Therefore, the correlation coefficient is bounded by

$$C(x_n, y_n) \quad = \quad \frac{\langle x_{n+1} y_{n+1} \rangle - \langle x_n \rangle^2}{\langle x_n^2 \rangle - \langle x_n \rangle^2} \leq r. \tag{3.54}$$

We can conclude that for the piecewise linear map with $r \approx 1$, an enhancement of the correlation can not occur.

Chapter 4

Dynamics in the period-2 regime

In the previous chapter we have studied the Moran effect in the fixed-point regime. However, one of the most remarkable results from Fig. 1.5(a) in the introductory chapter 1 is the sharp reduction of r_p at the transition to the period-2 regime (at $a = 3$). In this chapter we study this effect. As we show this de-correlation can be understood from transitions between states of phase and anti-phase locking. Therefore we use symbolic dynamics, calculate transition probabilities and study the approach of Markov models.

4.1 Description of desynchronization

4.1.1 Primer of the period-2 regime

In this chapter we are mostly concerned with a logistic map (3.11) with additive Gaussian noise in the period-2 regime. Because it will be important in the following, we shortly recapture the bifurcation diagram in this regime. The fixed point of the logistic map g, $x_* = 1 - 1/a$, becomes unstable for $a > 3$ (see Fig. 4.1). Through the bifurcation at $a = 3$ two stable fixed points $x_{1,2}$ of the second iterate g^2 emerge, so that $g(x_1) = x_2$, and $g(x_2) = x_1$. These points $x_{1,2} = (1 + a \pm \sqrt{(a+1)(a-3)})/2a$ are stable for $3 < a < 1 + \sqrt{6} \approx 3.445$. The unstable fixed point x_* separates the basin of attraction of x_1 and this of x_2. In equilibrium there are two possible states for the system, $x_{1,2}$, between those the system switches consecutively. With noise the situation changes: The system switches not only between these two discrete states, but between the basins of attractions of $x_{1,2}$. The fixed points $x_{1,2}$ of the second iterate have different distances from the unstable fixed point x_*. This asymmetry will show up throughout this chapter. For example, the fluctuations around x_1 are smaller than those at x_2 [67].

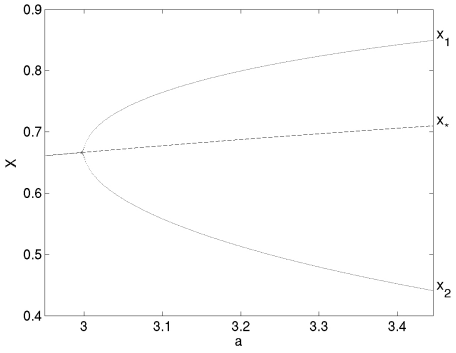

Figure 4.1: Enlargement of the bifurcation diagram of the logistic map in the period-2 regime. The fixed point x_* becomes unstable at $a = 3$ and two new points $x_{1,2}$ appear. Note the asymmetry.

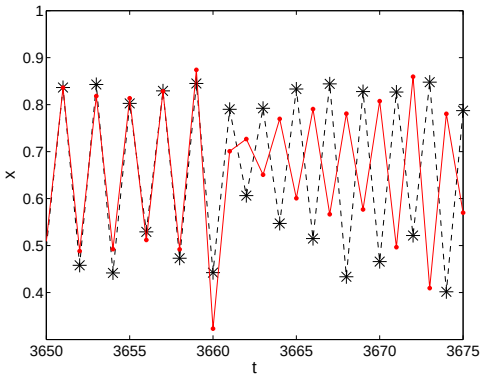

Figure 4.2: Time-series of two logistic maps in the period-2 regime with additive correlated Gaussian noise, $a = 3.3, \sigma = 0.02, r = 0.5$.

4.1.2 Decorrelation at the transition to the period-2 regime

In this section we describe the main mechanism of desynchronization. Furthermore we track special points like extrema and inflection points in the relative correlation of two systems with additive correlated Gaussian noise in order to uncover the mechanisms of desynchronization.

Two independent logistic maps in the period-2 regime are either highly correlated $r_p \approx 1$, or almost completely anticorrelated $r_p \approx -1$. If we add to each map correlated noise, with a noise intensity considerably smaller than the amplitude of the period-2 cycle, then from time to time rare jumps between these in-phase and out-of-phase solutions are induced. One of those jumps or phase-slips is depicted in Fig. 4.2. In the beginning, the two maps are synchronized, then one map experiences a noise shock and they are anticorrelated. Overall, this leads to contributions to the total correlation which cancel out each other, and averaging leads to a vanishing value of r_p.

In Fig. 1.5(b) the relative correlation coefficient r_p/r of two logistic maps with additive correlated noise in dependence on the noise intensity σ displays in the period-2 regime a local maximum at $\sigma_{\max}$ and a local minimum at $\sigma_{\min}$. The local minimum is also present in the fixed-point regime. In Fig. 4.3(a) the local extrema are plotted with their noise intensity and the corresponding bifurcation parameter for $r = 0.5$. The local minimum and maximum merge when the period-4 regime starts at $a_4 \approx 3.445$. Note that the maximal noise intensity of the local minimum occurs in the fixed-point regime at $a = 2.4, \max(\sigma_{\min}) = 0.2$. To the extremal noise intensities the following functions are fitted: $\sigma_{\max}(a) = 0.22a - 0.66(--)$, $\sigma_{\min}(a) = 0.25\sqrt{|a_\infty - a|}(-)$. For the Ricker map, Eq. (1.12) the noise intensity of the maximum $\sigma_{\max}$ is also a linear function of the bifurcation parameter, but for $\sigma_{\min}$ a function of $\sqrt{|a_4 - a|}$ seems more appropriate.

In the fixed-point regime the two identical systems are correlated (synchronized) with $r = 1$ in

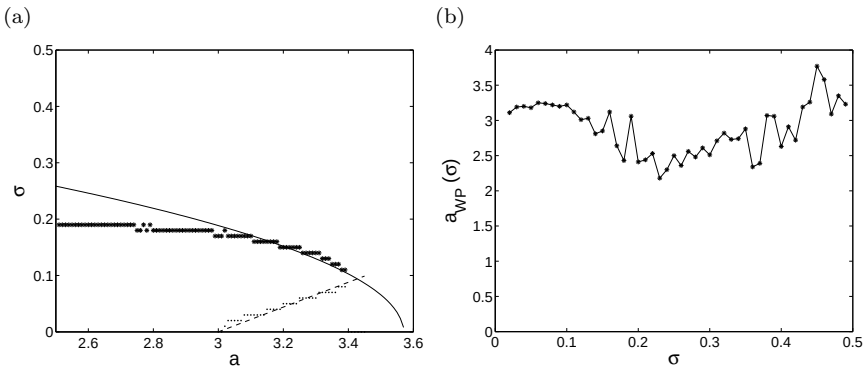

Figure 4.3: Tracking local special points in the relative correlation r_p/r of two logistic maps with correlated Gaussian noise in dependence of the bifurcation parameter a while varying the noise intensity σ, $r = 0.5$. Plotted are (a) the local maximum in the relative correlation at the noise intensity $\sigma_{\max}(\cdot)$, its linear fit $0.22a - 0.66$ (- -), the local minimum at $\sigma_{\min}(*)$ and the corresponding fit $0.25\sqrt{|a_\infty - a|}(-)$. (b) Displayed is the inflection point in r_p/r at a_{WP} while varying the noise intensity σ.

the case of zero noise. The desynchronization starts in the period-doubling regime at $a_2 = 3$. This is the starting point of the curve in Fig. 4.3(b), which displays the inflection point a_{WP} in the curve of the the relative correlation coefficient in dependence of the bifurcation parameter a that marks desynchronization. If both identical systems had different initial conditions, then in the period-2 regime both systems will be correlated a while and the other time anti-correlated and so the average correlation is zero for zero noise. For small noise intensities, i. e. smaller than the basin size $\max(x_1 - x_*) \approx 0.14$, the systems are still highly correlated in the period-2 regime, $a_{\mathrm{WP}} > 3$. For larger noise intensities the decorrelation sets in earlier, already in the fixed-point regime, $a_{\mathrm{WP}} < 3$. The minimum of $a_{\mathrm{WP}}(\sigma)$ is again around $(2.4, 0.12)$.

The relative correlation of two logistic maps correlated by noise in dependence on the bifurcation parameter a has a step at the beginning of the period-2 regime for weak noise. As a guess, we fit a sigmoid function to the relative correlation:

$$\frac{r_p}{r} = 1 - h(\sigma) + \frac{h(\sigma)}{1 + \exp\left(\frac{a-3-m(\sigma)}{b(\sigma)}\right)}. \tag{4.1}$$

This approach allows for the noise dependence on the height of the step $h(\sigma)$, the width $b(\sigma)$ and the mid $m(\sigma)$ of the step. We use the least-square method to fit Eq. (4.1) to the data of the relative correlation of two logistic maps with additive correlated Gaussian noise in dependence on the bifurcation parameter a. This is shown in Fig. 4.4(a) in comparison to the relative correlation of the time-series. Using the least-square method, one obtains also the dependencies of the details of this step on the noise intensity σ, which are depicted in Fig. 4.4(b). The

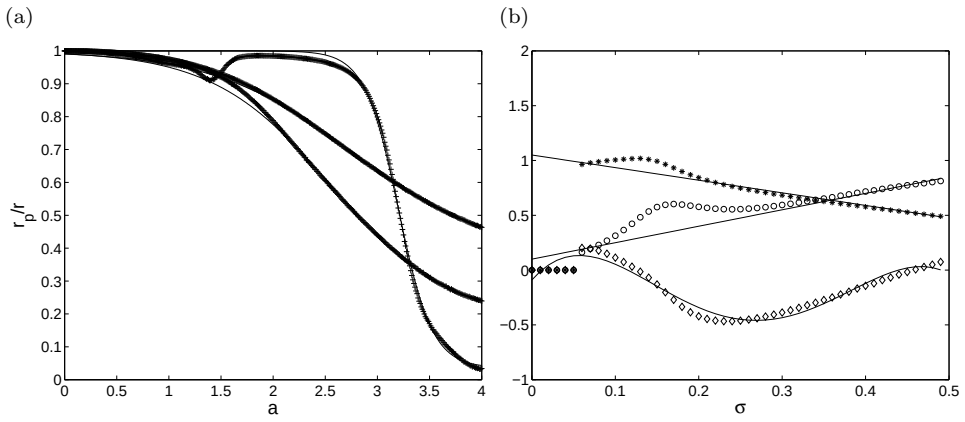

Figure 4.4: (a) Using the least-square method to fit the step-like function Eq. (4.1) (−) to the of the relative correlation (+) of two logistic maps correlated by Gaussian noise in dependence on the bifurcation parameter a. (b) Details of the step-like function Eq. (4.1): Mid $m(\sigma)(\diamond)$, width $b(\sigma)(\circ)$ and height $h(\sigma)(\star)$ for varying noise intensity and their fits for $\sigma = 0.06 \ldots 0.5$ (−), see Eq. (4.2).

following fits are chosen

$$\begin{aligned} b(\sigma) &= 1.5\sigma + 0.1, \\ h(\sigma) &= -1.15\sigma + 1.05, \\ m(\sigma) &= \alpha + \beta x + \gamma x^2 + \delta x^3 + \nu x^4, \end{aligned} \tag{4.2}$$

where $\alpha = -0.09, \beta = 8.8, \gamma = -102.6, \delta = 324$ and $\nu = -306.6$.

4.2 Invariant distribution in the period-2 regime

4.2.1 Invariant distribution of a single map

In the period-2 regime one can either apply the approach of section 3.2, i. e. linearize around the fixed points $x_{1,2}$ of the second iterate g^2 and calculate the moments. Or one can expand the probability distribution f of the map around the two points x_1, x_2 and solve the integral equation like in Sec. 3.3. This will be done in the following. An approach for the probability distribution of one logistic map with additive Gaussian noise is

$$f(x) = A_- p_{w_1}(x - x_1) + A_+ p_{w_2}(x - x_2), \tag{4.3}$$

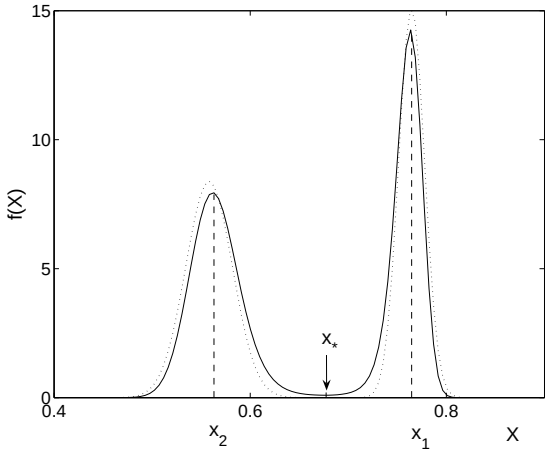

Figure 4.5: Probability distribution of the logistic map g with additive Gaussian noise in the period-2 regime ($-$). Indicated are the fixed points x_* of g and $x_{1,2}$ of g^2. Additionally plotted is the approach Eq.(4.3) as a sum of two Gaussian distributions ($\cdots$). The parameters are $a = 3.1, \sigma = 0.01$.

where $p_{w_i}(x)$ stands for the Gauss distribution and $A_\pm$ are normalization factors. The integral equation for the probability distribution, see App. A, reads as

$$f(x) = \iint_{-\infty}^{\infty} p_\sigma(\varepsilon)\, f(x')\delta(x - g(x') - \varepsilon)dx'd\varepsilon \tag{4.4}$$

$$= \int_{-\infty}^{\infty} p_\sigma(x - g(x'))\, f(x')dx'. \tag{4.5}$$

Entering Eq.(4.3) and expanding g around each point of the period-2 cycle leads to

$$f(x) \approx \frac{A_-}{g_1'} \int_{-\infty}^{\infty} p_{\sigma/g_1'} \left(\frac{x - x_2}{g_1'} - (x' - x_1) \right) p_{w_1}(x' - x_1)\, dx' + \tag{4.6}$$

$$+ \frac{A_+}{g_2'} \int_{-\infty}^{\infty} p_{\sigma/g_2'} \left(\frac{x - x_1}{g_2'} - (x' - x_2) \right) p_{w_2}(x' - x_2)\, dx'$$

$$= A_- p_{\sqrt{\sigma^2 + (w_1 g_1')^2}}(x - x_2) + A_+ p_{\sqrt{\sigma^2 + (w_2 g_2')^2}}(x - x_1), \tag{4.7}$$

where the abbreviation $g_i' = g'(x_i)$ was introduced. This is supposed to reproduce the ansatz (4.3), so we arrive at the conditions

$$w_2 \stackrel{!}{=} \sqrt{\sigma^2 + (w_1 g_1')^2},\ w_1 \stackrel{!}{=} \sqrt{\sigma^2 + (w_2 g_2')^2}, \tag{4.8}$$

which result in

$$w_2^2 = \sigma^2 \frac{1 + g_1'^2}{1 - g_1'^2 g_2'^2},\ w_1^2 = \sigma^2 \frac{1 + g_2'^2}{1 - g_1'^2 g_2'^2}. \tag{4.9}$$

For the amplitudes the approach yields $A_+ = A_-$, with $A_+ + A_- = 1$ we have $A_\pm = 1/2$.

Thus, as a first approximation, the probability distribution of one logistic map in the period-2 regime with additive noise can be approximated by two Gaussian distributions for small noise intensities.

4.2.2 Joint probability distribution of two maps

Now we explore the probability density in the product space of two logistic maps.

For two systems the integral equation for the joint probability distribution is

$$f(x,y) \quad = \quad \int\int_{-\infty}^{\infty} dx'dy' \; f(x',y')\, p\left(x-g(x'), y-g(y')\right). \tag{4.10}$$

We can approximate the distribution in the period-2 cycle by four Gaussian distributions, with, however, an unknown weight factor,

$$\begin{aligned} f(x,y) \quad \approx \quad & A_{--}p_{w_1}(x-x_1, y-x_1) + A_{-+}p_{w_2}(x-x_1, y-x_2) + \\ & + A_{+-}p_{w_3}(x-x_2, y-x_1) + A_{++}p_{w_4}(x-x_2, y-x_2). \end{aligned}$$

In order to obtain the relative weights, e. g. A_{--}, we have to calculate the probability that a pair (x,y) close to (x_1,x_1) is mapped not to a pair close to (x_2,x_2) but to a pair again close to (x_1,x_1) due to the noise.

4.3 Transition probabilities

Since the natural measure in phase space is concentrated around the four points (x_i,x_j), with $i,j \in \{1,2\}$, it is convenient to introduce a symbolic dynamics [86]. For this, we use a partition of the phase space, where the unstable fixed point x_* is used as a border for separating the states in the period-2 regime. For a single map we denote all points in the set $M_+ = \{x|x > x_*\}$ with the symbol "+" and all points $M_- = \{x|x \leq x_*\}$ with the symbol "-". The symbol set is denoted by $S = \{+,-\}$. Similar, in the product space we introduce the sets M_{++}, M_{+-}, M_{-+} and M_{--}, with e. g. $M_{++} = \{(x,y)|x > x_*, y > x_*\}$, and the corresponding symbol set $\hat{S} = \{++,+-,-+,--\}$. A sketch is depicted in Fig. 4.6. Further we denote the probabilities $A_+(A_-)$ to be in the set $M_+(M_-)$, with $A_- + A_+ = 1$. Correspondingly, A_{xy} is the probability to be in the set M_{xy}, $xy \in \hat{S}$, and $A_{++} + A_{+-} + A_{-+} + A_{--} = 1$.

In principle we have to consider sixteen transition rates which contribute to the joint distribution. The transition rate for two logistic maps in the period-2 regime with correlated noise can be expressed as:

$$\begin{aligned} \Gamma_{--\leftarrow++} \quad &= \quad \int\int\int\int_{x,y\in M_{--}}^{x',y'\in M_{++}} dxdydx'dy' f(x',y') p(x-g(x'), y-g(y')) \\ &=: \quad \Gamma_{--++}, \end{aligned} \tag{4.11}$$

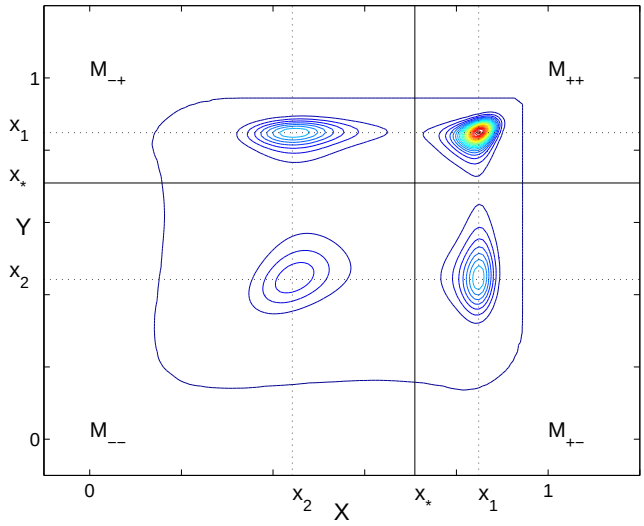

Figure 4.6: Contour plot of the joint probability distribution of two logistic maps with additive bivariate Gaussian noise. The highest probability densities are located at the points $x_{1,2}$ of the period-2 cycle. Indicated are the partitions of the phase space $M_{++} = \{(x,y)|x > x_*, y > x_*\}, M_{+-}, M_{-+}$ and M_{--}. The parameters are $a = 3.44, \sigma = 0.02, r = 0.5$.

where we omit the arrow from now for the sake of simplicity.

To obtain the transition probability, we have to normalize the above expression

$$w_{--++} \quad = \quad \frac{\Gamma_{--++}}{\mathcal{N}_{++}}, \tag{4.12}$$

with $\mathcal{N}_{++} = \iint_{x',y' \in M_{++}} dx'dy' f(x',y')$, so that $w_{----} + w_{+-++} + w_{-+++} + w_{++++} = 1$. If the noise is Gaussian, the integrals cannot be calculated except for special cases [1]. Here, $x_{1,2} \neq 0$, the only solvable case is uncorrelated Gaussian noise, $r = 0$, which leads to $r_p = 0$, independent of the bifurcation parameter or the noise intensity.

But nevertheless, the transition rates can be obtained from direct simulation of the system. In Fig. 4.7 the four transition probabilities for one logistic map with uniform noise are shown. The state "+" ($x > x_*$) is emptying for all noise intensities, $w_{++} < w_{-+}$. For a noise intensity $\sigma \gtrsim 0.12$ the probability to stay in the state "-" ($x < x_*$) is larger than the probability to jump away, $w_{+-} < w_{--}$. A possible explanation for this is that a noise intensity larger than $\max(x_1(a) - x_*(a)) \approx 0.13$ is necessary in order to stay in "-".

For two noisy logistic maps there are sixteen transition probabilities, which are shown in Fig. 4.8. Notice that, due to symmetry reasons, the two identical maps with symmetric noise are indistinguishable, which leaves only 10 different transition probabilities.

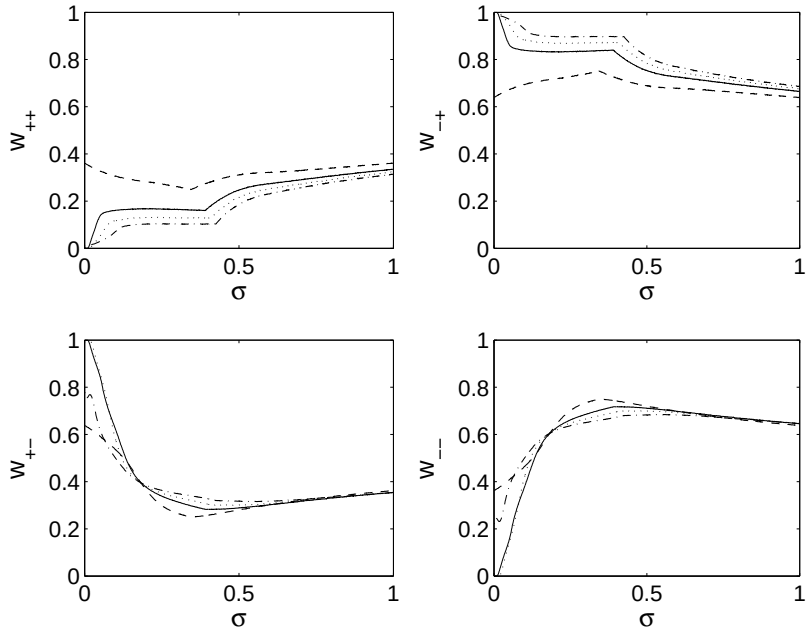

Figure 4.7: Transition probabilities of one logistic map with uniform noise as a function of the noise intensity σ for different bifurcation parameter values: $a = 2.8\,(--)$, $a = 3.1\,(-)$, $a = 3.44\,(\cdots)$ and $a = 3.8\,(-\cdot-)$.

4.3.1 Kramers' rate

Even though we are not able to write down the transition probabilities analytically, we study here a simple estimation of the transition rates in terms of the Kramers' theory. The idea is as follows. In the period-2 regime of the logistic map g, the system without noise switches consecutively between these two states. With additive noise it has the additional possibility to change between the basins of attraction of the fixed points of g^2 by means of a fluctuation and effectively stay in one state. This is the phase-slip depicted in Fig. 4.2. It corresponds to a jump in the second iterate g^2 of the logistic map. The smaller the fluctuations or the larger the distance between the two fixed points of g^2, the smaller is the possibility to stay in one state. This jump to the other fixed point of the second iterate g^2 is a noise-induced escape from a metastable state. The escape rate r_K over the barrier of a metastable potential has been derived by H.A. Kramers [65] in 1940:

$$r_K = \kappa \exp\left(\frac{-\Delta U}{D}\right), \tag{4.13}$$

where ΔU is the potential barrier to cross over and the diffusion constant $D = \sigma^2$ is here the standard deviation of the noise. The exponential term is also called the Arrhenius factor, and it was already mentioned by Arrhenius in the theory of chemical reactions (1889). The pre-exponential term κ depends only weakly on the noise and on the details of the potential.

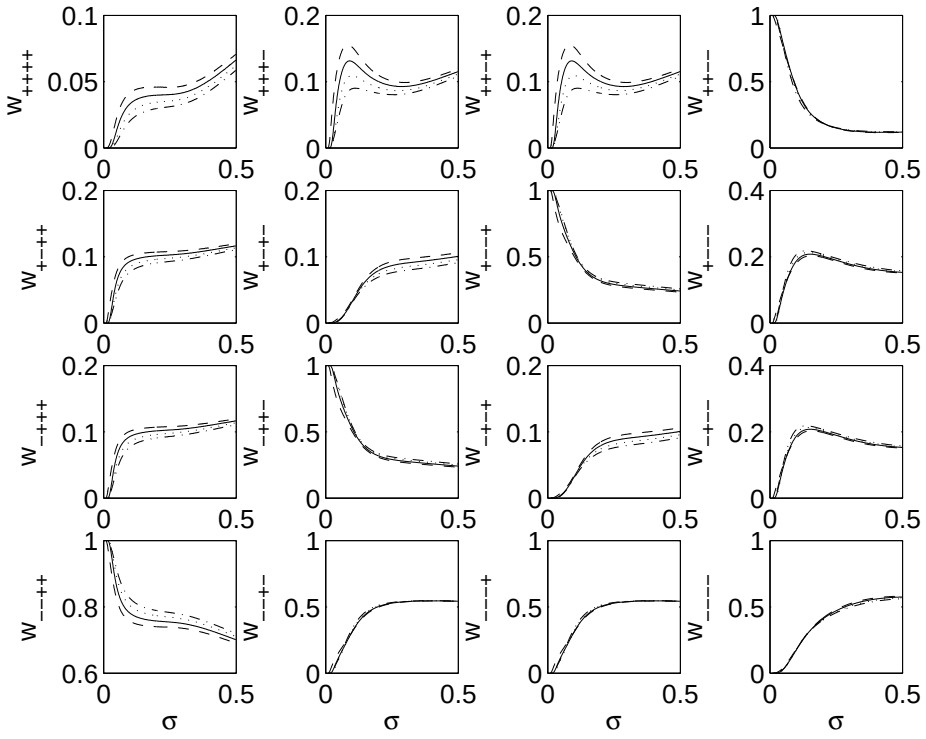

Figure 4.8: Transition probabilities of two logistic maps with additive correlated ($r = 0.5$) Gaussian noise for different bifurcation parameter values: $a = 3.1\,(--), a = 3.2\,(-), a = 3.3\,(\cdots)$ and $a = 3.4(-\cdot-)$ in dependence of the noise intensity σ. Shown are simulation results averaged over 100 realizations. For each realization both the transient time and the runtime are 10^6 steps.

The inverse of the escape rate is the mean first passage time $\langle\tau\rangle$ of the barrier crossing

$$\langle\tau\rangle = \frac{1}{\kappa} e^{\frac{\Delta U}{D}}. \tag{4.14}$$

If the system has no potential, that means it is not in thermodynamical equilibrium under the influence of noise, the theory of quasipotentials [66, 50] may be applied to calculate invariant densities or mean first passage exit times. In this study we do not enter this discussion, but we examine if the Kramers' theory holds in our case.

In Fig. 4.9 we compare the Kramers' theory (4.13) with a direct simulation of the rates. Plotted are the probabilities to stay , w_{++} and w_{--}, for one noisy logistic map (solid line) and their approximation by the Kramers' rate (dashed line), see Fig. 4.9(a). The other two transition probabilities can be derived from them $w_{-+} = 1 - w_{++}, w_{+-} = 1 - w_{--}$. The probabilities are computed by averaging 100 realizations of the simulated system. For comparison, the confidence interval for the confidence level of 95% is also shown $(\cdots)$, that means the interval $[x \pm 2\sigma_x]$ contains at least 95% of the predictions; where σ_x denotes the standard deviation. But of course

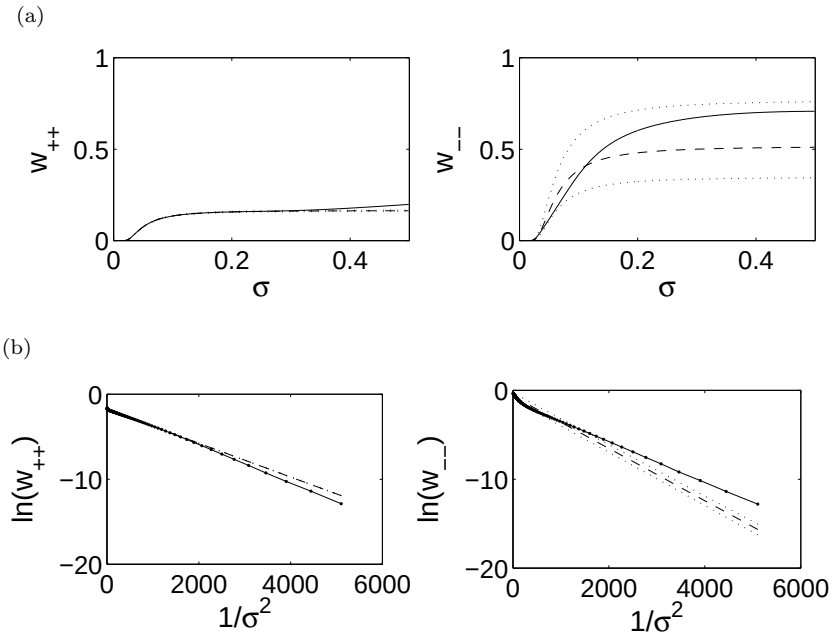

Figure 4.9: Transition probabilities w_{++} and w_{--} (a) and their logarithms (b) from the numerical simulation of one logistic map, $a = 3.25$, with Gaussian noise ($-$) and the fit (- -) of the Kramers' rate (4.13) for $\sigma = 0.024 \ldots 0.2$. Further indicated is the confidence interval of the confidence level 95% of the fit($\cdots$). Averaged over 100 realizations, each transient and runtime are 10^6 steps.

as mentioned at the end of Sec. 1.2, this test assumes that the data is independent and Gaussian distributed which is not true here. In order to test for the Kramers' rate, in Fig. 4.9(b) we also plot $\ln(w)$ versus $1/\sigma^2$ which should yield a straight line.

In Fig. 4.9 we find that the Kramers' theory is a good description as the semilogarithmical plot 4.9(b) displays a nearly straight line. The slope of the line should be height of the potential barrier. Now we seek to find the dependence on the bifurcation parameter a. In Fig. 4.10(a) the 'potential barrier' ΔU and in Fig. 4.10(b) the pre-exponential term $\ln(\kappa)$ are plotted. If the point $x_2(a)$ of the period-2 cycle is for the first time smaller than the super-stable point $x = 0.5$, this happens at $a = 1+\sqrt{5} \approx 3.236$, then the slope of the potential and the slope of the pre-exponential term changes its sign. However, there does not seem to be a simple dependence of the potential on a.

As we have shown, the transition rates in the period-2 regime for small noise intensities can be well approximated as a Markov process where the rates are given by the Kramers' theory. In the following we come back to the Moran problem.

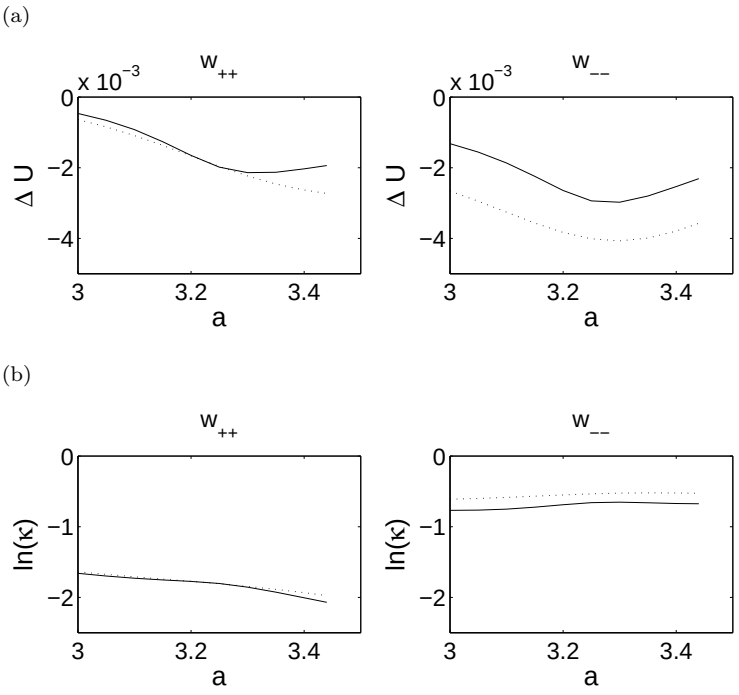

Figure 4.10: Verifying the validity of the Kramers' Ansatz Eq. (4.13) for the transition probabilities w_{++} and w_{--} of one logistic map with Gaussian noise. Displayed are in (a) the 'potential barrier' ΔU and in (b) the pre-exponential term $\ln(\kappa)$ with fits for $\sigma = 0.024 \ldots 0.2$ $(-)$, also shown in Fig. 4.9, and for $\sigma = 0.039 \ldots 0.2$ $(\cdots)$. Averaged over 100 realizations of a simulation where each transient and runtime steps are 10^6.

4.4 Markov-model with correlated noise

In the next sections, we build a Markov-model for the logistic map in the period-2 regime. We use a Markov process [56, 102] and see which features of the nonlinear logistic map in the period-2 regime it describes. This approach is more appropriate for small noise intensities.

4.4.1 Approximation as a Markov process

In section 4.3 we introduced a partition of the phase space in the states "+" and "-". Given this discretization of the space, the time-series of the logistic map translates into a sequence of symbols, which we model in this section by a Markov process. We denote the probability that a random variable X has a value $s(t)$ at time t by $P(s,t) = P_s(t)$, where $s \in S = \{+,-\}$. The joint probability $P(s_1,t_1;s_2,t_2)$ is the probability that the random variable has value s_1 at time t_1 and value s_2 at time t_2. A process is called stationary if

$$P_s(t) = P_s \qquad \forall t. \tag{4.15}$$

The conditional probability $P(s, t+1|s', t)$, here called transition probability, is the probability that the random variable X is in the state s at time $t+1$ given that it was before in the state s' at time t. We denote the transition probability with

$$P(s, t+1|s', t) =: w_{s \leftarrow s'} =: w_{ss'}. \tag{4.16}$$

If the random variable has memory only of its immediate past, the joint conditional probability $P(s_n, t_n|s_1, t_1; \ldots; s_{n-1}, t_{n-1})$, where $t_1 < t_2 < \cdots < t_n$, must have the form

$$P(s_n, t_n|s_1, t_1; \ldots; s_{n-1}, t_{n-1}) = P(s_n, t_n|s_{n-1}, t_{n-1}). \tag{4.17}$$

A process for which Eq. (4.17) is satisfied is called a *Markov process* (of first order).

Let us introduce the transition matrix $\mathbf{T}$, whose elements are the transition probabilities

$$\mathbf{T} = \begin{pmatrix} w_{++} & w_{+-} \\ w_{-+} & w_{--} \end{pmatrix}.$$

The transition matrix is a stochastic matrix, that is the sum over each column is equal to one, $\sum_i t_{ij} = 1$, and each element is a probability: $0 \leq t_{ij} \leq 1$ [102]. In other words, transition probabilities with the same initial state are arranged in the same column and transition probabilities with the same final state are in the same row. The transition matrix, $\mathbf{T}$, in general is not a symmetric matrix. Therefore, the left and right eigenvectors of $\mathbf{T}$ will be different. The stationary state of the system, $\vec{P}_{stat}$, is the eigenvector to the left eigenvalue 1,

$$\mathbf{T} \cdot \vec{P}_{stat} = 1 \cdot \vec{P}_{stat}, \tag{4.18}$$

with $\vec{P}_{stat} = (P_+, P_-)$.

Now we apply this theory to the logistic map in the period-2 regime. With noise the system has the possibility to stay in one state: If the system is in the state "-" and it happens that the noise is negative and with a large absolute value, the logistic function maps it to "+" but the negative noise brings it back to "-". On the other hand, if the system is in the state "+", only large positive noise lets it stay in "+". This is illustrated in Fig. 4.11. The described transition probabilities to stay in a state for Gaussian noise, $w_{--} = 1/2\,\mathrm{erfc}((x_1 - x_*)/(\sqrt{2}\sigma))$ and $w_{++} = 1/2\,\mathrm{erfc}((x_* - x_2)/(\sqrt{2}\sigma))$, are indicated as gray-shaded areas.

Thus a random number ε is drawn (e. g. throwing a dice) and depending on a threshold value the next state is chosen. The dynamic rules for the Markov model are the following:

$$\begin{array}{ll} + \longrightarrow + : & \frac{1}{2}\,\mathrm{erfc}\left(-\varepsilon/\sqrt{2}\right) \leq p \\ + \longrightarrow - : & \frac{1}{2}\,\mathrm{erfc}\left(-\varepsilon/\sqrt{2}\right) > p \\ - \longrightarrow + : & \frac{1}{2}\,\mathrm{erfc}\left(-\varepsilon/\sqrt{2}\right) < 1 - q \\ - \longrightarrow - : & \frac{1}{2}\,\mathrm{erfc}\left(-\varepsilon/\sqrt{2}\right) \geq 1 - q \end{array} \tag{4.19}$$

This is a Markov process with the transition rates $w_{++} = p$ and $w_{--} = q$. For $p = q = 0$, the system switches between the two states constantly. The random number ε is Gaussian distributed, in order to obtain positive values between in $[0, 1]$ we use the complementary error function.

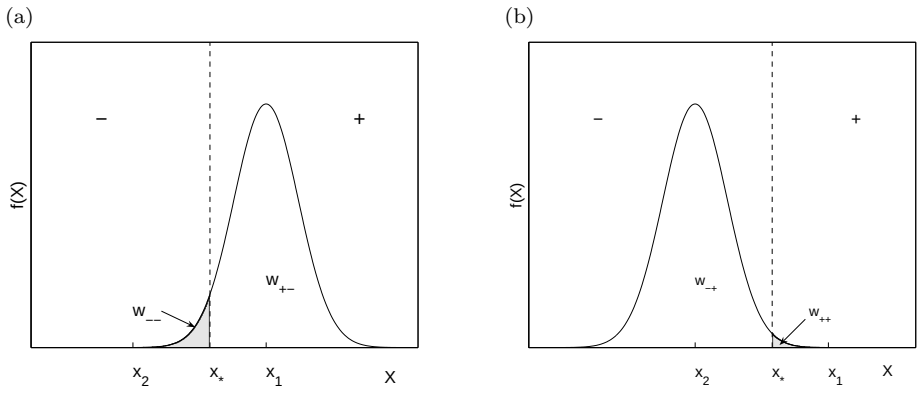

Figure 4.11: Gaussian distributed noise centered at the fixed points $x_{1,2}$ of the second iterate of the logistic map $g(x)$. Drawn as gray-shaded area are the probabilities to stay (a) in the state "-", $w_{--} = 1/2\,\mathrm{erfc}((x_1 - x_*)/(\sqrt{2}\sigma))$ and (b) in the state "+", $w_{++} = 1/2\,\mathrm{erfc}((x_* - x_2)/(\sqrt{2}\sigma))$. Further indicated are the fixed point x_* of g and the partitioning of the phase space. The parameters are $a = 3.1, \sigma = 0.05$.

4.4.2 Correlated Markov processes

Now we take two of the systems Eq. (4.19) with correlated random numbers, so to say the two dices are connected with a ribbon. The joint probability density function of the noises ε and η acting each on one of the processes is a bivariate Gaussian

$$p_{r,\sigma}(\varepsilon, \eta) = \frac{\exp(-\frac{\varepsilon^2 + \eta^2 - 2r\varepsilon\eta}{2\sigma^2(1-r^2)})}{2\pi\sigma^2\sqrt{1-r^2}}. \tag{4.20}$$

We set the standard deviation to one. Note that $p(\varepsilon, \eta) \neq p(-\varepsilon, \eta)$ (except for zero correlation, i. e. $r = 0$).

The transition probability that the random variables X_1 and X_2 are in the state s_1 respectively s_2 at time $t+1$ given that they were before in the state s_1' respectively s_2' at time t is denoted by

$$P((s_1, s_2), t+1 | (s_1', s_2'), t) =: w_{s_1 s_2 s_1' s_2'}, \tag{4.21}$$

with $s_i, s_i' \in S = \{+, -\}$. The transition matrix for these two correlated Markov systems (4.19) is

$$\mathbf{T} = \begin{pmatrix} w_{++++} & w_{+++-} & w_{++-+} & w_{++--} \\ w_{+-++} & w_{+-+-} & w_{+--+} & w_{+---} \\ w_{-+++} & w_{-++-} & w_{-+-+} & w_{-+--} \\ w_{--++} & w_{--+-} & w_{---+} & w_{----} \end{pmatrix}, \tag{4.22}$$

and has due to the symmetry of the probability distribution, $p(\varepsilon, \eta) = p(-\varepsilon, -\eta) = p(\eta, \varepsilon)$, the

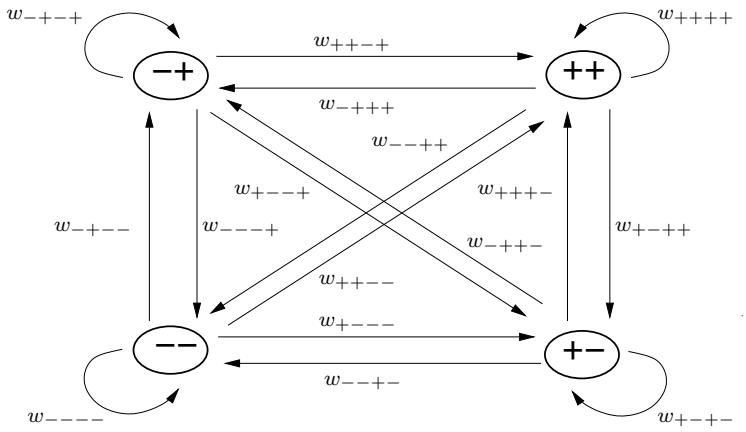

Figure 4.12: Possible states of the Markov model (4.19) and the corresponding transition probabilities

form

$$\begin{pmatrix} t_1 & t_4 & t_4 & t_8 \\ t_2 & t_5 & t_6 & t_9 \\ t_2 & t_6 & t_5 & t_9 \\ t_3 & t_7 & t_7 & t_{10} \end{pmatrix}, \tag{4.23}$$

where $t_i \in [0,1]$ for $i = 1 \ldots 10$. The same structure of the transition matrix displays the system of two logistic maps with additive, symmetrically correlated noise too, see Fig. 4.8. From the transition matrix $\mathbf{T}$ the correlation of the two systems can be calculated. The stationary state of the whole system is denoted by $\vec{P}_{stat} = (P_{++}, P_{+-}, P_{-+}, P_{--})$. The mean value of the first system can be calculated by

$$\langle X_1 \rangle = \sum_{s_1,s_2 \in S} s_1 P_{s_1 s_2} = (+1)P_{++} + (+1)P_{+-} + (-1)P_{-+} + (-1)P_{--}. \tag{4.24}$$

More generally, the m-th moment of the i-th variable of this process reads as

$$\langle X_i^m \rangle = \sum_{s_1,s_2 \in S} s_i^m P_{s_1 s_2}, \tag{4.25}$$

with $i \in \{1, 2\}$. The cross correlation can be expressed as

$$\langle X_1 X_2 \rangle = \sum_{s_1,s_2 \in S} s_1 s_2 P_{s_1 s_2}. \tag{4.26}$$

By inserting the calculated moments in Eq. (2.1), the linear correlation coefficient of two systems described by Eq. (4.19) reads as

$$r_T := \frac{P_{--} + P_{++} - P_{-+} - P_{+-} - (P_{++} + P_{+-} - P_{--} - P_{-+})(P_{-+} + P_{++} - P_{--} - P_{+-})}{\sqrt{1 - (P_{++} + P_{+-} - P_{--} - P_{-+})^2}\sqrt{1 - (P_{-+} + P_{++} - P_{--} - P_{+-})^2}}. \tag{4.27}$$

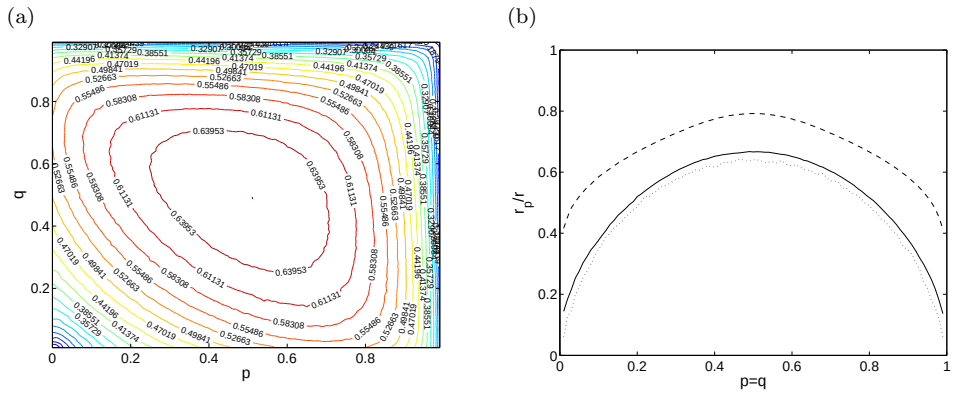

Figure 4.13: The relative correlation r_p/r of two correlated Markov systems (4.19):
(a) contour-plot of r_p/r for the threshold parameters p and $q, r = 0.5$, and
(b) section of $p = q$ for different random number correlations: $r = 0.1\,(\cdots), r = 0.5\,(-)$ and $r = 0.9\,(--)$. Both plots are averaged over 10 realizations, each transient and runtime are 10^6 steps.

For a Markov process of first order the linear correlation obtained from its time-series, r_p, and the correlation from the transition matrix, r_T, are equal due to the lack of further memory terms, i. e. $r_T = r_p$.

In Fig. 4.13(a) the relative correlation r_p/r of the two Markov systems (4.19) with correlated Gaussian random numbers is shown in dependence of the transition probabilities p, q. Additionally the section of $p = q$ for different correlation coefficients of the random numbers is displayed in Fig. 4.13(b). In the following we calculate analytically the correlation of the Markov systems (4.19) in some special cases.

The transition probability that both systems are staying in the state "+" is

$$w_{++++} = \int\int_{-\infty}^{\sqrt{2}\,\mathrm{erf}^{-1}(2p-1)} d\varepsilon\, d\eta\, p_{r,1}(\varepsilon,\eta), \tag{4.28}$$

$$= L(\sqrt{2}\,\mathrm{erf}^{-1}(1-2p), \sqrt{2}\,\mathrm{erf}^{-1}(1-2p), r), \tag{4.29}$$

where $L(h,k,r)$ is the bivariate normal probability function [1]. This integral is in general not analytically solvable except for special cases, see App. C. These special cases are indicated in the integral limits of Eq. (4.28) and are given in the following:

- Uncorrelated noise $r = 0$
  The two systems act independently and the probabilities just multiply $w_{++++} = p^2, w_{+-++} = p(1-p), \ldots$ The moments factorize $\langle xy\rangle = \langle x\rangle\langle y\rangle$ and thus the linear correlation coefficient is zero,

$$r_T = 0. \tag{4.30}$$

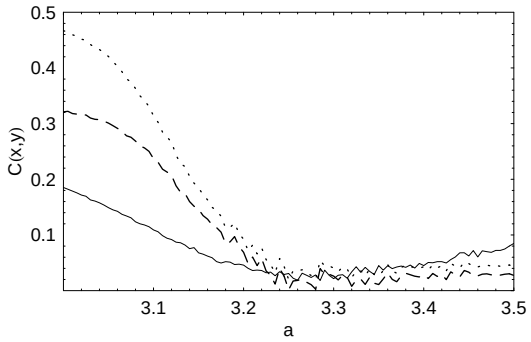

Figure 4.14: Linear correlation of two logistic maps as a function of the bifurcation parameter The correlation of two Markov systems (4.19), each with the transition probabilities of one logistic map with additive Gaussian noise obtained by direct numerical simulation, is drawn as solid line. As a comparison the correlation of the symbolic dynamics of two logistic maps with correlated Gaussian noise computed with Eq. (4.27) is shown $(\cdots)$ and the correlation of their time-series (- -). The parameters are $\sigma = 0.02, r = 0.5$.

- Equiprobable states $p = q = 1/2$
  Writing down the integrals for the transition probabilities reveals additional symmetries and the transition matrix has the following structure

$$\begin{pmatrix} t_1 & t_1 & t_1 & t_1 \\ t_2 & t_2 & t_2 & t_2 \\ t_2 & t_2 & t_2 & t_2 \\ t_1 & t_1 & t_1 & t_1 \end{pmatrix}. \tag{4.31}$$

  The correlation can be expressed as

$$r_T = -1 + w_{++++} = \frac{2}{\pi}\arcsin(r) \leq r. \tag{4.32}$$

  This is the maximal correlation, compare Fig. 4.13(b).

Application to the logistic maps

In the following we take the transition probabilities w_{++}, w_{--} of one logistic map with Gaussian noise obtained by direct numerical simulation and use them as transition probabilities p, q for the Markov model. The correlation of these Markov models is compared in Fig. 4.14 to the correlation of two logistic maps with correlated Gaussian noise. The time-series of the logistic maps is reduced like in Sec. 4.3 to the symbols "+,-" and the correlation is then computed by Eq. (4.27). For larger noise intensities the approximation gets worse. The reason is that the correlation of two logistic maps cannot be reduced to that of its symbols because fluctuations around the points $x_{1,2}$ are neglected.

4.5 Two piecewise constant maps

Suppose two identical piecewise constant maps with correlated noise. This is an exact realization of the previously described correlated Markov process and has the advantage, that fluctuations around the period-2 orbits are not neglected.

One piecewise constant maps looks as follows

$$x_{n+1} = \begin{cases} a+\varepsilon_n & x_n \le 0 \\ c+\varepsilon_n & x_n > 0 \end{cases}, \tag{4.33}$$

with $c<0, a>0$. For negative values of the bifurcation parameter a the map has a fixed point in a; for positive a the map has a period-2 cycle, switching between c and a.

Now we could proceed as in the last section with Gaussian noise, but the analytics were not satisfying. Thus we take symmetrically correlated uniform noise, introduced in Chap. 2:

$$\varepsilon = \sigma\sqrt{\frac{1+r}{2}}\xi + \sigma\sqrt{\frac{1-r}{2}}\xi', \tag{4.34}$$

$$\eta = \sigma\sqrt{\frac{1+r}{2}}\xi - \sigma\sqrt{\frac{1-r}{2}}\xi'. \tag{4.35}$$

The properties of the noise are: $\langle\varepsilon\rangle = 0$, $\langle\varepsilon^2\rangle = \sigma^2$, $\langle\varepsilon\eta\rangle = r\sigma^2$, where ξ and ξ' are uniformly distributed between $[-\sqrt{3},\sqrt{3}]$ to assure $\langle\xi^2\rangle = 1$. The joint probability density function can be calculated (see appendix B):

$$\begin{aligned} p(\varepsilon,\eta) = & \frac{1}{12\sqrt{1-r^2\sigma^2}}\Theta\left(\sqrt{6}\sigma\sqrt{1+r}-(\varepsilon+\eta)\right)\Theta\left(\sqrt{6}\sigma\sqrt{1+r}+(\varepsilon+\eta)\right) \\ & \times\Theta\left(\sqrt{6}\sigma\sqrt{1-r}-(\varepsilon-\eta)\right)\Theta\left(\sqrt{6}\sigma\sqrt{1-r}+(\varepsilon-\eta)\right). \end{aligned} \tag{4.36}$$

The integral equation for the joint distribution of the two maps reads as:

$$f(x,y) = \iint_{-\infty}^{\infty} dx'dy'\, f(x',y')p(x-g(x'),y-g(y')). \tag{4.37}$$

Using the piecewise constant map (4.33) we arrive at

$$\begin{aligned} f(x,y) = & \iint_0^\infty dx'dy'\, f(x',y')p(x-c,y-c) + \int_0^\infty dx'\int_{-\infty}^0 dy'\, f(x',y')p(x-c,y-a) + \\ & + \iint_{-\infty}^0 dx'dy'\, f(x',y')p(x-a,y-a) + \int_{-\infty}^0 dx'\int_0^\infty dy'\, f(x',y')p(x-a,y-c). \end{aligned}$$

This is also a zeroth order approximation for the noise-correlated logistic maps in the period-2 regime if we choose $g(x') = x_{1,2}$. As in Sec.4.3 we label the state $x_n > x_* = 0$ "+", and $x_n < 0$ "-". The probability that both systems are in state "+" is

$$A_{++} := \iint_0^\infty dxdy\, f(x,y) \tag{4.38}$$

$$\begin{aligned} = & A_{++}\iint_0^\infty dxdy\, p(x-c,y-c) + A_{+-}\iint_0^\infty dxdy\, p(x-c,y-a) + \\ & + A_{-+}\iint_0^\infty dxdy\, p(x-a,y-c) + A_{--}\iint_0^\infty dxdy\, p(x-a,y-a). \end{aligned} \tag{4.39}$$

The integral pre-factors of the probabilities A_{++}, A_{+-}, A_{-+} and A_{--} in Eq. (4.39) are the transition probabilities. The transition probabilities are defined leftward like in the previous section: $w_{++++} := w_{++\leftarrow++}$.

In App. D we calculate this transition probability exemplarily

$$\begin{aligned} w_{++++} &= \int_0^\infty dx \int_0^\infty dy\ p(x-c, y-c) \qquad (4.40) \\ &= \int_{-c}^\infty dx \int_{-c}^\infty dy\, \Theta\left(\sqrt{6}\sigma\sqrt{1+r} - (x+y)\right) \Theta\left(\sqrt{6}\sigma\sqrt{1+r} + (x+y)\right) \\ &\quad \times \frac{1}{12\sqrt{1-r^2\sigma^2}} \Theta\left(\sqrt{6}\sigma\sqrt{1-r} - (x-y)\right) \Theta\left(\sqrt{6}\sigma\sqrt{1-r} + (x-y)\right). \end{aligned}$$

For convenience we introduce the abbreviation $\sigma_+ = \sqrt{3}\sigma\sqrt{1+r}$, $\sigma_- = \sqrt{3}\sigma\sqrt{1-r}$. Solving the integrals leads to

$$\begin{aligned} w_{++++} &= \frac{1}{12\sqrt{1-r^2\sigma^2}} \Big[2\sigma_- \left(\sigma_+ + \sqrt{2}c - \sigma_-\right) \Theta\left(\sigma_+ - \sigma_- + \sqrt{2}c\right) \Theta\left(\sigma_+ + \sigma_- - \sqrt{2}c\right) \\ &\quad + 4\sigma_+\sigma_- \Theta\left(\sqrt{2}c - \sigma_+ - \sigma_-\right) \Theta\left(\sqrt{2}c - \sigma_+\right) \\ &\quad + 4\sqrt{2}c\sigma_+ \Theta\left(\sigma_- - \sqrt{2}c - \sigma_+\right) \Theta\left(\sqrt{2}c - \sigma_+\right) \\ &\quad + \left(\sigma_+ + \sqrt{2}c\right)^2 \Theta\left(\sigma_- - \sqrt{2}c - \sigma_+\right) \Theta\left(\sigma_+ + \sqrt{2}c\right) \Theta\left(-\sqrt{2}c + \sigma_+\right) \\ &\quad + \left(\sigma_-^2 - \left(\sigma_+ - \sqrt{2}c\right)^2\right) \Theta\left(\sigma_+ - \sigma_- + \sqrt{2}c\right) \Theta\left(\sqrt{2}c - \sigma_+\right) \Theta\left(\sigma_- + \sigma_+ - \sqrt{2}c\right) \\ &\quad + \sigma_-^2 \Theta\left(\sigma_+ - \sigma_- + \sqrt{2}c\right) \Theta\left(-\sqrt{2}c + \sigma_+\right) \Big]. \qquad (4.41) \end{aligned}$$

The other transition probabilities can be computed by solving the Frobenius-Perron equation, analogously to w_{++++}, or by constructing geometrically the areas in phase space which correspond to the transition probabilities, like in Fig. 4.11.

From the ten transition probabilities, only three have to be calculated, all others can be derived from them through transformations. One transition probability is noted already, see Eq. (4.41), the other two are also calculated in appendix D. Calculating the stationary state of the transition matrix, the correlation r_T of these two piecewise constant maps with additive correlated noise can be computed with Eq. (4.27). This correlation is depicted in Fig. 4.15(a) with the line of diamonds ($\diamond$).

With the use of the formula (2.6) for the correlation of two additive noises the correlation of the time-series can also be calculated, because the noise is an additive process to the Markov process. The variance of this Markov process is $((a-c)/2)^2$, so the correlation reads as

$$C(x,y) = \frac{r_T \left(\frac{a-c}{2}\right)^2 + r\sigma^2}{\left(\frac{a-c}{2}\right)^2 + \sigma^2}, \qquad (4.42)$$

where r denotes the correlation and σ the variance of the additive noise. This is the dashed line in Fig. 4.15(a) and it corresponds to the correlation of the simulated process (line of stars

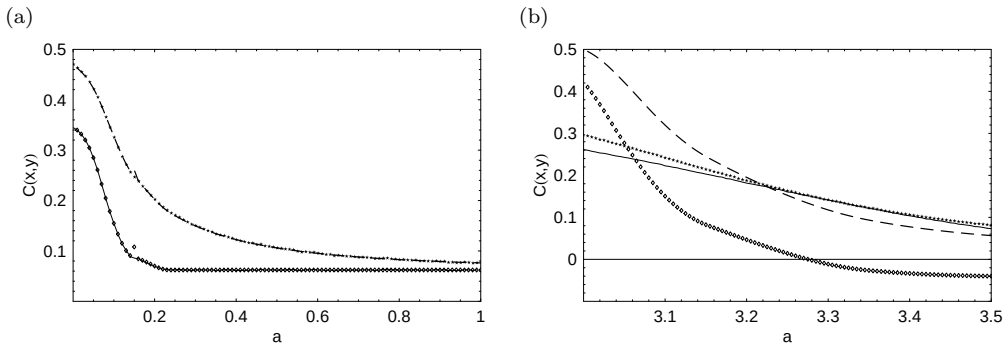

Figure 4.15: Correlation $C(x, y)$ of two (a) piecewise constant and (b) logistic maps in zeroth order with symmetrically correlated additive uniform noise when changing the bifurcation parameter a. Plotted is the correlation of the simulated time-series ($\star$), the correlation computed with Eq. (4.27) from the analytically derived transition matrix ($\diamond$) r_T and from the transition matrix acquired by simulation ($-$) and the correlation for two additive noises calculated in Eq. (4.42) ($--$). The parameters are for (a) $\sigma = 0.1, c = -0.1, r = 0.5$ and (b) $\sigma = 0.1, r = 0.5$; the simulations are averaged over 10 realizations.

($\star$)). The correlation of the symbolic dynamics of this process is depicted as the solid line in Fig. 4.15(a) and coincides with the analytically derived correlation ($\diamond$). If in the transition probabilities of the logistic map, Eq. (4.11), with uniform noise the map g is only expanded to zeroth order, i. e. $g(x' > x_*) = x_2$, then the transition probabilities are reduced to those of the piecewise constant map, compare Eq. (4.39). The corresponding fixed points of the second iterate are $a = x_1 - x_*, c = x_2 - x_*$. This comparison is shown in Fig. 4.15(b).

Special cases of two piecewise constant maps with additive correlated noise, which we could solve are the following:

- Uncorrelated noise $r = 0$
  The two systems act independently and the correlation vanishes.
- Case $a = -c = 0$ and large noise intensities $\sigma \longrightarrow \infty$, i. e. $\sigma \gg \max(\|a\|, \|c\|)$
  The transition matrix has the structure

$$\begin{pmatrix} t_1 & t_1 & t_1 & t_1 \\ t_2 & t_2 & t_2 & t_2 \\ t_2 & t_2 & t_2 & t_2 \\ t_1 & t_1 & t_1 & t_1 \end{pmatrix}. \tag{4.43}$$

  Thus the correlation of the symbolic dynamics reduces to

$$r_T = -1 + 4w_{++++}, \tag{4.44}$$

  and using Eq. (2.6) the correlation of the time-series yields

$$r_p = r. \tag{4.45}$$

More precisely, for uniform noise the correlation computes to $r_T = -1+\left(2-\sqrt{\frac{1-r}{1+r}}\right)\Theta(r)+\sqrt{\frac{1+r}{1-r}}\Theta(-r)$, and for Gaussian noise to $r_T = \frac{2}{\pi}\arcsin(r) \leq r$.

- Symmetric case $a = -c$
  This implies another symmetry to the transition matrix, which now looks like

$$\begin{pmatrix} t_1 & t_4 & t_4 & t_3 \\ t_2 & t_5 & t_6 & t_2 \\ t_2 & t_6 & t_5 & t_2 \\ t_3 & t_4 & t_4 & t_1 \end{pmatrix}. \tag{4.46}$$

  The corresponding correlations yield

$$r_T = \frac{w_{+++-} - w_{-+++}}{w_{+++-} + w_{-+++}}, \tag{4.47}$$

$$r_p = \frac{r_T a^2 + r\sigma^2}{a^2 + \sigma^2}. \tag{4.48}$$

  In the special case that there are no jumps between the two states, i. e. $a = -c > 2\sigma$, the 'transition matrix' reads as

$$\begin{pmatrix} 0 & & & 1 \\ & & 1 & \\ & 1 & & \\ 1 & & & 0 \end{pmatrix}, \tag{4.49}$$

  with $r_T = \pm 1$, because the eigenvalue 1 is twice degenerated.

Chapter 5

Amplification of the correlation

In the previous chapters we saw always that the correlation of the processes is smaller (or equal) the correlation of the added noises. In this chapter we discuss two different ways in which an amplification of the correlation can appear, so that the correlation r_p of the two systems is larger than that of the noise, $r_p > r$.

5.1 X-noise

We show that a counterintuitive amplification of the correlation can arise if the joint noise probability distribution is structured. The most simple example is given by the following joint distribution

$$f(\varepsilon,\eta) \quad = \quad q\,p(\varepsilon)\delta(\varepsilon-\eta) + (1-q)p(\varepsilon)\delta(\varepsilon+\eta). \tag{5.1}$$

The particular noise distribution $p(\varepsilon)$ can be of any kind, in the following a Gaussian is assumed. The joint noise distribution is a simple case of Eq. (2.2), a mixture of a perfect correlated and an anti-correlated component, where q is the mixing parameter. An example for this kind of noise in the ecological context could be climate with a distinct correlated and a distinct anticorrelated component. For noise satisfying $\langle\varepsilon\rangle = \langle\eta\rangle = 0, \langle\varepsilon^2\rangle = \langle\eta^2\rangle = \sigma^2$, the linear correlation coefficient reads as $C(\varepsilon,\eta) = 2q-1$. In Fig. 5.1(a) the joint probability density of noise corresponding to Eq. (5.1) is depicted. Due to the shape of the distribution we call this X-noise. For $q = 1/2$, the linear correlation coefficient is zero, although the distribution is apparently dependent: From the knowledge of ε the absolute value of η can be predicted.

If we now apply this uncorrelated X-noise additively to uncoupled logistic maps, the distribution of the maps is smeared out and slightly biased compared to the noise distribution, see Fig. 5.1(b). Varying the noise correlation in Fig. 5.2(a) reveals an amplification regime $r_p > r$, e. g. for $r \in [-0.1, 0.63]$ with $a = 2.4, \sigma = 0.2$. This result is at first glance astonishing. For uncorrelated X-noise in the fixed-point regime of the logistic map a resonance-like dependence on the noise

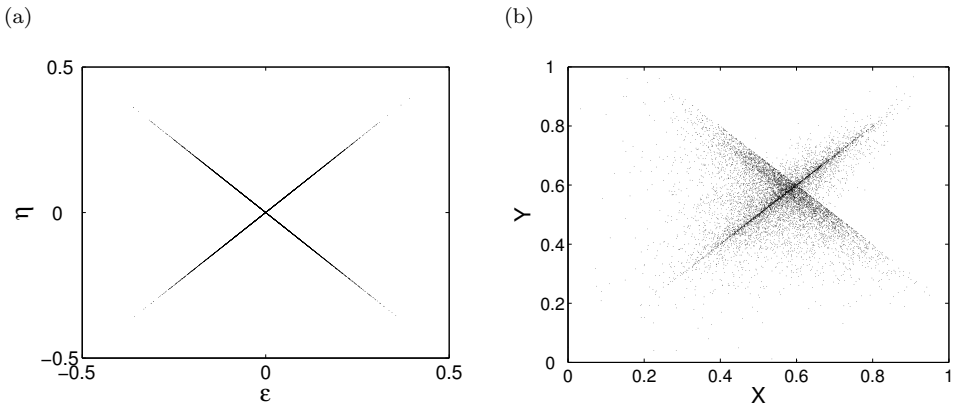

Figure 5.1: (a) Density distribution of Gaussian X-noise Eq. (5.1), $q = 0.5, \sigma = 0.1$ and (b) the density distribution of two logistic maps with this uncorrelated Gaussian X-noise, $a = 2.4, q = 0.5, \sigma = 0.1$. Both plots show an ensemble of 10^4 realizations with each 10^6 iteration steps.

intensity σ is observed in Fig. 5.2(b). Additionally we vary the bifurcation parameter in order to see in which regime the amplification of the noise correlation through the system is most pronounced. In Fig. 5.3(b) we see that for the logistic map in the fixed-point regime, $a \in [1, 3]$, the correlation is most enhanced.

Following the naming of other noise-related resonance effects, we denote the effect as *correlation resonance*. *Stochastic resonance* [11] is observed in a broad class of nonlinear systems, e. g. bistable or excitable, that are driven by an external signal and noise. A finite optimal noise intensity results in a maximal response of the system to the signal. Too large noise destroys the cooperative effect of noise and the external signal. Excitable systems with additive noise, which lack an external signal, show also a resonant behavior if the noise intensity corresponds to the eigenfrequency of the system [37]. This is called *coherence resonance* (CR) [92] or autonomous stochastic resonance [76]. A detailed analysis of coherence and stochastic resonance is given in [73]. As a measure of the resonance effect the signal-to-noise ratio (SNR) is used. Coherence resonance was reported by Neiman et al. [85] for one noisy logistic map or two coupled noisy logistic maps. The authors interpreted CR as a noisy precursor of a period-doubling bifurcation at subcritical control parameter values.
The difference to coherence resonance is that correlation resonance is a mutual phenomenon of two nonlinear systems that have a structured noise distribution. Therefore we use as a measure the correlation (coeffcient).

We have tested correlated Laplacian noise with a probability distribution $p(x) = 1/\sqrt{2}e^{-|x|\sqrt{2}}$, correlated uniform noise, correlated dichotomous noise where the four points are not on the diagonals of the joint noise distribution and correlated uniform noise distributed on the unit disk $\{(x, y)|x^2 + y^2 < 1\}$, all correlated symmetrically according to Eq. (2.12). If the four points of the dichotomous joint distribution are on the diagonals like in [39], the correlation is zero. The comparison of the correlation coefficient of two logistic maps with the mentioned

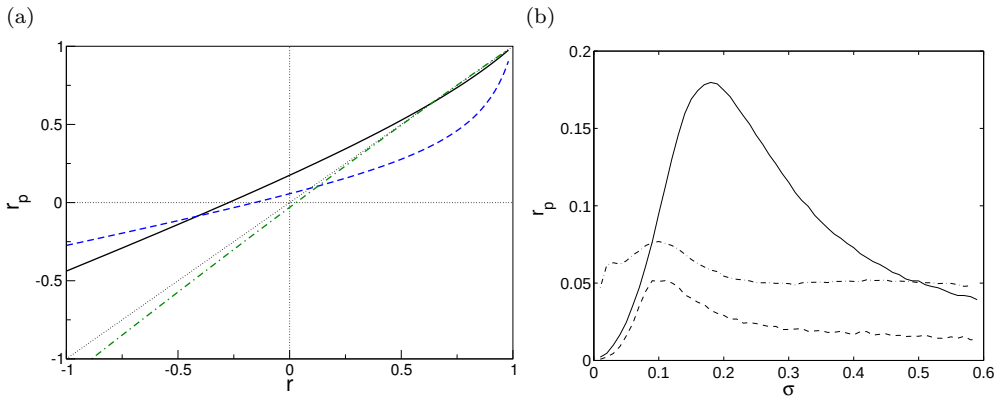

Figure 5.2: Amplification of the noise: (a) The correlation coefficient r_p of two logistic maps with r correlated Gaussian X-noise Eq. (5.1), $\sigma = 0.2$. (b) The correlation coefficient r_p of two logistic maps with additive Gaussian X-noise Eq. (5.1), $q = 0.5$. Shown are results for bifurcation parameters in the fixed-point regime $a = 1.6\,(-\cdot-), a = 2.4\,(-)$ and in the period-2 regime $a = 3.3\,(--)$. Averaged over 100 realizations with runtime 10^6 steps.

different structured noise distributions is shown in Fig. 5.4. For the logistic maps the maximal amplification is around $a = 2.4, \sigma = 0.2$, independent of the structured noise distribution. Though the amplification factor depends on the particular distribution as shown in Fig. 5.4. Our numerics suggests that this effect plays a role for every non-Gaussian noise to a different degree. Simulations indicate that for the Ricker map, Eq. (1.12), the maximal amplification is also in the fixed-point regime at $a \in [1.3, 1.4]$ for $\sigma \in [0.55, 0.65]$. The amplification is most pronounced for linearly uncorrelated noise $r = 0$. Note, that there is no correlation resonance in linear systems.

Nevertheless, the mutual information of the two logistic maps with additive X-noise is always smaller than that of the X-noise. So we do not have an information gain transmitting the noise signals through the nonlinear systems. This can be seen in Fig. 5.3(a)-(b). The uncertainty coefficient [96], a normalized mutual information, yields no different results to the mutual information. But the resonance effect still holds when measuring the dependence of these two systems with the mutual information. Concludingly, one can say that the linear correlation coefficient, which measures how well a straight line fits the data, is a not well suited measure for this kind of structured noise distribution.

5.2 Autocorrelated noise

So far we have always neglected correlations in time in the noises. However, in natural systems the environment is often temporally correlated [115, 124]. In the following we show that correlation enhancement can be achieved for linear systems with additive, autocorrelated noise.

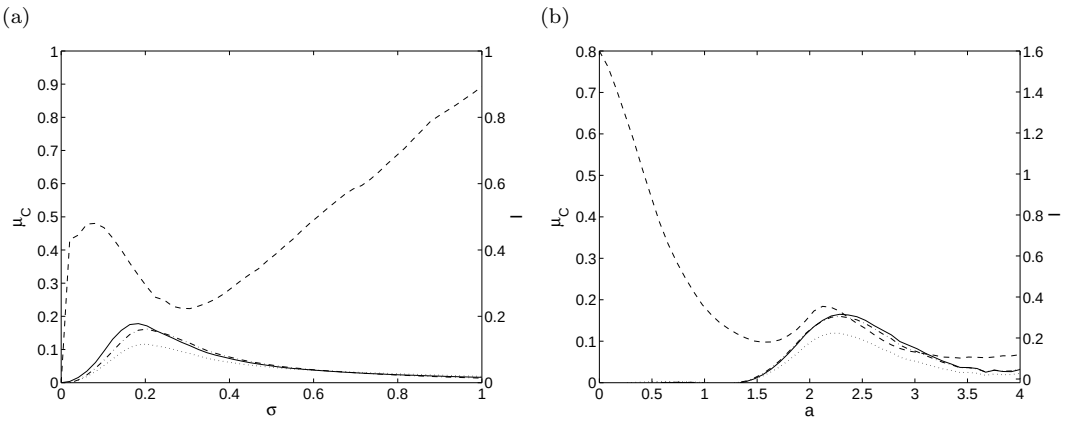

Figure 5.3: Dependence of various correlation measures μ_C as a function of the noise intensity σ (a) and the bifurcation parameter a (b) of two logistic maps with additive Gaussian X-noise Eq. (5.1). Shown are Spearman's rank correlation $(-\cdot-)$, Pearson's correlation coefficient $(-)$, Kendall's Tau $(\cdots)$ and the mutual information I of the two logistic maps $(--)$. The mutual information of the Gaussian X-noise is $I(\varepsilon,\eta) \approx 1.6$, the other correlation measures of the noise are zero. Parameters are $q = 0.5$ and for (a) $a = 2.4$, for (b) $\sigma = 0.2$, and both plots are averaged over 10 realizations of each transient and runtime 10^4 steps.

Autocorrelated noise can be modeled with the help of the theory of autoregressive processes, which have well known statistical properties [56]. A first order autoregressive (AR(1)) process reads as

$$\begin{aligned} \varepsilon_{t+1} &= \alpha\varepsilon_t + \xi_t, \\ \eta_{t+1} &= \beta\eta_t + \xi_t', \end{aligned} \tag{5.2}$$

where $\alpha, \beta \in [-1, 1]$ are the autocorrelation parameters, independent of time. The generating noises $\xi_t, \xi_t^{'}$ are drawn from a bivariate Gaussian distribution with correlation coefficient $C(\xi_t, \xi_t') = \rho$, zero mean and variance σ^2. The autocorrelation parameter, e. g. α, determines the 'color' of the resulting time-series $\{\varepsilon_t\}$: For $\alpha > 0$, the time-series is positively correlated (red-shifted) with long-period cycles, whereas $\alpha < 0$ results in negative correlation (blue-shifted) and short-period cycles. Negatively autocorrelated noise is unlikely to be important in nature and might be harder to detect. If there is no autocorrelation at all, the times-series is white Gaussian noise.

The following computations are done analogously to section 3.1.1. Calculating the first moments of the autocorrelated noise yields

$$\langle \varepsilon_t^2 \rangle = \frac{\sigma^2}{1-\alpha^2}, \quad \langle \varepsilon_t \eta_t \rangle = \frac{\rho\sigma^2}{1-\alpha\beta}. \tag{5.3}$$

The correlation coefficient of the generated autocorrelated noise reads as

$$C(\varepsilon_t, \eta_t) = \rho \frac{\sqrt{1-\beta^2}\sqrt{1-\alpha^2}}{1-\alpha\beta}. \tag{5.4}$$

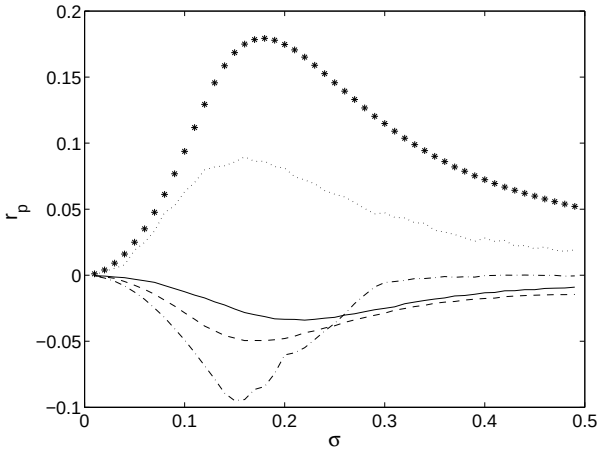

Figure 5.4: Comparison of two logistic maps with additive uncorrelated ($r = 0$) different noises according to Eq. (2.12). The correlation coefficient r_p in dependence of the noise intensity σ is shown for Gaussian X-noise Eq. (5.1) ($\star$), Laplacian noise ($\cdots$), noise distributed on the unit disk ($-$), uniform noise ($--$) and dichotomous noise ($- \cdot -$). The simulations are averaged over 10 realizations with transient and runtime 10^6 steps. $a = 2.4$.

Rewriting the correlation gives an estimation in dependence of the correlation of the generating noise

$$C(\varepsilon_t, \eta_t) = \rho \frac{\sqrt{(1-\beta^2)(1-\alpha^2)}}{\sqrt{(1-\alpha^2)(1-\beta^2)+(\alpha-\beta)^2}} \leq \rho. \tag{5.5}$$

Therefore, if $\alpha \neq \beta$, the correlation of the environmental processes will always be smaller than the correlation of the generating noise. If the environmental processes have very different autocorrelation or just one process is very unstable ($|\alpha| \approx 1$), they are unlikely to be substantially correlated. Note, that given simple, first order population processes, Eq.(5.5) offers a correction of the Moran theorem for the case of nonidentical populations.

The simplest possible model for a time-discrete, one species, two populations model around the population equilibrium is

$$\begin{aligned} x_{t+1} &= a x_t + \varepsilon_t, \\ y_{t+1} &= a y_t + \eta_t, \end{aligned} \tag{5.6}$$

with autocorrelated noises ε_t, η_t described by Eq. (5.2). The process depends on the slope of the recruitment function $a(|a| < 1)$ at the population equilibrium and on the noise.

Now the variance and the first joint moment of the two AR(1) processes can be calculated

$$\langle x_t^2 \rangle = \frac{\sigma^2(1+a\alpha)}{(1-a^2)(1-\alpha^2)(1-a\alpha)}, \tag{5.7}$$

$$\langle x_t y_t \rangle = \frac{\rho\sigma^2(1-a^2\alpha\beta)}{(1-a^2)(1-\alpha\beta)(1-a\beta)(1-a\alpha)}. \tag{5.8}$$

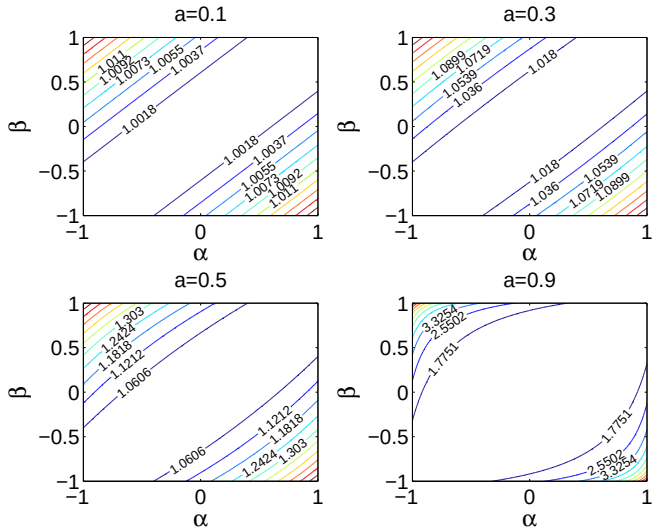

Figure 5.5: Table of the correlation enhancement of two linear maps with autocorrelated noise, Eq. (5.6). Shown is the amplification factor Eq. (5.11) depending on the autocorrelation parameters α, β of the noise for different bifurcation parameter values of the maps $a = 0.1, 0.3, 0.5, 0.9$.

The variance corresponds to the one calculated in [105, 106]. Finally the correlation coefficient of two AR(1) processes with autocorrelated noise computes to

$$C(x_t, y_t) \quad = \quad C(\varepsilon_t, \eta_t) \frac{(1 - a^2\alpha\beta)}{\sqrt{(1 - a^2\beta^2)(1 - a^2\alpha^2)}}. \tag{5.9}$$

From Eq. (5.9) it can be deduced that the sign of the correlation of the two processes is determined by the sign of the correlation of the noise, because all other terms are positive. Rewriting the correlation coefficient of the two AR(1) processes according to Eq. (5.5), yields

$$C(x_t, y_t) \quad = \quad C(\varepsilon_t, \eta_t) \frac{\sqrt{(1 - a^2\alpha^2)(1 - a^2\beta^2) + a^2(\alpha - \beta)^2}}{\sqrt{(1 - a^2\beta^2)(1 - a^2\alpha^2)}} \geq C(\varepsilon_t, \eta_t). \tag{5.10}$$

The correlation of the two processes is always higher than or equal to that the correlation of the added autocorrelated noise. The correlation enhancement is most pronounced if one noise is “red” and the other “blue”, i. e. a short- and a long-period environmental noise is used.

The exact condition for the correlation enhancement is

$$1 - a^2 \operatorname{sgn}(\alpha) \operatorname{sgn}(\beta) |\alpha||\beta| > \sqrt{(1 - a^2\alpha^2)(1 - a^2\beta^2)}, \tag{5.11}$$

where $\operatorname{sgn}(x)$ denotes the signum function, $\operatorname{sgn}(x > 0) = 1, \operatorname{sgn}(x < 0) = -1, \operatorname{sgn}(0) = 0$. In Fig. 5.5 the amplification factor Eq. (5.11) depending on the autocorrelation parameters α, β of the noise for different bifurcation parameter values a of the maps is shown. If both autocorrelation parameters are equal, $\alpha = \beta$, the Moran effect is reproduced. The correlation enhancement is most pronounced for unstable systems $a \approx 1$ and different signs of large autocorrelation parameters.

Note that the correlation of the processes is nevertheless always smaller than the correlation of the generating noises, $C(x_t, y_t) \leq \rho$. But in nature often the correlation of the generating noises or even the generating noises itself are unknown, so a correlation enhancement might be observable in nature.

Chapter 6

Summary and Perspectives

In the first part of this thesis we have systematically studied noise-induced correlation of nonlinear maps.

In Chap. 2 we have given a simple expression for the correlation coefficient of processes which consists of pairs of additive correlated noise. Moreover, we have expressed the Moran theorem differently in terms of the mutual information. This expression is valid for two one-dimensional maps in the fixed-point regime with weak or very strong Gaussian noise.

The second order analytical approximation of the Moran theorem in Chap. 3 for weak noise in the fixed-point regime of quadratic maps is a novel result. We have shown that in the fixed-point regime of a one-dimensional quadratic map there is no correlation enhancement possible for small additive Gaussian noise. This result is also valid for the fixed-point regime of the nth iterate of the map. Additionally, boundary conditions have been shown to account for a local minimum in the correlation coefficient at the first transcritical bifurcation of the logistic map.

In Chap. 4 we have described the desynchronization mechanism of one-dimensional maps in the period-2 regime. The transition rates between phase and antiphase dynamics of two noise-correlated logistic maps in the period-2 regime for very small noise intensities could be well approximated as a Markov process where the rates are given by the Kramers' theory. Nevertheless this approach of using a Markov process of first order remains a coarse approximation to calculate the correlation of noise-correlated logistic maps. In addition we have introduced correlated Markov processes and we have examined it using the example of two noise-correlated piecewise constant maps. The notion of correlated Markov processes should be closer investigated.

In the period-n regime of the logistic map the Markov approach of partitioning the phase space to analyze transition probabilities may be used, but it gets more tedious as n increases. Solving the Frobenius-Perron integral equation to calculate the stationary joint probability density function also in the chaotic regime is numerically feasible, analytically it is a challenge.

In Chap. 5 we wanted to emphasize the possibility of a larger linear correlation coefficient of the populations than that of the noise. We have suggested two possible methods to create correlation enhancement, either by using a structured joint noise distribution or by using spatially and temporally correlated noise, which to our knowledge have not been reported before. Using the mutual information as a measure for the dependence of the two systems, this yielded no information gain transmitting the noise through the nonlinear systems. Nevertheless, the resonance effect still held. But these methods still leave open questions, which are discussed below.

The mechanism of the correlation resonance in the case of a structured noise distribution is to be uncovered. Furthermore, an analytic expression for the resonance curve is worthwile. A noisy precursor of the period-doubling bifurcation at subcritical bifurcation parameter values can be ruled out as a mechanism of the enhancement, because the amplification does not increase with vanishing distance to the bifurcation, instead it decreases.

An experimental verification of both methods for correlation enhancement is desirable. The effect of correlated environmental noise with positive or no temporal autocorrelation on population dynamics in aquatic microcosms has been experimentally studied [23, 34, 89]. Negative temporal autocorrelation of the environment would be a prerequisite for the correlation enhancement, but has not, to our knowledge, been realized. A structured joint noise distribution could be implemented in experiments by using correlated noise with identical amplitudes and opposite signs with respect to a mean value. This would represent environmental noise with a positively correlated and an anticorrelated component.

It would be interesting to transfer the achieved results to spatially extended systems and to incorporate coupling between the systems. Especially it would be tantalizing to study the effect of coupling on the phenomenon of correlation resonance.

Furthermore, the environment is known [68] to cause a change in the fitness of species. In this sense a possible direction for further research could be the analysis of the influence of correlated environments on the evolution of uncoupled species.

Part II

Automatic control of phase synchronization

Chapter 7

Control of phase synchronization in two coupled oscillators

In this chapter we investigate the synchronization properties of two nonlinear oscillators, which are coupled by a feedback loop which is inspired from phase-locked loops. In contrast to other, usually diffusively coupling schemes, the presented approach supposes the existence of a special controller, which allows to change the parameters of the controlled systems. First, we study the simplest possible case of two regular oscillators for which the typical synchronization properties (synchronization threshold, Arnold tongues etc.) can easily be derived. Finally we apply this method of phase synchronization to foodweb models.

7.1 Introduction

Considering the models of coupled systems in biology, neuroscience or ecology, one can see that in many of them the coupling between interacting elements is nonlinear. Such a coupling serves as the basis of an internal self-organization mechanism leading to a balanced motion in these systems. Coupled neurons [99], phase transitions in human hand movement [48] or ecological systems [84], are only some well known examples of balanced cooperative oscillatory motion, caused by a nonlinear coupling. In engineering, nonlinear coupling, is used, for example, in coupled lasers [129]. Usually this coupling has the form of a quadratic function of the interacting elements [121]. This type of coupling is able to lock the oscillators' phase and therefore leads to synchronization.

Different methods for controlling the behavior of dynamical systems have been used for chaos control [87, 98]. For a review of control techniques and algorithms see Boccaletti et al. [17]. An adaptation of these methods for the stabilization of a chaotic trajectory of one system to a chaotic trajectory of another identical system, i. e. for a control of complete synchronization, was

presented in [71, 78]. In [94] it was shown that the main problems of complete synchronization, being regarded as a control problem, can be solved on the basis of control theory methods. On the other hand, the problem of phase synchronization (PS) has not been formulated and hence considered before as a control theory problem.

In contrast to the aforementioned methods, our novel approach is directed at controlling the phases via characteristic time scales of two (or many) different interacting oscillators. We propose an automatic control method to achieve phase locking of regular and chaotic non-identical oscillations, when all subsystems interact via a feedback [5, 7]. This method is based on the well known principle of feedback control which takes place in nature and is successfully used in engineering. This principle of obtaining synchronization is effectively used in applications of phase-locked loops (PLL) in a large number of radio- and telecommunication devices, e. g. radio-location [74]. Before we introduce our control method, we review shortly the phase synchronization of coupled oscillators.

7.2 Review: Two coupled limit cycle systems

Recall the usual equations of two diffusively coupled phase oscillators [119]

$$\begin{aligned} \dot{\phi_1} &= \omega_1 + \varepsilon\,\Gamma(\phi_2 - \phi_1), \\ \dot{\phi_2} &= \omega_2 + \varepsilon\,\Gamma(\phi_1 - \phi_2). \end{aligned} \tag{7.1}$$

Here, ε is the coupling strength, $\omega_{1,2}$ is the natural frequency and $\phi_{1,2}$ the phase of the oscillators. The function $\Gamma(\phi_2 - \phi_1)$ determines the interaction between the oscillators. Usually, it is assumed that the interaction disappears for vanishing phase difference. Therefore, it is customary to set $\Gamma(0) = 0$. The simplest 2π-periodic function with this property is the sinus function and leads to the Kuramoto model [69, 93]

$$\begin{aligned} \dot{\phi_1} &= \omega_1 + \varepsilon\sin(\phi_2 - \phi_1), \\ \dot{\phi_2} &= \omega_2 + \varepsilon\sin(\phi_1 - \phi_2). \end{aligned} \tag{7.2}$$

To study the synchronization properties we investigate the time evolution of the phase difference $\theta = \phi_2 - \phi_1$

$$\dot{\theta} = \Delta\omega - 2\varepsilon\sin(\theta), \tag{7.3}$$

where $\Delta\omega = \omega_2 - \omega_1$. In Fig. 7.1(a) the difference of observed frequencies $\Delta\Omega = 2\pi/\int_0^{2\pi} d\theta/\dot{\theta} = \sqrt{(\Delta\omega)^2 - 4\varepsilon^2}$ is plotted against the coupling parameter ε. If the coupling exceeds a threshold $\varepsilon_c = \Delta\omega/2$, the frequency difference disappears, $\Delta\Omega = 0$, and the oscillators are synchronized to a common frequency. The synchronization takes place for $\varepsilon > \varepsilon_c$ independent of the initial values of the variables. In this regime the system is characterized by the phase difference $\theta^* = \arcsin\left(\frac{\Delta\omega}{2\varepsilon}\right)$.

The fact that the phase difference in the synchronized state is bounded, $|\theta(t)| < \text{const.}$, is called phase locking or *phase synchronization* (PS). In Fig. 7.1(b) the synchronized region, the

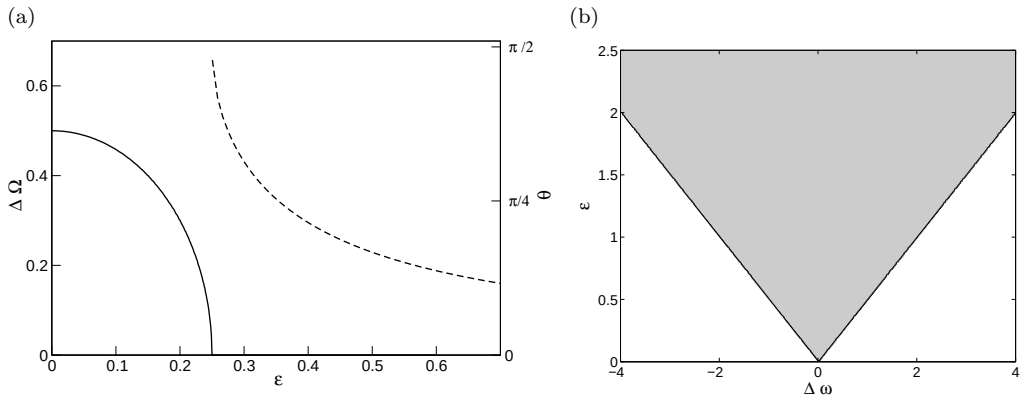

Figure 7.1: Discussion of the Kuramoto model Eq. (7.2) (a) Frequency difference $\Delta\Omega$ (solid line) and phase difference θ (dashed line) of the two phase oscillators as a function of the coupling strength ε. (b) Locking region (Arnold tongue) of the oscillators in dependence of the natural frequency difference $\Delta\omega$ and the coupling strength ε. The upper gray part is the synchronization region.

so called Arnold tongue, is described by the condition

$$\varepsilon > \frac{|\Delta\omega|}{2}. \tag{7.4}$$

In the synchronized regime, the locked oscillators rotate with the mean observed frequency,

$$\bar{\Omega} := \frac{\dot{\phi}_1 + \dot{\phi}_2}{2} = \frac{\omega_1 + \omega_2}{2} = \bar{\omega}, \tag{7.5}$$

which is simply given by the mean of the natural frequencies (as can be seen from Eq. (7.2))

7.3 General principle of automatic phase synchronization

To begin with, we describe automatic phase locking for two arbitrary regular or chaotic oscillators

$$\dot{x}_{1,2} = F_{1,2}(x_{1,2}, \omega_{1,2}), \tag{7.6}$$

where $x_{1,2}$ and $F_{1,2}$ are n-dimensional vectors, $\omega_{1,2}$ are parameters defining the time dependence rate (in some cases, frequencies) of oscillators $x_{1,2}(t)$. Often, the time dependence rates (or frequencies) can be expressed in terms of multipliers of the right hand parts: $\dot{x}_{1,2} = \omega_{1,2} F_{1,2}(x_{1,2})$. In contrast to direct unidirectional (Fig. 7.2(a) and direct bidirectional (Fig. 7.2(b) coupling, the approach presented here supposes the existence of a special controller, which allows to change the parameters of the controlled systems (Fig. 7.2(c). Our purpose is to synchronize such two oscillators by using a feedback control of the time scales of the coupled oscillators in such a way that the new characteristic time scales $\Omega_{1,2}^{-1}$ become identical. Here $\Omega_{1,2}$ are the

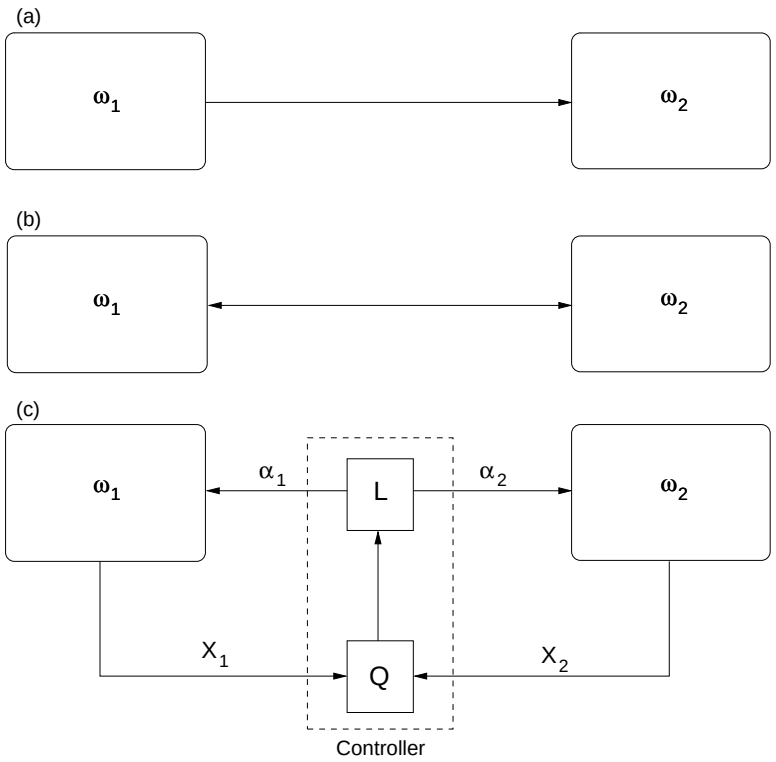

Figure 7.2: Three main schemes of inter-element coupling between two oscillators having natural frequencies ω_1 and ω_2: a) direct unidirectional, b) direct bidirectional, and c) coupling via a feedback loop with a controller composed of a quadratic form Q, Eq. (7.9), and a linear operator L, Eq. (7.8).

mean observed frequencies of the controlled oscillators. In addition to the comparison of the observed frequencies of the controlled systems, we are also interested in the evolution of their phase difference, which is typically used in the study of PS. In order to synchronize the coupled subsystems, we apply a feedback control in the following form:

$$\begin{aligned} \dot{x}_{1,2} &= F_{1,2}(x_{1,2}, \omega_{1,2}(1 + \alpha_{1,2}u)), \\ Lu &= Q(x_1, x_2). \end{aligned} \tag{7.7}$$

Here L is a linear operator

$$L = \gamma_k \frac{d^k}{dt^k} + \gamma_{k-1} \frac{d^{k-1}}{dt^{k-1}} + ... + \gamma_1 \frac{d}{dt} + \gamma_0 \tag{7.8}$$

acting as a low-pass filter, where all γ_k are non-negative constants. $Q(x_1, x_2)$ is a quadratic form

$$Q = x_1^T H x_2, \tag{7.9}$$

where H is a $n \times n$ matrix, which is usually taken as a diagonal matrix. The variables $\alpha_{1,2}$ are the feedback controlling coefficients, acting on the subsystems 1 and 2, respectively, and $u(t)$ is

the control variable, which is added in the first equation of (7.7) in such a way that it is able to change the characteristic time scales of the interacting subsystems.

The scheme modeled by Eqs. (7.7)-(7.9) works in the following simple manner: First, the two signals x_1 and x_2 taken from both interacting systems are fed to the multiplier, $Q(x_1, x_2)$, which is acting as a correlator between the variables of the interacting systems (first part Q of the "Controller" presented in Fig. 7.2(c). The spectrum of oscillations $Q(t)$ consists of a "low" part defined by the difference $\Omega_2 - \Omega_1$ and a "high" part defined by the sum $\Omega_2 + \Omega_1$. Then, the signal $Q(t)$ is conducted through the low-pass filter (second part L of the "Controller" presented in Fig. 7.2(c), which damps the "high" frequency part due to a specially designed transfer function. Hence, the control variable $u(t)$ becomes a slow-varying function in time, whose spectral band goes to zero. After the filtering, $u(t)$ is added to both interacting systems (7.7) in such a way that it may change their characteristic time scales. The main goal is that this procedure provides a balance between the new time scales, i. e. $\Omega_2 = \Omega_1$. Note, that due to the boundedness of the form $Q(x_1^*, x_2^*)$ at the attractor and due to the stability of the operator L, the control variable u is bounded too, i. e. $||u(t)|| < K$, where $K = \text{const}$.

7.4 Two coupled Poincaré systems.

As the simplest case, we consider feedback control of PS in two coupled Poincaré systems

$$\begin{aligned}
\dot{x}_1 &= -\omega_1(1+\alpha_1 u)y_1 - \lambda(x_1^2 + y_1^2 - p^2)x_1, \\
\dot{y}_1 &= \omega_1(1+\alpha_1 u)x_1 - \lambda(x_1^2 + y_1^2 - p^2)y_1, \\
\dot{x}_2 &= -\omega_2(1+\alpha_2 u)y_2 - \lambda(x_2^2 + y_2^2 - p^2)x_2, \\
\dot{y}_2 &= \omega_2(1+\alpha_2 u)x_2 - \lambda(x_2^2 + y_2^2 - p^2)y_2, \\
\tau\dot{u} &= -\gamma u + \beta x_1 x_2 \ .
\end{aligned} \tag{7.10}$$

Here, (x_i, y_i) describe the Cartesian coordinates of two Poincaré systems and u is the control variable. The coefficients $\omega_{1,2}$ are the frequencies of the systems, p is the amplitude of oscillations and $\lambda > 0$ determines the relaxation to the limit cycle. β and γ are the parameters of the controller. The constants $\alpha_{1,2}$ determine the coupling scheme. In contrast to the Kuramoto phase model (7.2), there are overall three coupling parameters $\alpha_1, \alpha_2, \beta$. By a simple modification of α_i it is possible to realize both bidirectional ($\alpha_i \neq 0$, $i \in \{1, 2\}$) or unidirectional coupling ($\alpha_i = 0$, $\alpha_j \neq 0$). Notice, that in this scheme the coupling parameter α_i may as well take negative numbers. In Eq. (7.10) we have chosen very simple analytic forms for the quadratic form $Q(x_1, x_2) = \beta x_1 x_2$ and the linear operator $L = \tau\frac{d}{dt} + \gamma$. However, we note that also different, more sophisticated, functions may be used with similar results.

Using polar coordinates $x_i = \rho_i \cos\phi_i, y_i = \rho_i \sin\phi_i$, we rewrite system (7.10) in the form:

$$\begin{aligned}
\dot{\rho}_{1,2} &= \lambda\rho_{1,2}(p^2 - \rho_{1,2}^2), \\
\dot{\phi}_{1,2} &= \omega_{1,2}(1+\alpha_{1,2}u), \\
\tau\dot{u} &= -\gamma u + \beta\rho_1\rho_2\cos(\phi_1)\cos(\phi_2).
\end{aligned} \tag{7.11}$$

The product of cosine functions in Eq. (7.11) can be decomposed into a slow and a rapidly oscillating term. In the limit $\omega_1 + \omega_2 > \gamma$, the low pass filter L is damping out the 'high' frequencies, which further simplifies the dynamics. Let $\omega_2 = \omega_1 + \Delta\omega$. After relaxation of the radial equation, $\dot{\rho}_i = 0$, the amplitude of each oscillator is fixed to $\rho_i = p$. Thus, after averaging we arrive at the following simplified equations for the control variable u and the phase difference $\theta = \phi_2 - \phi_1$:

$$\begin{aligned} \dot{\theta} &= \Delta\omega + (\alpha_2\omega_2 - \alpha_1\omega_1)u, \\ \tau\dot{u} &= -\gamma u + \frac{\beta\, p^2}{2}\cos\theta. \end{aligned} \tag{7.12}$$

Rewritten as a second order differential equation this leads to

$$\tau\ddot{\theta} + \gamma\dot{\theta} - \gamma\Delta\omega - \frac{\beta}{2}p^2(\alpha_2\omega_2 - \alpha_1\omega_1)\cos\theta = 0. \tag{7.13}$$

This pendulum-like equation for the evolution of the phase difference describes the synchronization regime of the two oscillators interacting via feedback control. The existence of this regime is defined by a stable steady state in Eq. (7.12) with the coordinates

$$\cos\theta^* = \frac{2\gamma}{\beta p^2}u^*, \quad u^* = \frac{\Delta\omega}{\alpha_1\omega_1 - \alpha_2\omega_2}, \tag{7.14}$$

which does exist in the range

$$\frac{\beta p^2}{2\gamma} > \left|\frac{\Delta\omega}{\alpha_2\omega_2 - \alpha_1\omega_1}\right|. \tag{7.15}$$

Synchronization is achieved when the effective coupling strength, here $\varepsilon_{\text{eff}} = \beta p^2/(2\gamma)$, is larger than a function of the frequencies, i. e. $\varepsilon_{\text{eff}} > |\Delta\omega/(\alpha_2\omega_2 - \alpha_1\omega_1)|$. Note the similarity to Eq. (7.4). However, we want to stress that here the synchronization threshold, Eq. (7.15), depends on the amplitude of oscillation, p. Larger values of p lead to an onset of phase synchronization at smaller values of the coupling strength β.

In Fig. 7.3 the locking (or synchronization) regions of system (7.12), as described by condition (7.15), are plotted in the parameter plane of effective coupling and natural frequency difference. By variations of different coupling schemes, i. e. uni- and bidirectional coupling, basically four different scenarios for the form of the locking regions can be found. Obviously in the feedback coupling scheme, depending on the values of α_i, the locking regions are not necessarily defined by straight lines. Furthermore there are specific values of the natural frequencies, ($\alpha_2\omega_2 = \alpha_1\omega_1$), which arise from the singularities of Eq. (7.15), for which synchronization can never be achieved. These special frequency values divide the parameter plane into different locking regimes. In some regions of $\Delta\omega$, synchronization is inhibited. In compensation, in other regimes of parameter space the synchronization is strongly promoted and the border of synchronization is moved toward smaller values of effective coupling strength.

Further indicated in Fig. 7.3 is also the phase difference of the two oscillators at the onset of synchronization. As a consequence of the cosine term in Eq.(7.13), the phase difference may be either 0° or 180°. Therefore, for the minimal coupling strength when synchronization sets in,

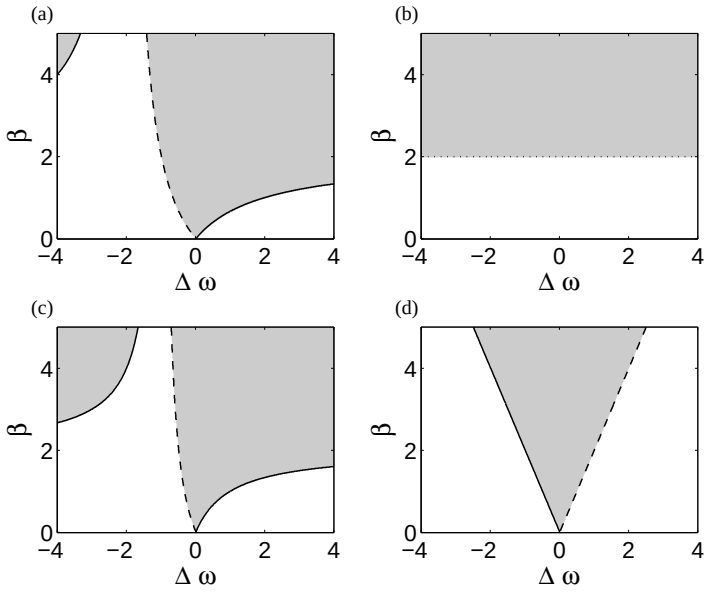

Figure 7.3: Synchronization regions (gray) of two Poincaré oscillators Eq. (7.13) as described by condition (7.15) for different coupling scenarios and fixed $\omega_1 = 1, \gamma = 1, p = 1$. a) $\alpha_2 = -\alpha_1 = 1$, b) $\alpha_2 = \alpha_1 = 1$, c) $\alpha_1 = 0, \alpha_2 = 1$, d) $\alpha_1 = 1, \alpha_2 = 0$. Further indicated is the phase difference of both oscillators at the synchronization threshold, which is either $\theta^* = 0°$ (solid line), $\theta^* = 180°$ (dashed line), or undetermined, if the transition leads to oscillation death (dotted line). Compare to Fig.7.1(b).

the time lag between two nearby maxima of $x_i(t)$ is either 0 or $\pi/\bar{\Omega}$, where we have used the mean observed frequency

$$\bar{\Omega} = \left\langle \frac{\dot{\phi_1} + \dot{\phi_2}}{2} \right\rangle . \tag{7.16}$$

Consequently, at the onset of synchronization the two limit cycle oscillators are either fully synchronized or fully anti-synchronized.

Before the synchronization sets in, the observed frequency difference in the small coupling regime can be calculated in the case $\tau \ll 1$ as

$$\Delta\Omega = \frac{2\pi}{\int_0^{2\pi} d\theta/\dot{\theta}} = \sqrt{\Delta\omega^2 - \frac{\beta^2 p^4}{4\gamma^2}(\alpha_2\omega_2 - \alpha_1\omega_1)^2}. \tag{7.17}$$

In the following we compare this analytical approximation with numerical simulations of Eq. (7.10). The phase of a limit cycle can be computed in the form

$$\phi_{1,2} = \arctan\left(\frac{y_{1,2}}{x_{1,2}}\right), \tag{7.18}$$

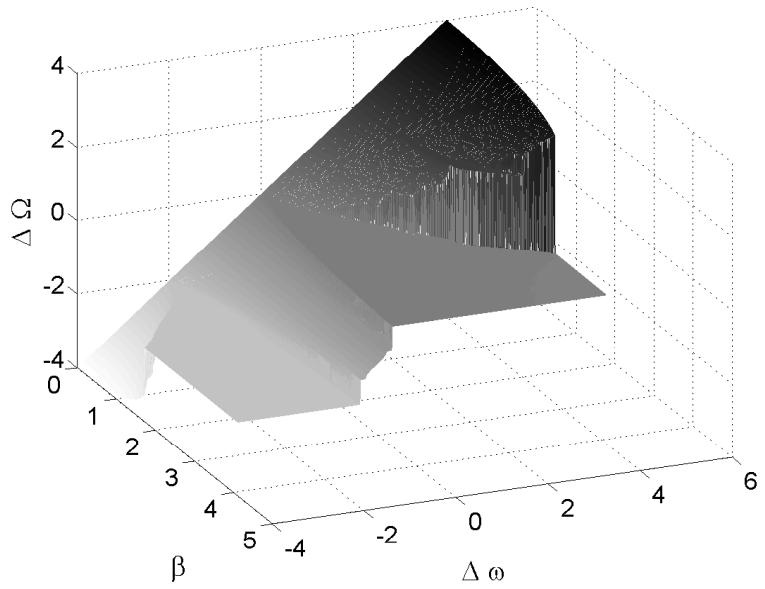

Figure 7.4: Locking regions of two Poincaré oscillators Eq. (7.10) for unidirectional coupling $\alpha_1 = 0, \alpha_2 = 1$ in dependence on the coupling strength β and the natural frequency difference $\Delta\omega$. $\gamma = 1, p = 1, \omega_1 = 1$. In order to ensure synchronization, i. e. to avoid the multistability regime discussed in Sec. 7.4.3, we use the initial state in the middle of the two fixed points $\theta = \pi$ on the $\dot{\theta} = 0$ nullcline.

and the respective mean frequency as

$$\Omega_{1,2} = \lim_{T\to\infty} \frac{\phi_{1,2}(T) - \phi_{1,2}(0)}{T}. \tag{7.19}$$

The numerically calculated values of $\Delta\Omega$ can also be used to visualize the locking regions. A numerically computed synchronization surface is shown in Fig. 7.4. Compare this to the analytically derived Fig. 7.3(c).

7.4.1 Impossibility of synchronization with symmetrical coupling

We now study the special case of symmetrical coupling where $\alpha_1 = \alpha_2$. Inspection of Fig. 7.3 reveals the special role which is played by this coupling scheme because seemingly the synchronization threshold in this case is independent of the natural frequency difference between the oscillators. This result can also be found from Eq. (7.15). However, the picture is somewhat misleading because as we now show in this case it is impossible to synchronize the two oscillators at all. In order to calculate the mean observed frequency (7.16) of two Poincaré systems (7.11) in the locked state, we require

$$\dot{\phi}_1 + \dot{\phi}_2 = \omega_1 + \omega_2 + u^*(\alpha_1\omega_1 + \alpha_2\omega_2). \tag{7.20}$$

After inserting the steady state value of the control variable u^*, Eq. (7.14), this results in

$$\bar{\Omega} = \frac{\omega_1 + \omega_2}{2} + \frac{\alpha_1\omega_1 + \alpha_2\omega_2}{\alpha_1\omega_1 - \alpha_2\omega_2}\frac{\Delta\omega}{2}, \tag{7.21}$$

and replaces the usual formula $\bar{\Omega} = \bar{\omega}$, Eq. (7.5), for two simply symmetrically directly coupled phase oscillators.

In the case of symmetrical coupling Eq. (7.21) this has the implication that the mean observed frequency disappears

$$\alpha_1 = \alpha_2 \quad \rightarrow \quad \bar{\Omega} = \frac{\dot{\phi}_1 + \dot{\phi}_2}{2} = 0. \tag{7.22}$$

Since in the synchronized state further $\Delta\Omega = 0$, we follow that $\Omega_1 = \Omega_2 = 0$ and the oscillators effectively stop to rotate. This result is also evident by going back to the feedback coupling scheme (Fig. 7.2). If $\alpha_1 = \alpha_2$, then both oscillators always obtain identical feedback. The only way in which then the observed frequencies can become identical is when they are controlled to zero, i. e. to oscillation death. This is also valid if u is introduced only in the second equation of system (7.10), whereas for different oscillator types in this case this does not hold, see section 7.5.

7.4.2 Anti-symmetrical coupling

A special interest attains the scheme of anti-symmetrical coupling, where the feedback to the two oscillators has the same strength but opposite sign, $\alpha_1 = -\alpha_2$. In this case, obviously the mean coupling parameter disappears, $\bar{\alpha} = \frac{\alpha_1+\alpha_2}{2} = 0$, which leads with $\dot{u} = 0$ to the simplified phase equation (7.12)

$$\dot{\theta} = \Delta\omega + \alpha\,\frac{\beta\,\bar{\omega}p^2}{\gamma}\cos(\theta). \tag{7.23}$$

Similarly, the synchronization regime in the parameter space simplifies to

$$\alpha\,\frac{\beta\,\bar{\omega}p^2}{\gamma} > |\Delta\omega|\,. \tag{7.24}$$

This expression for the synchronization threshold resembles very much the usual synchronization of two coupled oscillators (compare Fig. 7.1(b) and Fig. 7.3(a). However, note that even in this case there remain important differences. For example, synchronization sets in with a phase difference of either 0° or 180°.

We again calculate the mean locking frequency in the synchronized state

$$\dot{\phi}_1 + \dot{\phi}_2 = \omega_1 + \omega_2 + \frac{(\omega_1 - \omega_2)^2}{\omega_1 + \omega_2}, \tag{7.25}$$

which leads to

$$\bar{\Omega} = \frac{\omega_1^2 + \omega_2^2}{\omega_1 + \omega_2}. \tag{7.26}$$

Therefore, in the case of anti-symmetrical coupling the observed mean frequency in general is not the arithmetic mean of the natural frequencies.

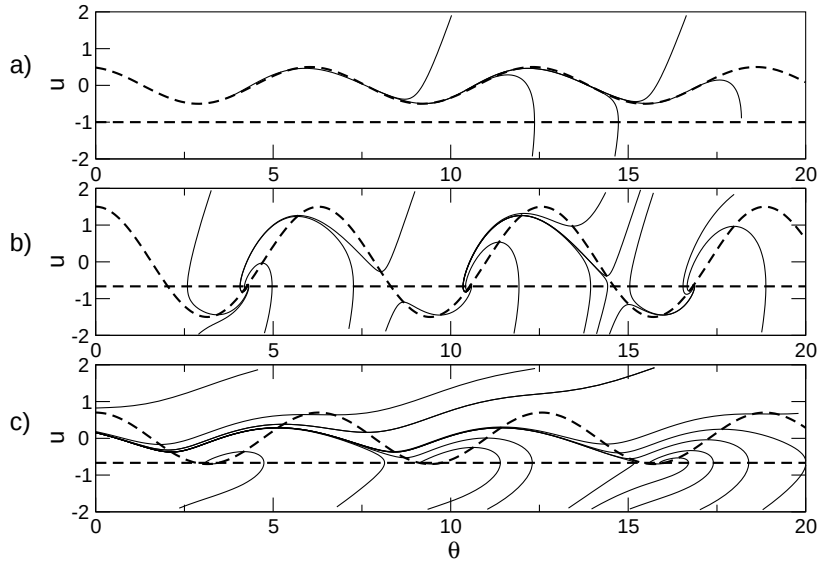

Figure 7.5: Typical phase flow of Eq. (7.12) in three different parameter regimes. a) No synchronization. For all initial values the phase difference is drifting (parameters $\alpha_1 = \alpha_2 = 1$, $\gamma = 1$, $\beta = 1$, $\omega_1 = 1.3$, $\omega_2 = 1$). b) Global stability of locked state (parameters $\alpha_1 = \alpha_2 = 1$, $\gamma = 1$, $\beta = 3$, $\omega_1 = 1.3$, $\omega_2 = 1$). c) Bistability between locking and drifting solutions (parameters $\alpha_1 = \alpha_2 = 1.5$, $\gamma = 1.5$, $\beta = 2.1$, $\omega_1 = 4$, $\omega_2 = 2$). The dashed lines indicate the nullclines. $p = 1$.

It is also straightforward to calculate the forbidden frequency ratio, i. e. the ratio for which synchronization cannot be achieved in the scheme with antisymmetrical coupling. We are led to the condition $\bar{\omega} = 0$ or $\omega_2 = -\omega_1$. Therefore, synchronization cannot be achieved when both oscillators rotate in opposite direction with exactly the same frequency. In contrast to the Kuramoto phase model (7.3), here in the limit $\bar{\omega} \to 0$ the mean observed frequency goes to infinity $\bar{\Omega} \to \infty$ and not $\bar{\Omega} \to 0$.

7.4.3 Bistability of phase locking

Eq. (7.15) seems to imply that in the case when locking can be achieved in the model (u, ϕ), this leads to synchronization for all initial values. However this is not the case. To explore this in more detail, we now analyze the phase plane of Eq. (7.12). In Fig. 7.5 we depict the nullclines given by Eq. (7.14) and the phase flow for three different parameter sets. The fixed points are located at the intersection of the nullclines. If there are no fixed points, of course, synchronization does not occur.

When varying the coupling strength, we can distinguish between three different dynamical regimes: For small values of the coupling strength β the nullclines do not intersect and there is no synchronization. In contrast for large values of β a locking regime is found. When increasing

parameter β over the critical level, two fixed points are created in a saddle node bifurcation. However for coupling parameter values in the transition regime near the bifurcation point, we find multistability. Depending on the initial states of the two Poincaré systems, they may synchronize or not. Starting above the nullclines in the phase space, the system is only able to reach a periodic, non synchronized state. This scenario can be seen in Fig. 7.5(c). Recall that such bistable behavior is absent in the Kuramoto model. However, similar bistability is known to arise in two coupled oscillators with varying nonisochronicities [4].

7.5 Coupled foodweb models

In this section we apply the method of automatic phase synchronization to foodweb models from ecology. First, we study the synchronization of two coupled limit-cycle Rosenzweig-MacArthur [84] systems

$$\begin{aligned} \dot{x}_{1,2} &= a x_{1,2}\,(1 - x_{1,2}/K) - k f_H(x_{1,2}, y_{1,2}), \\ \dot{y}_{1,2} &= -b_{1,2}\,(1 + \alpha_{1,2} u)\, y_{1,2} + k f_H(x_{1,2}, y_{1,2}), \\ \dot{u} &= -\gamma u + \beta y_1 y_2. \end{aligned} \tag{7.27}$$

Here, $x_{1,2}$ denotes the prey and $y_{1,2}$ the predator species, a and $b_{1,2}$ are the birth and death rates, K is the prey carrying capacity, k the predation rate and κ the half saturation constant of the Holling type II functional response $f_H(x, y) = xy/(1 + \kappa x)$. Throughout this section we use the parameter values $a = 1, k = 3, K = 3, \kappa = 1$. The two oscillators are nonidentical and vary in the value of predator death rates $b_1 = 1.0$ and $b_2 = 0.95$.

The control variable u is introduced into the model as in the previous models. Ecologically, quadratic forms Q of Eq. (7.9) can arise very naturally as Lotka-Volterra interactions. Here, u either represents a species that is affected and grows only in the presence of the predator $y_{1,2}$ of both sites and has a mortality γ. On the other hand, the predators' death rates $b_{1,2}$ are modified by the abundance of the species u. In a different interpretation of Eq. (7.27) u represents an abiotic environmental variable. In the absence of predators the environmental variable u decays with rate γ to the ground state $u = 0$, however with positive predator density u is disturbed to a positive value. Positive (negative) values of α_i imply that the predator mortality increases (decreases) with u. It is assumed that the mortality of the predators depends linearly on the environment. This is described multiplicatively, i. e. the presence of both predator species is necessary to change the environment.

Without coupling, system (7.27) is well known to exhibit limit cycle oscillations with a frequency roughly determined by $\omega_i = \sqrt{ab_i}$. Nevertheless, feedback control can induce synchronization, see Fig. 7.6. Depending on the coupling scheme synchronization may be achieved or not. Note that in Fig. 7.6 the control parameter α is varied in the whole range from negative to positive values.

Interestingly, in system (7.27) synchronization can be achieved even in the symmetrical scheme where the values of α are identical, i. e. $\alpha_1 = \alpha_2 = \alpha$. This is astonishing because then the

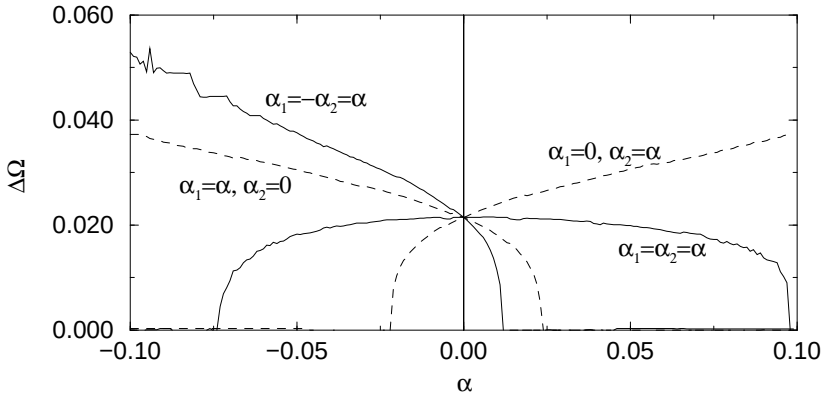

Figure 7.6: Transition to synchronization for two limit cycle predator-prey models Eq.(7.27) coupled via feedback loop. Solid lines) bidirectional coupling with either symmetric ($\alpha_1 = \alpha_2 = \alpha$) or antisymmetric ($\alpha_1 = -\alpha_2 = \alpha$) coupling scheme; dashed lines) unidirectional coupling ($\alpha_1 = 0$ or $\alpha_2 = 0$).

parameters in both systems (and consequently also the natural frequencies) are modified by exactly the same amount $b_i(1+\alpha u)$. This is in contrast to the simple theory with two Poincaré oscillators Eq. (7.10) where identical α_i only lead to oscillation death, see Section 7.4.1. Of course, in the foodweb case u is only introduced into the second equation of system (7.27) and not also to $\dot{x}$ as in Eq. (7.10). However, the principal behavior of the Poincaré system remains unchanged even if u is only introduced into the second equation, i. e. symmetrical coupling only results in oscillation death. Similar behavior, i. e. synchronization in symmetrical coupling, was also observed in the Rössler system, if u is affecting only the equation of the $\dot{y}$-variable [7].

Next, we study feedback control in a model for chaotic predator-prey cycles, which has been proposed in [13, 15]

$$\begin{aligned}
\dot{x}_{1,2} &= a x_{1,2} - e\, f_H(x_{1,2}, y_{1,2}), \\
\dot{y}_{1,2} &= -b_{1,2}(1+\alpha_{1,2}u) y_{1,2} + e\, f_H(x_{1,2}, y_{1,2}) - g\, y_{1,2}\, z_{1,2}, \\
\dot{z}_{1,2} &= -c(z_{1,2} - z_0) + g\, y_{1,2}\, z_{1,2}, \\
\dot{u} &= -\gamma u + \beta y_1 y_2 \ .
\end{aligned} \tag{7.28}$$

This model describes a three trophic "vertical" food chain where the vegetation x is consumed by herbivores y which themselves are preyed upon by the top predator z. In the absence of interspecific interactions the dynamics is linearly expanded around the steady state $(0, 0, z_0)$ with coefficients a, $b_{1,2}$ and c that represent the respective nett growth and death rates of each species. Predator-prey and consumer-resource interactions are incorporated into the equations via either the Lotka-Volterra term xy, or the Holling type II term $f_H(x, y) = xy/(1 + \kappa x)$ with strengths set by the coefficients e and g. Again, feedback control is implemented by the biotic or abiotic variable u. Despite their minimal structure, the above equations might sketch the major ecological transfers involved in the Canadian lynx-hare-vegetation foodweb [13, 15].

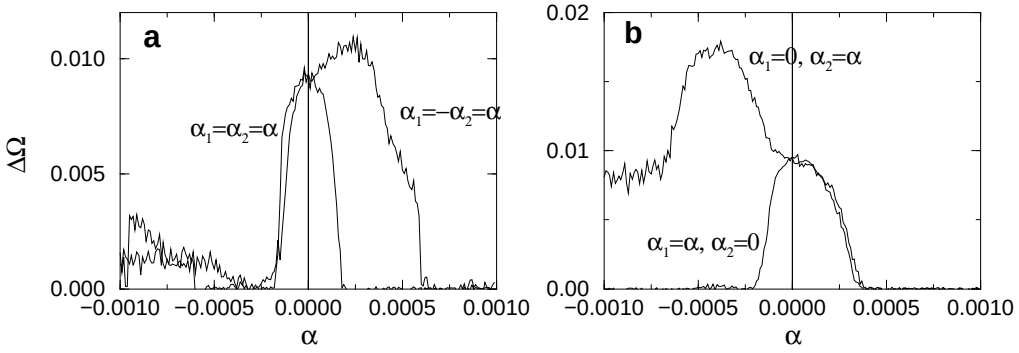

Figure 7.7: Transition to synchronization for two chaotic foodweb models coupled via feedback loop. a) Bidirectional coupling with either symmetric ($\alpha_1 = \alpha_2 = \alpha$) or antisymmetric ($\alpha_1 = -\alpha_2 = \alpha$) coupling scheme; b) unidirectional coupling ($\alpha_1 = 0$ or $\alpha_2 = 0$).

For simulation runs reported here, parameter values are taken as in [13, 15]: $a = 1, c = 10, e = 0.2, g = 1,\ \kappa = 0.05, z_0 = 0.006$. The parameter mismatch between the two oscillators is given by $b_1 = 0.96$; $b_2 = 0.98$. In this parameter range the model shows phase coherent chaotic dynamics, where the trajectory rotates with nearly constant frequency in the (x, y)-plane but with chaotic dynamics that appear as irregular spikes in the top predator z. This behavior of the foodweb model is reminiscent to the Rössler system [86] and therefore one might expect similar synchronization properties in both systems.

Simulation results are shown in Fig. 7.7. Also in the chaotic ecological model synchronization in phase can be obtained. However, we find a rich behavior. In the unidirectional coupling scheme for positive α, synchronization is achieved in both cases. For negative α synchronization is achieved only in the case $\alpha_2 = 0$, see Fig. 7.7(b). In the bidirectional coupling schemes, depicted in Fig. 7.7(a), synchronization is found in all cases if the absolute value of α is sufficiently large. In the antisymmetric coupling scheme, e. g. $\alpha_1 = -\alpha_2 = \alpha$, for positive values of α the transition to synchronization is characterized by the fact that with the onset of coupling the frequency difference is first increasing with a maximal difference for intermediate values (here $\alpha \approx 0.00025$). Whereas frequencies become attracted and locking arises only for larger values of the coupling strength. Similar behavior is known to arise also in two diffusively coupled foodweb models and has been called anomalous phase synchronization [14, 79].

7.6 Summary and Perspectives

In contrast to the directly coupled limit cycles of the Kuramoto phase model (7.3), in the feedback coupling scheme we obtain a frequency-dependent coupling. One consequence is the existence of specific values of natural frequencies for which synchronization in principle cannot be achieved, in particular when $\alpha_1\omega_1 = \alpha_2\omega_2$. As we have shown for Poincaré oscillators, for symmetrical bidirectional coupling, $\alpha_1 = \alpha_2$, the critical coupling value is independent of the

natural frequency ratio, and synchronization can never be achieved: In this case strong coupling leads to oscillation death. Whereas in the case if the control variable u only influences the y-variable directly, for Rosenzeig-McArthur or Rössler systems synchronization could be achieved even for symmetrical coupling. This deserves closer investigation.

In the PLL coupling scheme the increase of coupling acts somewhat counterintuitive. Take the case where both oscillators rotate identically at the onset of synchronization. With further increase of coupling strength, the two oscillators are more and more driven out of phase. Until finally, in the limit of very large coupling, they are related with a phase difference of $\pi/2$. This is just the opposite behavior of the Kuramoto phase model, where at threshold the oscillators are related with phase difference of $|\theta^*| = \pi/2$, whereas in the limit of large coupling $\theta^* \to 0$. Therefore, in the feedback coupled model the interaction does not disappear in the limit of large coupling.

Another difference is the extra equation for u, which gives rise to an additional degree of freedom in the phase space of the system. Thus, the phase difference is determined by a second order equation. This allows for new rich behavior. Whereas in the usual case the phase difference must necessarily approach the equilibrium locking state monotonically, here damped oscillations around this locked state are possible (see Fig. 7.5). Further, depending on initial values of u the phase difference can increase (or decrease) several multiples of 2π before reaching synchronization. In principle this new degree of freedom allows for new applications. For example by external forcing it might be possible to excite such oscillating modes of the frequency difference.

The advantages of this novel feedback control method compared to more conventional schemes are the following:

- The effect of the amplitudes of the interacting subsystems on the difference of their phases provides a high efficiency of this approach: large amplitudes lead to a small phase difference.
- The proposed method can be used for automatic synchronization of oscillators of different nature (regular and chaotic).
- Phase synchronization already sets in at very small values of control parameters, which is very important from an energetical point of view. On the other hand, for specific parameter values synchronization can not be obtained at all, that seems to be a trade-off.

It is important to emphasize that this principle can be applied not only to coupled self-oscillatory systems [5, 7]. Note that this method can also be applied to synchronize oscillators of different topology (e .g. coupled Rössler and Lorenz oscillators) and complexity (e. g. chaotic and hyperchaotic Rössler oscillators). Furthermore, the method can also be used to synchronize elements coupled in chains and lattices. In the latter case the coupling can be local or global [6, 7]. An experimental realization of our method is desired.

Appendix A

Derivation of the Frobenius-Perron equation

In this appendix we derive the integral equation for the stationary density, the so called Frobenius-Perron equation, and clarify the methods used for its calculation. The dynamical equations under consideration are

$$x_{n+1} = g(x_n) + \varepsilon_n, \tag{A.1}$$

$$y_{n+1} = g(y_n) + \eta_n. \tag{A.2}$$

The random variables ε and η are correlated. From these equations, we obtain a condition for the correlated stationary (i. e. $f_{n+1} = f_n \equiv f$) distribution density

$$\begin{aligned} f(x,y) &= \iint_{-\infty}^{\infty} d\varepsilon_n d\eta_n \iint_{-\infty}^{\infty} dx_n dy_n \, f(x_n,y_n)\, p(\varepsilon_n,\eta_n)\, \delta(x-x_{n+1})\delta(y-y_{n+1}) \qquad \text{(A.3)} \\ &= \iint_{-\infty}^{\infty} d\varepsilon_n d\eta_n \iint_{-\infty}^{\infty} dx_n dy_n \, f(x_n,y_n)\, p(\varepsilon_n,\eta_n)\, \delta(x-g(x_n)-\varepsilon_n)\delta(y-g(y_n)-\eta_n), \end{aligned}$$

the so called Frobenius-Perron-Equation. This is the probability density that the system is after infinite iteration steps in the state (x, y). The averaging is meant as an average over all simulations with different initial conditions. We rename $(x_n, y_n) \to (x', y')$ and perform the noise-average

$$f(x,y) = \int_{-\infty}^{\infty} dx' \int_{-\infty}^{\infty} dy' \; f(x',y')\, p\left(x-g(x'), y-g(y')\right). \tag{A.4}$$

Eq. (A.4) is discretized on a equidistant grid with gridsize Δ; the integrals are approximated by Riemann sums. With the definitions

$$\begin{aligned} x &\longrightarrow x_i, \\ f(x,y) &\longrightarrow f_{\{ij\}} \equiv f(x_i,y_j), \\ p\left(x-f(u), y-g(v)\right) &\longrightarrow K_{\{ij\}\{mn\}} \equiv p\left(x_i-g(u_m), y_j-g(v_n)\right)\Delta^2, \end{aligned}$$

it takes the form

$$f_{\{ij\}} = \sum_{\{mn\}} K_{\{ij\}\{mn\}} f_{\{mn\}}. \tag{A.5}$$

One should think of the pair $\{ij\}$ as *one* vector index. This makes $f_{\{ij\}}$ a vector and $K_{\{ij\}\{mn\}}$ a matrix. Depending on taste and efficiency of available numerical packages, the equation can be considered as

(a) system of homogeneous linear equations

$$0 = \sum_{\{mn\}} \left(K_{\{ij\}\{mn\}} - \delta_{\{ij\}\{mn\}} \right) f_{\{mn\}} \, \forall \{ij\} \tag{A.6}$$

(b) integral equation (A.4)

(c) eigenvalue equation, where only the left eigenvalue $\Lambda = 1$ is of interest

$$\Lambda \vec{f} = \underline{\mathcal{K}} \, \vec{f}$$

(d) iteration equation for the population

$$\vec{f}[j+1] = \underline{\mathcal{K}} \, \vec{f}[j]$$

Once, this integral equation is solved, the cross correlation

$$C(x,y) = \frac{\langle xy \rangle - \langle x \rangle \, \langle y \rangle}{\sqrt{(\langle x^2 \rangle - \langle x \rangle^2)(\langle y^2 \rangle - \langle y \rangle^2)}} \tag{A.7}$$

can be obtained from integrals such as

$$\langle xy \rangle \quad = \quad \int_{-\infty}^{\infty} dx \int_{-\infty}^{\infty} dy \, f(x,y) \, xy = \sum_{\{ij\}} f_{\{ij\}} \, x_i x_j \, \Delta^2. \tag{A.8}$$

Appendix B

Uniform correlated noise

In this appendix we calculate the probability distribution function of symmetrically correlated uniform noise and derive some of its properties. The corresponding noise equations are:

$$\varepsilon = \sigma\sqrt{\frac{1+r}{2}}\xi + \sigma\sqrt{\frac{1-r}{2}}\xi', \tag{B.1}$$

$$\eta = \sigma\sqrt{\frac{1+r}{2}}\xi - \sigma\sqrt{\frac{1-r}{2}}\xi'. \tag{B.2}$$

The properties of the noise are: $\langle\varepsilon\rangle = 0$, $\langle\varepsilon^2\rangle = \sigma^2$, $\langle\varepsilon\eta\rangle = r\sigma^2$, where ξ and ξ' are independent and uniformly distributed in the interval $[-\sqrt{3}, \sqrt{3}]$ to assure $\langle\xi^2\rangle = 1$. The linear correlation coefficient $C(\varepsilon, \eta) = r$ lies in the interval $[-1, 1]$ by definition. The joint distribution of ξ and ξ' reads as follows:

$$p(\xi, \xi') = \frac{1}{12}\Theta(\sqrt{3}+\xi)\Theta(\sqrt{3}-\xi)\Theta(\sqrt{3}+\xi')\Theta(\sqrt{3}-\xi'). \tag{B.3}$$

With the use of the construction formula

$$p(\varepsilon, \eta) = \frac{p(\xi(\varepsilon,\eta), \xi'(\varepsilon,\eta))}{|\det(J)|}, \quad J = \begin{pmatrix} \frac{\partial\varepsilon}{\partial\xi} & \frac{\partial\varepsilon}{\partial\xi'} \\ \frac{\partial\eta}{\partial\xi} & \frac{\partial\eta}{\partial\xi'} \end{pmatrix}, \tag{B.4}$$

see [56], and $\xi = \frac{1}{\sqrt{2}\sigma\sqrt{1+r}}(\varepsilon+\eta)$, $\xi' = \frac{1}{\sqrt{2}\sigma\sqrt{1-r}}(\varepsilon-\eta)$, we arrive at:

$$\begin{aligned} p(\varepsilon, \eta) = {} & \frac{1}{12\sqrt{1-r^2\sigma^2}}\Theta\left(\sqrt{6}\sigma\sqrt{1+r} - (\varepsilon+\eta)\right)\Theta\left(\sqrt{6}\sigma\sqrt{1+r} + (\varepsilon+\eta)\right) \\ & \times\Theta\left(\sqrt{6}\sigma\sqrt{1-r} - (\varepsilon-\eta)\right)\Theta\left(\sqrt{6}\sigma\sqrt{1-r} + (\varepsilon-\eta)\right). \end{aligned} \tag{B.5}$$

One can easily compute the area of the rectangle created by the Θ-functions if we make a transformation into a 45°-rotated and at the new x-axis mirrored coordinate system, depicted in Fig. B.1. The transformation is given by

$$\varepsilon' = \frac{\varepsilon+\eta}{\sqrt{2}}, \; \eta' = \frac{\varepsilon-\eta}{\sqrt{2}}, \tag{B.6}$$

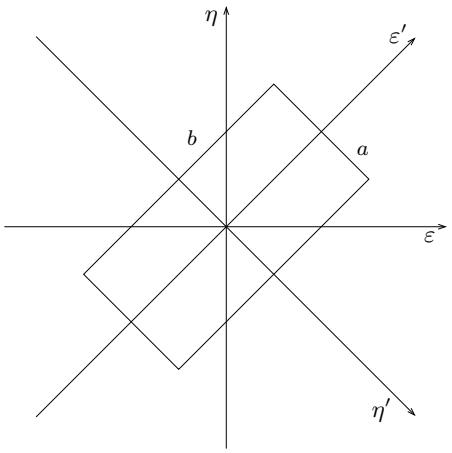

Figure B.1: Transformation of the coordinate system (ε, η) to (ε', η') with $\varepsilon' = (\varepsilon+\eta)/\sqrt{2}$, $\eta' = (\varepsilon - \eta)/\sqrt{2}$. Indicated are the boundaries a and b of the probability density function of symmetrically correlated noise, Eq. (B.7).

and the matching determinant of the Jacobian $\det(J) = -1$. This yields the following joint distribution function:

$$\begin{aligned} p(\varepsilon', \eta') &= \frac{1}{12\sqrt{1-r^2}\sigma^2} \Theta\left(\sqrt{3}\sigma\sqrt{1+r} - \varepsilon'\right) \Theta\left(\sqrt{3}\sigma\sqrt{1+r} + \varepsilon'\right) \\ &\quad \times \Theta\left(\sqrt{3}\sigma\sqrt{1-r} - \eta'\right) \Theta\left(\sqrt{3}\sigma\sqrt{1-r} + \eta'\right), \end{aligned} \tag{B.7}$$

which indicates the area of the rectangle in Fig. B.1:

$$ab = 2\sqrt{3}\sigma\sqrt{1-r}\, 2\sqrt{3}\sigma\sqrt{1+r} = 12\sigma^2\sqrt{1-r^2}.$$

This is of course exactly the normalization constant.

In this thesis we often have to compute intersections of probability density function with one of the four quadrants, for example in Sect. 4.5. The intersections represent here transition probabilities. An exemplary transition probability might read as

$$w = \int_0^\infty dx \int_0^\infty dy\ p(x - c_1, y - c_2) = \int_{c_1}^\infty dx \int_{c_2}^\infty dy\ p(x, y). \tag{B.8}$$

To calculate this, we use the above transformation (B.6) respecting the integral limits

$$w = \int_{c_1'}^\infty dx' \int_{c_2' - (x' - c_1')}^{c_2' + (x' - c_1')} dy'\ p(x', y'). \tag{B.9}$$

The integral limits transform accordingly to the transformation (B.6)

$$c_1' = (c_1 + c_2)/\sqrt{2},\ c_2' = (c_1 - c_2)/\sqrt{2}, \tag{B.10}$$

which factorizes the integral

$$w = \int_{\frac{c_1+c_2}{\sqrt{2}}}^\infty dx'\ p(x') \int_{\sqrt{2}c_1 - x'}^{-\sqrt{2}c_2 + x'} dy'\ p(y'). \tag{B.11}$$

Appendix C

Bivariate Normal probability function

In this appendix we discuss the transition probabilities of two correlated Gaussian noise, mentioned in Sec. 4.3 and 4.4. Exemplarily we derive the quadrant probability

$$\begin{aligned} w_{++\leftarrow++} &= \int_h^\infty d\varepsilon \int_k^\infty d\eta \; p_{r,\sigma}(\varepsilon,\eta), \\ &= \frac{1}{2\pi\sigma^2\sqrt{1-r^2}} \int_h^\infty d\varepsilon \int_k^\infty d\eta \; \exp\left(-\frac{\varepsilon^2+\eta^2-2r\varepsilon\eta}{2\sigma^2(1-r^2)}\right). \end{aligned}$$

Using the transformation $s = \varepsilon/(\sqrt{2}\sigma)$, $t = (\eta - r\varepsilon)/(\sigma\sqrt{2(1-r^2)})$ with the Jacobi-Matrix $\begin{pmatrix} \sigma\sqrt{2} & 0 \\ r\sigma\sqrt{2} & \sigma\sqrt{2(1-r^2)} \end{pmatrix}$, the probability reads as

$$\begin{aligned} w_{++\leftarrow++} &= \frac{1}{\pi} \int_{h/\sigma\sqrt{2}}^\infty ds \; \exp(-s^2) \int_{\frac{k-r\sigma\sqrt{2}s}{\sigma\sqrt{2(1-r^2)}}}^\infty dt \; \exp(-t^2), \\ &= \frac{1}{2\sqrt{\pi}} \int_{h/\sigma\sqrt{2}}^\infty ds \; \exp(-s^2) \operatorname{erfc}\left(\frac{k-r\sigma\sqrt{2}s}{\sigma\sqrt{2(1-r^2)}}\right). \end{aligned}$$

The solution of the integral

$$\int_0^\infty dx \; \operatorname{erf}(ax) e^{-px-cx^2} \tag{C.1}$$

leads to the confluent hypergeometric function of two variables Ψ_1, see 2.8.6.5 in [97]. A review of multiple Gaussian (confluent) hypergeometric series is e. g. given in [114]. But the hypergeometric functions of two variables are not yet implemented in numerical software like Mathematica, Matlab, Maple, GSL.

Therefore we define the bivariate normal probability function L following [1] as

$$L(h,k,r) := \frac{1}{2\pi\sqrt{1-r^2}} \int_h^\infty dx \int_k^\infty dy \; \exp\left(-\frac{x^2+y^2-2rxy}{2(1-r^2)}\right) \tag{C.2}$$

with $h, k \in \mathbb{R}$. It is related to the cumulative bivariate normal distribution function by $\Phi(h,k,r) = L(-h,-k,r)$. Solvable cases are

$$L(h,k,0) = \frac{1}{4}\operatorname{erfc}\left(\frac{h}{\sqrt{2}}\right)\operatorname{erfc}\left(\frac{k}{\sqrt{2}}\right), \tag{C.3}$$

$$L(0,0,r) = \frac{1}{4} + \frac{1}{2\pi}\arcsin(r), \tag{C.4}$$

$$L\left(h,0,\frac{1}{\sqrt{2}}\right) = \frac{1}{2}\operatorname{erfc}\left(\frac{h}{\sqrt{2}}\right) - \frac{1}{8}\operatorname{erfc}^2\left(\frac{h}{\sqrt{2}}\right). \tag{C.5}$$

A package for calculating $L(h,k,r)$ numerically in Fortran or Matlab is given in [38]. Another way of numerically solving it is using the MultinormalDistribution package of Mathematica.

Appendix D

Transition probabilities of two piecewise constant maps

In this appendix we display the transition probabilities of two identical piecewise constant maps with uniform, symmetric correlated noise, discussed in Sect. 4.5. As discussed there, only three of the sixteen transition probabilities have to be calculated, the others can be derived from them due to the symmetry $p(\epsilon,\eta) = p(\eta,\epsilon) = p(-\epsilon,-\eta)$.

First, we calculate the following transition probability examplarily

$$\begin{aligned} w_{++++} &= \int_0^\infty dx \int_0^\infty dy\; p(x-c, y-c) \qquad \text{(D.1)} \\ &= \int_{-c}^\infty dx \int_{-c}^\infty dy\, \Theta\left(\sqrt{6}\sigma\sqrt{1+r} - (x+y)\right) \Theta\left(\sqrt{6}\sigma\sqrt{1+r} + (x+y)\right) \\ &\quad \times \frac{1}{12\sqrt{1-r^2\sigma^2}} \Theta\left(\sqrt{6}\sigma\sqrt{1-r} - (x-y)\right) \Theta\left(\sqrt{6}\sigma\sqrt{1-r} + (x-y)\right). \end{aligned}$$

For convenience we introduce the abbreviation $\sigma_+ = \sqrt{3}\sigma\sqrt{1+r}$, $\sigma_- = \sqrt{3}\sigma\sqrt{1-r}$. The transformation $x' = (x+y)/\sqrt{2}$, $y' = (x-y)/\sqrt{2}$ with the matching determinant of the Jacobian $\det(J) = -1$ leaves us with distinctions of cases to solve the integral

$$\begin{aligned} w_{++++} &= \frac{1}{12\sqrt{1-r^2\sigma^2}} \int_{-\sqrt{2}c}^\infty dx' \int_{-\sqrt{2}c-x'}^{\sqrt{2}c+x'} dy'\, \Theta\left(\sigma_+ - x'\right) \Theta\left(\sigma_+ + x'\right) \\ &\quad \times \Theta\left(\sigma_- - y'\right) \Theta\left(\sigma_- + y'\right). \qquad \text{(D.2)} \end{aligned}$$

To distinct the cases it is useful to remember the conditions $\sigma > 0$ and $-1 < r < 1$. At the integration in y' we have to distinguish between $\sqrt{2}c + x' > \sigma_-$ and $\sqrt{2}c + x' < \sigma_-$:

$$\begin{aligned} w_{++++} &= \frac{1}{12\sqrt{1-r^2\sigma^2}} \int_{-\sqrt{2}c}^\infty dx'\, \Theta\left(\sigma_+ - x'\right) \Theta\left(\sigma_+ + x'\right) \qquad \text{(D.3)} \\ &\quad \times \left[\int_{-\sigma_-}^{\sigma_-} dy'\, \Theta\left(\sqrt{2}c + x' - \sigma_-\right) + \int_{-\sqrt{2}c-x}^{\sqrt{2}c+x} dy'\, \Theta\left(\sigma_- - \sqrt{2}c - x'\right) \right]. \end{aligned}$$

The first integral leaves two choices being $x' > \sigma_- - \sqrt{2}c > -\sqrt{2}c$ and $x' > -\sigma_+ > \sigma_- - \sqrt{2}c$. whereas in the second integral there are four cases: $\sigma_- - \sqrt{2}c > \sigma_+ > x' > -\sqrt{2}c > -\sigma_+$, $\sigma_+ > \sigma_- - \sqrt{2}c > x' > -\sqrt{2}c$, $\sigma_- - \sqrt{2}c > \sigma_+ > x' > -\sigma_+ > -\sqrt{2}c$ and $\sigma_+ > \sigma_- - \sqrt{2}c > x' > -\sqrt{2}c > -\sigma_+$. So collecting all cases sums up to

$$\begin{aligned} w_{++++} &= \frac{1}{12\sqrt{1-r^2\sigma^2}}\Big[2\sigma_-\left(\sigma_+ + \sqrt{2}c - \sigma_-\right)\Theta\left(\sigma_+ - \sigma_- + \sqrt{2}c\right)\Theta\left(\sigma_+ + \sigma_- - \sqrt{2}c\right) \\ &\quad + 4\sigma_+\sigma_-\Theta\left(\sqrt{2}c - \sigma_+ - \sigma_-\right)\Theta\left(\sqrt{2}c - \sigma_+\right) \\ &\quad + 4\sqrt{2}c\sigma_+\Theta\left(\sigma_- - \sqrt{2}c - \sigma_+\right)\Theta\left(\sqrt{2}c - \sigma_+\right) \\ &\quad + \left(\sigma_+ + \sqrt{2}c\right)^2\Theta\left(\sigma_- - \sqrt{2}c - \sigma_+\right)\Theta\left(\sigma_+ + \sqrt{2}c\right)\Theta\left(-\sqrt{2}c + \sigma_+\right) \\ &\quad + \left(\sigma_-^2 - \left(\sigma_+ - \sqrt{2}c\right)^2\right)\Theta\left(\sigma_+ - \sigma_- + \sqrt{2}c\right)\Theta\left(\sqrt{2}c - \sigma_+\right)\Theta\left(\sigma_- + \sigma_+ - \sqrt{2}c\right) \\ &\quad + \sigma_-^2\Theta\left(\sigma_+ - \sigma_- + \sqrt{2}c\right)\Theta\left(-\sqrt{2}c + \sigma_+\right)\Big]. \end{aligned} \tag{D.4}$$

The derived transition probabilities are

$$\begin{aligned} w_{----} &= w_{++++}(-a,-a), \\ w_{--++} &= w_{++++}(-c,-c), \\ w_{++--} &= w_{++++}(a,a). \end{aligned}$$

From $w_{+--+}(a,c) = \int\int_0^\infty dxdy\, p(x-a,-y-c)$ can be deduced by transformation of one variable

$$\begin{aligned} w_{-+++} &= w_{+--+}(c,c), \\ w_{+---} &= w_{+--+}(a,a), \\ w_{-+-+} &= w_{+--+}(c,a). \end{aligned}$$

And finally from $w_{--+-}(c,a) = \int\int_0^\infty dxdy\, p(x+c,y+a)$ can be derived

$$w_{+++-} = w_{--+-}(-c,-a).$$

$$
\begin{aligned}
w_{+--+} \;=\; & \frac{1}{12\sqrt{1-r^2\sigma^2}}\Bigg\{2\sigma_+\left(\frac{a-c}{\sqrt{2}}+\sigma_-\right)\Theta\left(\sigma_--\frac{a-c}{\sqrt{2}}\right)\Theta\left(\frac{a-c}{\sqrt{2}}+\sigma_-\right)\Theta\left(-\frac{a+c}{\sqrt{2}}-\sigma_+\right)\Theta\left(\frac{a+c}{\sqrt{2}}-\sigma_+\right)\\
& +4\sigma_-\sigma_+\Theta\left(\frac{a-c}{\sqrt{2}}-\sigma_-\right)\Theta\left(\sqrt{2}a-\sigma_--\sigma_+\right)\Theta\left(-\sqrt{2}c-\sigma_--\sigma_+\right)\\
& +2\sigma_+\left(\sigma_--\sqrt{2}c-\sigma_+\right)\Theta\left(\sqrt{2}(a+c)\right)\Theta\left(\sigma_--\sqrt{2}c-\sigma_+\right)\Theta\left(\frac{a+c}{\sqrt{2}}+\sigma_+\right)\Theta\left(\sqrt{2}c+\sigma_-+\sigma_+\right)\\
& +2\sigma_+\left(\sqrt{2}a+\sigma_--\sigma_+\right)\Theta\left(-\sqrt{2}(a+c)\right)\Theta\left(\sqrt{2}a+\sigma_--\sigma_+\right)\Theta\left(\sigma_+-\frac{a+c}{\sqrt{2}}\right)\Theta\left(\sigma_--\sqrt{2}a+\sigma_+\right)\\
& +\left((\sigma_+-\sqrt{2}a)^2-\sigma_-^2+\sqrt{2}(a-c)\left(-\sqrt{2}a+\sigma_-+\sigma_+\right)\right)\Theta\left(\sqrt{2}(a+c)\right)\Theta\left(\frac{a-c}{\sqrt{2}}-\sigma_-\right)\Theta\left(\sqrt{2}a+\sigma_--\sigma_+\right)\Theta\left(\sigma_--\sqrt{2}a+\sigma_+\right)\\
& +2\sqrt{2}(a-c)\sigma_-\Theta\left(\frac{a-c}{\sqrt{2}}-\sigma_-\right)\Theta\left(-\sqrt{2}a-\sigma_-+\sigma_+\right)\Theta\left(\sqrt{2}c-\sigma_-+\sigma_+\right)\\
& +\left(\sigma_-^2-\frac{1}{2}(c-a)^2+\sqrt{2}(a-c)\left(\frac{a-c}{\sqrt{2}}+\sigma_-\right)\right)\Theta\left(\sigma_--\frac{a-c}{\sqrt{2}}\right)\Theta\left(\frac{a-c}{\sqrt{2}}+\sigma_-\right)\Theta\left(\sigma_+-\sqrt{2}a-\sigma_-\right)\Theta\left(\sqrt{2}c-\sigma_-+\sigma_+\right)\\
& +\left((\sigma_+-\sqrt{2}a)^2-\frac{1}{2}(c-a)^2+\sqrt{2}(a-c)\left(\sigma_+-\frac{a+c}{\sqrt{2}}\right)\right)\Theta\left(\sqrt{2}(a+c)\right)\Theta\left(\sigma_--\frac{a-c}{\sqrt{2}}\right)\Theta\left(\sqrt{2}a+\sigma_--\sigma_+\right)\Theta\left(\sigma_+-\frac{a+c}{\sqrt{2}}\right)\\
& +\left((\sigma_++\sqrt{2}c)^2-\frac{1}{2}(c-a)^2+\sqrt{2}(a-c)\left(\frac{a+c}{\sqrt{2}}+\sigma_+\right)\right)\Theta\left(-\sqrt{2}(a+c)\right)\Theta\left(\sigma_--\frac{a-c}{\sqrt{2}}\right)\Theta\left(\sigma_--\sqrt{2}c-\sigma_+\right)\Theta\left(\frac{a+c}{\sqrt{2}}+\sigma_+\right)\\
& +\left((\sigma_++\sqrt{2}c)^2-\sigma_-^2+\sqrt{2}(a-c)\left(\sqrt{2}c+\sigma_-+\sigma_+\right)\right)\Theta\left(-\sqrt{2}(a+c)\right)\Theta\left(\frac{a-c}{\sqrt{2}}-\sigma_-\right)\Theta\left(\sigma_--\sqrt{2}c-\sigma_+\right)\Theta\left(\sqrt{2}c+\sigma_-+\sigma_+\right)\\
& +2\sigma_-\left(\sqrt{2}a+\sigma_+\right)\Theta\left(\frac{a-c}{\sqrt{2}}-\sigma_-\right)\Theta\left(-\sqrt{2}c-\sigma_--\sigma_+\right)\Theta\left(\sigma_+-\sqrt{2}a-\sigma_-\right)\Theta\left(\sqrt{2}a-\sigma_-+\sigma_+\right)\\
& +\left(\frac{\sigma_-^2}{2}-\frac{1}{2}\left(\sigma_++\sqrt{2}c\right)^2+\left(\sigma_--\sqrt{2}c-\sigma_+\right)\left(\sqrt{2}a+\sigma_+\right)\right)\Theta\left(\sigma_--\sqrt{2}c-\sigma_+\right)\Theta\left(\frac{a+c}{\sqrt{2}}+\sigma_+\right)\Theta\left(\sigma_+-\sqrt{2}a-\sigma_-\right)\Theta\left(\sqrt{2}c+\sigma_-+\sigma_+\right)\Theta\left(\sqrt{2}(a+c)+2\sigma_+\right)\\
& +\left(\frac{\sigma_-^2}{2}-\frac{1}{4}(a-c)^2+\left(\frac{a-c}{\sqrt{2}}+\sigma_-\right)\left(\sqrt{2}a+\sigma_+\right)\right)\Theta\left(\frac{a-c}{\sqrt{2}}+\sigma_-\right)\Theta\left(\frac{c-a}{\sqrt{2}}+\sigma_-\right)\Theta\left(-\frac{a+c}{\sqrt{2}}-\sigma_+\right)\Theta\left(\sigma_+-\sqrt{2}a-\sigma_-\right)\Theta\left(\frac{a+c}{\sqrt{2}}+\sigma_+\right)\\
& +\left(\frac{1}{2}\left(\sigma_+-\sqrt{2}a\right)^2-\frac{\sigma_-^2}{2}+\left(\sqrt{2}a+\sigma_+\right)\left(\sigma_--\sqrt{2}a+\sigma_+\right)\right)\Theta\left(\frac{a-c}{\sqrt{2}}-\sigma_-\right)\Theta\left(-\sqrt{2}c-\sigma_--\sigma_+\right)\Theta\left(\sqrt{2}a+\sigma_--\sigma_+\right)\Theta\left(\sqrt{2}a-\sigma_-+\sigma_+\right)\Theta\left(\sigma_--\sqrt{2}a+\sigma_+\right)\\
& +\left(a^2-c^2-\sqrt{2}(a+c)\sigma_+-\sqrt{2}(a+c)\left(\sqrt{2}a+\sigma_+\right)\right)\Theta\left(-\sqrt{2}(a+c)\right)\Theta\left(\sqrt{2}a+\sigma_--\sigma_+\right)\Theta\left(\frac{a+c}{\sqrt{2}}+\sigma_+\right)\Theta\left(\sqrt{2}c+\sigma_-+\sigma_+\right)\Theta\left(\sqrt{2}(a+c)+2\sigma_+\right)\\
& +\left(\frac{1}{2}(\sigma_+-\sqrt{2}a)^2-\frac{1}{4}(a-c)^2+\left(\sqrt{2}a+\sigma_+\right)\left(\sigma_+-\frac{a+c}{\sqrt{2}}\right)\right)\Theta\left(\frac{c-a}{\sqrt{2}}+\sigma_-\right)\Theta\left(-\frac{a+c}{\sqrt{2}}-\sigma_+\right)\Theta\left(\sqrt{2}a+\sigma_--\sigma_+\right)\Theta\left(\sigma_+-\frac{a+c}{\sqrt{2}}\right)\Theta\left(\frac{a+c}{\sqrt{2}}+\sigma_+\right)\\
& +\left(\frac{\sigma_-^2}{2}-\frac{1}{2}\left(\sqrt{2}a+\sigma_+\right)^2+\left(\sqrt{2}a+\sigma_+\right)\left(\sqrt{2}a+\sigma_-+\sigma_+\right)\right)\Theta\left(-\sqrt{2}(a+c)-2\sigma_+\right)\Theta\left(-\frac{a+c}{\sqrt{2}}-\sigma_+\right)\Theta\left(\sigma_--\sqrt{2}a-\sigma_+\right)\Theta\left(\sigma_+-\sqrt{2}a-\sigma_-\right)\Theta\left(\sqrt{2}a+\sigma_-+\sigma_+\right)
\end{aligned}
$$

$$
\begin{aligned}
&+\left(-2\sqrt{2}a\sigma_+ + 2\sigma_+\left(\sqrt{2}a+\sigma_+\right)\right)\Theta\left(-\sqrt{2}(a+c)-2\sigma_+\right)\Theta\left(-\frac{a+c}{\sqrt{2}}-\sigma_+\right)\Theta\left(\sigma_- -\sqrt{2}a-\sigma_+\right)\Theta\left(\sqrt{2}a+\sigma_- -\sigma_+\right)\\
&+2\sigma_-\left(\sigma_+-\sqrt{2}c\right)\Theta\left(\frac{a-c}{\sqrt{2}}-\sigma_-\right)\Theta\left(\sqrt{2}a-\sigma_- -\sigma_+\right)\Theta\left(\sigma_+-\sqrt{2}c-\sigma_-\right)\Theta\left(\sqrt{2}c-\sigma_-+\sigma_+\right)\\
&+\left(\frac{\sigma_-^2}{2}-\frac{1}{2}\left(\sigma_+-\sqrt{2}a\right)^2+\left(\sqrt{2}a+\sigma_- -\sigma_+\right)\left(\sigma_+-\sqrt{2}c\right)\right)\Theta\left(\sqrt{2}a+\sigma_- -\sigma_+\right)\Theta\left(\sigma_+-\frac{a+c}{\sqrt{2}}\right)\Theta\left(\sqrt{2}c-\sigma_-+\sigma_+\right)\Theta\left(\sigma_- -\sqrt{2}a+\sigma_+\right)\Theta\left(2\sigma_+-\sqrt{2}(a+c)\right)\\
&+\left(\frac{\sigma_-^2}{2}-\frac{1}{4}(c-a)^2+\left(\frac{a-c}{\sqrt{2}}+\sigma_-\right)\left(\sigma_+-\sqrt{2}c\right)\right)\Theta\left(\frac{a-c}{\sqrt{2}}+\sigma_-\right)\Theta\left(\frac{c-a}{\sqrt{2}}+\sigma_-\right)\Theta\left(\sigma_+-\frac{a+c}{\sqrt{2}}\right)\Theta\left(\sqrt{2}c-\sigma_-+\sigma_+\right)\Theta\left(\frac{a+c}{\sqrt{2}}-\sigma_+\right)\\
&+\left(\frac{1}{2}\left(\sqrt{2}c+\sigma_+\right)^2-\frac{\sigma_-^2}{2}+\left(\sigma_+-\sqrt{2}c\right)\left(\sqrt{2}c+\sigma_-+\sigma_+\right)\right)\Theta\left(\frac{a-c}{\sqrt{2}}-\sigma_-\right)\Theta\left(\sqrt{2}a-\sigma_- -\sigma_+\right)\Theta\left(\sigma_- -\sqrt{2}c-\sigma_+\right)\Theta\left(\sigma_+-\sqrt{2}c-\sigma_-\right)\Theta\left(\sqrt{2}c+\sigma_-+\sigma_+\right)\\
&+\left(c^2-a^2+\sqrt{2}(a+c)\sigma_++\sqrt{2}(a+c)\left(\sigma_+-\sqrt{2}c\right)\right)\Theta\left(\sqrt{2}(a+c)\right)\Theta\left(\sigma_- -\sqrt{2}c-\sigma_+\right)\Theta\left(\sigma_+-\frac{a+c}{\sqrt{2}}\right)\Theta\left(\sigma_- -\sqrt{2}a+\sigma_+\right)\Theta\left(2\sigma_+-\sqrt{2}(a+c)\right)\\
&+\left(\frac{1}{2}\left(\sigma_++\sqrt{2}c\right)^2-\frac{1}{4}(a-c)^2+\left(\sigma_+-\sqrt{2}c\right)\left(\frac{a+c}{\sqrt{2}}+\sigma_+\right)\right)\Theta\left(\frac{c-a}{\sqrt{2}}+\sigma_-\right)\Theta\left(\sigma_- -\sqrt{2}c-\sigma_+\right)\Theta\left(\sigma_+-\frac{a+c}{\sqrt{2}}\right)\Theta\left(\frac{a+c}{\sqrt{2}}+\sigma_+\right)\Theta\left(\frac{a+c}{\sqrt{2}}-\sigma_+\right)\\
&+\left(\frac{\sigma_-^2}{2}-\frac{1}{2}\left(\sqrt{2}c-\sigma_+\right)^2+\left(\sigma_+-\sqrt{2}c\right)\left(\sigma_- -\sqrt{2}c+\sigma_+\right)\right)\Theta\left(\sqrt{2}(a+c)-2\sigma_+\right)\Theta\left(\sqrt{2}c+\sigma_- -\sigma_+\right)\Theta\left(\sqrt{2}c-\sigma_-+\sigma_+\right)\Theta\left(\sigma_- -\sqrt{2}c+\sigma_+\right)\Theta\left(\frac{a+c}{\sqrt{2}}-\sigma_+\right)\\
&+\left(2\sqrt{2}c\sigma_+ + 2\sigma_+\left(\sigma_+-\sqrt{2}c\right)\right)\Theta\left(\sqrt{2}(a+c)-2\sigma_+\right)\Theta\left(\sigma_- -\sqrt{2}c-\sigma_+\right)\Theta\left(\sqrt{2}c+\sigma_- -\sigma_+\right)\Theta\left(\frac{a+c}{\sqrt{2}}-\sigma_+\right)\Bigg\}
\end{aligned}
$$

$$
\begin{aligned}
w_{--+-} \;=\; & \frac{1}{12\sqrt{1-r^2}\sigma^2}\Big\{2\sigma_+\left(\sigma_- - \sqrt{2}a\right)\Theta\left(-\frac{a+c}{\sqrt{2}} - \sigma_+\right)\Theta\left(-\sqrt{2}c - \sigma_+ - \sigma_-\right)\Theta\left(\sigma_- - \sqrt{2}a - \sigma_+\right)\Theta\left(\sqrt{2}a - \sigma_+ + \sigma_-\right) \\
& + \left(\frac{\sigma_+^2}{2} - \frac{1}{2}\left(\sqrt{2}c + \sigma_-\right)^2 + \left(\sigma_+ - \sqrt{2}c - \sigma_-\right)\left(\sigma_- - \sqrt{2}a\right)\right)\Theta\left(\sigma_+ - \sqrt{2}c - \sigma_-\right)\Theta\left(\frac{c-a}{\sqrt{2}} + \sigma_-\right)\Theta\left(\sqrt{2}a - \sigma_+ + \sigma_-\right)\Theta\left(\sqrt{2}c + \sigma_+ + \sigma_-\right)\Theta\left(\sqrt{2}(c-a) + 2\sigma_-\right) \\
& + \left(\frac{\sigma_+^2}{2} - \frac{1}{4}(a+c)^2 + \left(\sigma_+ - \frac{a+c}{\sqrt{2}}\right)\left(\sigma_- - \sqrt{2}a\right)\right)\Theta\left(\frac{a-c}{\sqrt{2}} - \sigma_-\right)\Theta\left(\sigma_+ - \frac{a+c}{\sqrt{2}}\right)\Theta\left(\frac{a+c}{\sqrt{2}} + \sigma_+\right)\Theta\left(\frac{c-a}{\sqrt{2}} + \sigma_-\right)\Theta\left(\sqrt{2}a - \sigma_+ + \sigma_-\right) \\
& + \left(\frac{1}{2}\left(\sqrt{2}a + \sigma_-\right)^2 - \frac{\sigma_+^2}{2} + \left(\sqrt{2}a + \sigma_+ + \sigma_-\right)\left(\sigma_- - \sqrt{2}a\right)\right)\Theta\left(-\frac{a+c}{\sqrt{2}} - \sigma_+\right)\Theta\left(-\sqrt{2}c - \sigma_+ - \sigma_-\right)\Theta\left(\sigma_+ - \sqrt{2}a - \sigma_-\right)\Theta\left(\sigma_- - \sqrt{2}a - \sigma_+\right)\Theta\left(\sqrt{2}a + \sigma_+ + \sigma_-\right) \\
& + \left(a^2 - c^2 + \sqrt{2}(a-c)\sigma_- + \sqrt{2}(a-c)\left(\sigma_- - \sqrt{2}a\right)\right)\Theta\left(\sqrt{2}(a-c)\right)\Theta\left(\sigma_+ - \sqrt{2}a - \sigma_-\right)\Theta\left(\frac{c-a}{\sqrt{2}} + \sigma_-\right)\Theta\left(\sqrt{2}c + \sigma_+ + \sigma_-\right)\Theta\left(\sqrt{2}(c-a) + 2\sigma_-\right) \\
& + \left(\frac{1}{2}\left(\sqrt{2}a + \sigma_-\right)^2 - \frac{1}{4}(a+c)^2 + \left(\sigma_- - \sqrt{2}a\right)\left(\frac{a-c}{\sqrt{2}} + \sigma_-\right)\right)\Theta\left(\frac{a+c}{\sqrt{2}} + \sigma_+\right)\Theta\left(\frac{a-c}{\sqrt{2}} - \sigma_-\right)\Theta\left(\sigma_+ - \sqrt{2}a - \sigma_-\right)\Theta\left(\frac{a-c}{\sqrt{2}} + \sigma_-\right)\Theta\left(\frac{c-a}{\sqrt{2}} + \sigma_-\right) \\
& + \left(\frac{\sigma_+^2}{2} - \frac{1}{2}\left(\sqrt{2}a - \sigma_-\right)^2 + \left(\sigma_- - \sqrt{2}a\right)\left(\sigma_+ - \sqrt{2}a + \sigma_-\right)\right)\Theta\left(\sqrt{2}(a-c) - 2\sigma_-\right)\Theta\left(\frac{a-c}{\sqrt{2}} - \sigma_-\right)\Theta\left(\sqrt{2}a + \sigma_+ - \sigma_-\right)\Theta\left(\sqrt{2}a - \sigma_+ + \sigma_-\right)\Theta\left(\sigma_+ - \sqrt{2}a + \sigma_-\right) \\
& + \left(2(\sqrt{2}a\sigma_- + 2\sigma_-\left(\sigma_- - \sqrt{2}a\right)\right)\Theta\left(\sqrt{2}(a-c) - 2\sigma_-\right)\Theta\left(\frac{a-c}{\sqrt{2}} - \sigma_-\right)\Theta\left(\sigma_+ - \sqrt{2}a - \sigma_-\right)\Theta\left(\sqrt{2}a + \sigma_+ - \sigma_-\right) \\
& + 2\sigma_-\left(\sigma_+ - \frac{a+c}{\sqrt{2}}\right)\Theta\left(\sigma_+ - \frac{a+c}{\sqrt{2}}\right)\Theta\left(\frac{a+c}{\sqrt{2}} + \sigma_+\right)\Theta\left(\frac{a-c}{\sqrt{2}} - \sigma_-\right)\Theta\left(\frac{c-a}{\sqrt{2}} - \sigma_-\right) \\
& + 4\sigma_+\sigma_-\Theta\left(-\frac{a+c}{\sqrt{2}} - \sigma_+\right)\Theta\left(-\sqrt{2}a - \sigma_+ - \sigma_-\right)\Theta\left(-\sqrt{2}c - \sigma_+ - \sigma_-\right) \\
& + 2\sigma_-\left(\sigma_+ - \sqrt{2}a - \sigma_-\right)\Theta\left(\sqrt{2}(a-c)\right)\Theta\left(\sigma_+ - \sqrt{2}a - \sigma_-\right)\Theta\left(\frac{a-c}{\sqrt{2}} + \sigma_-\right)\Theta\left(\sqrt{2}a + \sigma_+ + \sigma_-\right) \\
& + 2\sigma_-\left(\sigma_+ - \sqrt{2}c - \sigma_-\right)\Theta\left(\sqrt{2}(c-a)\right)\Theta\left(\sigma_+ - \sqrt{2}c - \sigma_-\right)\Theta\left(\frac{c-a}{\sqrt{2}} + \sigma_-\right)\Theta\left(\sqrt{2}c + \sigma_+ + \sigma_-\right) \\
& + 2\sigma_-\left(\sigma_- - \sqrt{2}c\right)\Theta\left(-\frac{a+c}{\sqrt{2}} - \sigma_+\right)\Theta\left(-\sqrt{2}a - \sigma_+ - \sigma_-\right)\Theta\left(\sigma_- - \sqrt{2}c - \sigma_+\right)\Theta\left(\sqrt{2}c - \sigma_+ + \sigma_-\right) \\
& + \left(\frac{\sigma_+^2}{2} - \frac{1}{4}(a+c)^2 + \left(\sigma_+ - \frac{a+c}{\sqrt{2}}\right)\left(\sigma_- - \sqrt{2}c\right)\right)\Theta\left(\frac{c-a}{\sqrt{2}} - \sigma_+\right)\Theta\left(\sigma_+ - \frac{a+c}{\sqrt{2}}\right)\Theta\left(\frac{a+c}{\sqrt{2}} + \sigma_+\right)\Theta\left(\frac{a-c}{\sqrt{2}} + \sigma_-\right)\Theta\left(\sqrt{2}c - \sigma_+ + \sigma_-\right) \\
& + \left(\frac{\sigma_+^2}{2} - \frac{1}{2}\left(\sqrt{2}a + \sigma_-\right)^2 + \left(\sigma_+ - \sqrt{2}a - \sigma_-\right)\left(\sigma_- - \sqrt{2}c\right)\right)\Theta\left(\sigma_+ - \sqrt{2}a - \sigma_-\right)\Theta\left(\frac{a-c}{\sqrt{2}} + \sigma_-\right)\Theta\left(\sqrt{2}c - \sigma_+ + \sigma_-\right)\Theta\left(\sqrt{2}a + \sigma_+ + \sigma_-\right)\Theta\left(\sqrt{2}(a-c) + 2\sigma_-\right) \\
& + \left(\frac{1}{2}\left(\sqrt{2}c + \sigma_-\right)^2 - \frac{\sigma_+^2}{2} + \left(\sigma_- - \sqrt{2}c\right)\left(\sqrt{2}c + \sigma_+ + \sigma_-\right)\right)\Theta\left(-\frac{a+c}{\sqrt{2}} - \sigma_+\right)\Theta\left(-\sqrt{2}a - \sigma_+ - \sigma_-\right)\Theta\left(\sigma_+ - \sqrt{2}c - \sigma_-\right)\Theta\left(\sigma_- - \sqrt{2}c - \sigma_+\right)\Theta\left(\sqrt{2}c + \sigma_+ + \sigma_-\right) \\
& + \left(\frac{1}{2}\left(\sqrt{2}c + \sigma_-\right)^2 - \frac{1}{4}(a+c)^2 + \left(\sigma_- - \sqrt{2}c\right)\left(\frac{c-a}{\sqrt{2}} + \sigma_-\right)\right)\Theta\left(\frac{a+c}{\sqrt{2}} + \sigma_+\right)\Theta\left(\sigma_+ - \sqrt{2}c - \sigma_-\right)\Theta\left(\frac{a-c}{\sqrt{2}} + \sigma_-\right)\Theta\left(\frac{c-a}{\sqrt{2}} + \sigma_-\right)\Theta\left(\frac{c-a}{\sqrt{2}} - \sigma_-\right)
\end{aligned}
$$

$$
\begin{aligned}
&+\left(c^2-a^2-\sqrt{2}(c-a)\sigma_-+\sqrt{2}(c-a)\left(\sigma_--\sqrt{2}c\right)\right)\Theta\left(\sqrt{2}(c-a)\right)\Theta\left(\sigma_+-\sqrt{2}c-\sigma_-\right)\Theta\left(\frac{a-c}{\sqrt{2}}+\sigma_-\right)\Theta\left(\sqrt{2}a+\sigma_++\sigma_-\right)\Theta\left(\sqrt{2}(a-c)+2\sigma_-\right)\\
&+\left(\frac{\sigma_+^2}{2}-\frac{1}{2}\left(\sqrt{2}c-\sigma_-\right)^2+\left(\sigma_--\sqrt{2}c\right)\left(\sigma_+-\sqrt{2}c+\sigma_-\right)\right)\Theta\left(\sqrt{2}(c-a)-2\sigma_-\right)\Theta\left(\sqrt{2}c+\sigma_+-\sigma_-\right)\Theta\left(\sqrt{2}c-\sigma_++\sigma_-\right)\Theta\left(\sigma_+-\sqrt{2}c+\sigma_-\right)\Theta\left(\frac{c-a}{\sqrt{2}}-\sigma_-\right)\\
&+\left(2\sqrt{2}c\sigma_-+2\sigma_-\left(\sigma_--\sqrt{2}c\right)\right)\Theta\left(\sqrt{2}(c-a)-2\sigma_-\right)\Theta\left(\sigma_+-\sqrt{2}c-\sigma_-\right)\Theta\left(\sqrt{2}c+\sigma_+-\sigma_-\right)\Theta\left(\frac{c-a}{\sqrt{2}}-\sigma_-\right)\\
&-2\sigma_+\sqrt{2}(a+c)\Theta\left(-\frac{a+c}{\sqrt{2}}-\sigma_+\right)\Theta\left(\sqrt{2}a-\sigma_++\sigma_-\right)\Theta\left(\sqrt{2}c-\sigma_++\sigma_-\right)\\
&+\left(\sigma_+^2-\frac{1}{2}(a+c)^2-\sqrt{2}(a+c)\left(\sigma_+-\frac{a+c}{\sqrt{2}}\right)\right)\Theta\left(\sigma_+-\frac{a+c}{\sqrt{2}}\right)\Theta\left(\frac{a+c}{\sqrt{2}}+\sigma_+\right)\Theta\left(\sqrt{2}a-\sigma_++\sigma_-\right)\Theta\left(\sqrt{2}c-\sigma_++\sigma_-\right)\\
&+\left(\left(\sqrt{2}a+\sigma_-\right)^2-\sigma_+^2-\sqrt{2}(a+c)\left(\sqrt{2}a+\sigma_++\sigma_-\right)\right)\Theta\left(\sqrt{2}(c-a)\right)\Theta\left(-\frac{a+c}{\sqrt{2}}-\sigma_+\right)\Theta\left(\sigma_+-\sqrt{2}a-\sigma_-\right)\Theta\left(\sqrt{2}a+\sigma_++\sigma_-\right)\\
&+\left(\left(\sqrt{2}a+\sigma_-\right)^2-\frac{1}{2}(a+c)^2-\sqrt{2}(a+c)\left(\frac{a-c}{\sqrt{2}}+\sigma_-\right)\right)\Theta\left(\sqrt{2}(c-a)\right)\Theta\left(\frac{a+c}{\sqrt{2}}+\sigma_+\right)\Theta\left(-\sqrt{2}a+\sigma_++\sigma_-\right)\Theta\left(\frac{a-c}{\sqrt{2}}+\sigma_-\right)\\
&+\left(\left(\sqrt{2}c+\sigma_-\right)^2-\sigma_+^2-\sqrt{2}(a+c)\left(\sqrt{2}c+\sigma_++\sigma_-\right)\right)\Theta\left(\sqrt{2}(a-c)\right)\Theta\left(-\frac{a+c}{\sqrt{2}}-\sigma_+\right)\Theta\left(\sigma_+-\sqrt{2}c-\sigma_-\right)\Theta\left(\sqrt{2}c+\sigma_++\sigma_-\right)\\
&+\left(\left(\sqrt{2}c+\sigma_-\right)^2-\frac{1}{2}(a+c)^2-\sqrt{2}(a+c)\left(\frac{c-a}{\sqrt{2}}+\sigma_-\right)\right)\Theta\left(\sqrt{2}(a-c)\right)\Theta\left(\frac{a+c}{\sqrt{2}}+\sigma_+\right)\Theta\left(\sigma_+-\sqrt{2}c-\sigma_-\right)\Theta\left(\frac{c-a}{\sqrt{2}}+\sigma_-\right)\Bigg\}
\end{aligned}
$$

Bibliography

[1] Abramowitz, M. and Stegun, I. A. (1964). *Handbook of Mathematical Functions with Formulas, Graphs, and Mathematical Tables*. Dover, 9th edition.

[2] Allen, J. C., Schaffer, W. M., and Rosko, D. (1993). Chaos reduces species extinction by amplyfing local population noise. *Nature*, 364:229–235.

[3] Argyris, J. H., Faust, G., and Haase, M. (1995). *Die Erforschung des Chaos*. Vieweg.

[4] Aronson, D. G., Ermentrout, G. B., and Kopell, N. (1990). Amplitude response of coupled oscillators. *Physica D*, 41(3):403–449.

[5] Belykh, V. N., Kuckländer, N., Osipov, G. V., Blasius, B., and Kurths, J. (2005a). Automatic control of phase synchronization in coupled complex oscillators. In Fradkov, A. and Churilov, A. N., editors, *2005 International Conference Physics and Control Proceedings*, pages 92–99, St. Petersburg. IEEE.

[6] Belykh, V. N. and Osipov, G. V. (2004). Automatic phase synchronization in ensembles of regular and chaotic oscillators. *J. Commun. Technol. El+*, 49(8):891–895.

[7] Belykh, V. N., Osipov, G. V., Kuckländer, N., Blasius, B., and Kurths, J. (2005b). Automatic control of phase synchronization in coupled complex oscillators. *Physica D*, 200(1-2):81–104.

[8] Benton, T. G., Lapsley, C. T., and Beckerman, A. P. (2001a). Population synchrony and environmental variation: an experimental demonstration. *Ecol. Lett.*, 4:236–243.

[9] Benton, T. G., Lapsley, C. T., and Beckerman, A. P. (2002). The population response to environmental noise: population size, variance and correlation in an experimental system. *J. Anim. Ecol.*, 71:320–332.

[10] Benton, T. G., Ranta, E., Kaitala, V., and Beckerman, A. P. (2001b). Maternal effects and the stability of population ynamics in noisy environments. *J. Anim. Ecol.*, 70:590–599.

[11] Benzi, R., Sutera, A., and Vulpiani, A. (1981). The mechanism of stochastic resonance. *J. Phys. A.*, 14(11):L453–L457.

[12] Bjørnstad, O. N. and Bolker, B. (2000). Canonical functions for dispersal-induced synchrony. *Proc. R. Soc. Lond. B*, 267:1787–1794.

[13] Blasius, B., Huppert, A., and Stone, L. (1999). Complex dynamics and phase synchronization in spatially extended ecological systems. *Nature*, 399:354–359.

[14] Blasius, B., Montbrió, E., and Kurths, J. (2003). Anomalous phase synchronization in populations of nonidentical oscillators. *Phys. Rev. E*, 67:035204(R).

[15] Blasius, B. and Stone, L. (2000a). Chaos and phase synchronization in ecological systems. *Int. J. Bif. Chaos*, 10(10):2361–2380.

[16] Blasius, B. and Stone, L. (2000b). Nonlinearity and the Moran effect. *Nature*, 406:846–847.

[17] Boccaletti, S., Grebogi, C., Lai, Y.-C., Mancini, H., and Maza, D. (2000). The control of chaos: Theory and applications. *Phys. Rep.*, 329:103–197.

[18] Buonaccorsi, J. P., Elkington, J. S., Evans, S. R., and Liebhold, A. M. (2001). Measuring and testing for spatial synchrony. *Ecology*, 82(6):1668–1679.

[19] Cattadori, I. M., Haydon, D. T., and Hudson, P. J. (2005). Parasites and climate synchronize red grouse populations. *Nature*, 433:737–741.

[20] Cattadori, I. M., Merler, S., and Hudson, P. J. (2000). Searching for mechanisms of synchrony in spatially structured gamebird populations. *J. Anim. Ecol.*, 69:620–638.

[21] Cazelles, B. and Stone, L. (2003). Detection of imperfect population synchrony in an uncertain world. *J. Anim. Ecol.*, 72:953–968.

[22] Clutton-Brock, T. H., Price, O. F., Albon, S. D., and Jewell, P. A. (1991). Persistent instability and population regulation in Soay sheep. *J. Anim. Ecol.*, 60:593–608.

[23] Cohen, A. E., Gonzalez, A., Lawton, J. H., Petchey, O. L., Wildman, D., and Cohen, J. E. (1998). A novel experimental apparatus to study the impact of white noise and 1/f noise on animal populations. *Proc. R. Soc. Lond. B*, 265:11–15.

[24] Coulson, T., Catchpole, E. A., Albon, S. D., Morgan, B. J. T., Pemberton, J. M., Clutton-Brock, T. H., Crawley, M. J., and Grenfell, B. T. (2001). Age, sex, density, winter, weather, and population crashes in Soay sheep. *Science*, 292:1528–1531.

[25] Coulson, T., Clutton-Brock, T., and Milner-Gulland, E. J. (2000). The relative roles of density and climatic variation on population dynamics and fecundity rates in three contrasting ungulate species. *Proc. R. Soc. Lond. B*, 267:1771–1779.

[26] Crutchfield, J., Nauenberg, M., and Rudnick, J. (1981). Scaling for external noise at the onset of chaos. *Phys. Rev. Lett.*, 46(14):933–935.

[27] Crutchfield, J. P., Farmer, J. D., and Huberman, B. A. (1982). Fluctuations and simple chaotic dynamics. *Phys. Rep.*, 92(2):45–82.

[28] Cuddington, K. M. and Yodzis, P. (1999). Black noise and population persistence. *Proc. R. Soc. Lond. B*, 266:969–973.

[29] Earn, D. J. D., Levin, S. A., and Rohani, P. (2000). Coherence and conservation. *Science*, 290:1360–1363.

[30] Ellis, A. M. and Post, E. (2004). Population response to climate change: linear vs. non-linear modeling approaches. *BMC Ecology*, 4(2):1472–6785.

[31] Elton, C. and Nicholson, M. (1942). The ten-year cycle in numbers of the lynx in Canada. *J. Anim. Ecol.*, 11:215–244.

[32] Feigenbaum, M. J. (1978). Quantitative universality for a class of nonlinear transformations. *J. Stat. Phys.*, 19(1):25–52.

[33] Feigenbaum, M. J. and Hasslacher, B. (1982). Irrational decimation and path integrals for external noise. *Phys. Rev. Lett.*, 49(9):605–609.

[34] Fontaine, C. and Gonzalez, A. (2005). Population synchrony induced by resource fluctuations and dispersal in an aquatic microcosm. *Ecology*, 86(6):1463–1471.

[35] Forchhammer, M. C., Clutton-Brock, T. H., Lindström, J., and Albon, S. D. (2001). Climate and population density induce long-term cohort variation in a northern ungulate. *J. Anim. Ecol.*, 70:721–729.

[36] Forchhammer, M. C., Stenseth, N. C., Post, E., and Langvatn, R. (1998). Population dynamics in norwegian red deer: density-dependence and climatic variation. *Proc. R. Soc. Lond. B*, 265:341–350.

[37] Gang, H., Ditzinger, T., Ning, C. Z., and Haken, H. (1993). Stochastic resonance without external periodic force. *Phys. Rev. Lett.*, 71(6):807–810.

[38] Genz, A. (2004). Numerical computation of rectangular bivariate and trivariate normal and t probabilities. *Statistics and Computing*, 14(3):251–260.

[39] Greenman, J. V. and Benton, T. G. (2001). The impact of stochasticity on the behaviour of nonlinear population models: synchrony and the Moran effect. *Oikos*, 93(2):343–351.

[40] Greenman, J. V. and Benton, T. G. (2003). The amplification of environmental noise in population models: Causes and consequences. *Am. Nat.*, 161(2):225–239.

[41] Greenman, J. V. and Benton, T. G. (2005). The frequency spectrum of structured discrete time population models: its properties and their ecological implications. *Oikos*, 110(2):369–389.

[42] Grenfell, B. T., Wilson, K., Finkenstädt, B. F., Coulson, T. N., and Crawley, M. J. (2000). Reply. *Nature*, 406:847.

[43] Grenfell, B. T., Wilson, K., Finkenstädt, B. F., Coulson, T. N., Murray, S., Albon, S. D., Pemberton, J. M., Clutton-Brock, T. H., and Crawley, M. J. (1998). Noise and determinism in synchronized sheep dynamics. *Nature*, 394:674–677.

[44] Grenfell, B. T., Wilson, K., Isham, V., Boyd, H. E. G., and Dietz, K. (1995). Modelling patterns of parasite aggregation in natural populations: trichostrongylid nematode-ruminant interactions as a case study. *Parasitology*, 111:S135–S151.

[45] Grossmann, S. and Thomae, S. (1977). Invariant distributions and stationary correlation functions of one-dimensional discrete processes. *Z. Naturforsch. A*, 32:1353–1363.

[46] Gulland, F. M. D. (1992). The role of nematode parasites in Soay sheep mortality during a population crash. *Parasitology*, 105:493–503.

[47] Hadley, P. and Beasley, M. R. (1987). Dynamical states and stability of linear arrays of josephson junctions. *Appl . Phys. Lett.*, 50(10):621–623.

[48] Haken, H., Kelso, J. A. S., and Bunz, H. (1985). A theoretical model of phase transitions in human hand movements. *Biol. Cybern.*, 51:347–356.

[49] Hallett, T. B., Coulson, T., Pilkington, J. G., Clutton-Brock, T. H., Pemberton, J. M., and Grenfell, B. T. (2004). Why large-scale climate indices seem to predict ecological processes better than local weather. *Nature*, 430:71–75.

[50] Hamm, A. and Graham, R. (1992). Scaling for small random perturbations of golden critical maps. *Phys. Rev. A*, 46(10):323–333.

[51] Haydon, D. and Steen, H. (1997). The effects of large- and small-scale random events on the synchrony of metapopulation dynamics: a theoretical analysis. *Proc. R. Soc. Lond. B*, 264:1375–1381.

[52] Haydon, D. T., Greenwood, P. E., Stenseth, N. C., and Saitoh, T. (2003). Spatio-temporal dynamics of the grey-sided vole in hokkaido: identifying coupling using state-based markov-chain modeling. *Proc. R. Soc. Lond. B*, 270:435–445.

[53] Heino, M., Kaitala, V., Ranta, E., and Lindström, J. (1997). Synchronous dynamics and rates of extinction in spatially structured populations. *Proc. R. Soc. Lond. B*, 264:481–486.

[54] Herzel, H., Schmitt, A. O., and Ebeling, W. (1994). Finite sample effects in seqence analysis. *Chaos, Solitons & Fractals*, 4(1):97–113.

[55] Holmstad, P. R., Hudson, P. J., Vandvik, V., and Skorping, A. (2005). Can parasites synchronise the population fluctuations of sympatric tetranoids? - examining some minimum conditions. *Oikos*, 109(3):429–434.

[56] Honerkamp, J. (1990). *Stochastische Dynamische Systeme*. VCH.

[57] Hudson, P. J. and Cattadori, I. M. (1999). The Moran effect: a cause of population synchrony. *TREE*, 14(1):1–2.

[58] Ims, R. A. and Andreassen, H. P. (2000). Spatial synchronization of vole population dynamics by predatory birds. *Nature*, 408:194–196.

[59] Iwasa, Y. and Satake, A. (2004). Mechanisms inducing spatially extended synchrony in mast seeding: The role of pollen coupling and environmental fluctuation. *Ecol. Res.*, 19:13–20.

[60] Jones, J., Doran, P. J., and Holmes, R. T. (2003). Climate and food synchronize regional forest bird abundances. *Ecology*, 84(11):3024–3032.

[61] Kendall, B. E., Bjørnstad, O. N., Bascompte, J., Keitt, T. H., and Fagan, W. F. (2000). Dispersal, environmental correlation, and spatial synchrony in population dynamics. *Am. Nat.*, 155:628–636.

[62] Khoury, P., Lieberman, M., and Lichtenberg, A. (1996). Degree of synchronization of noisey maps on the circle. *Phys. Rev. E*, 54(4):3377–3388.

[63] Khoury, P., Lieberman, M. A., and Lichtenberg, A. J. (1998). Experimental measurement of the degree of chaotic synchronization using a distribution exponent. *Phys. Rev. E*, 57(5):5448–5466.

[64] Koenig, W. D. (2002). Global patterns of environmental synchrony and the Moran effect. *Ecography*, 25:283–288.

[65] Kramers, H. A. (1940). Brownian motion in a field of force and diffusion model of chemical reactions. *Physica*, 7(4):284–304.

[66] Kraut, S. (2001). *Multistable systems under the influence of noise*. PhD thesis, University of Potsdam.

[67] Kravtsov, Y. A., Bilchinskaya, S. G., Butkovskii, O. Y., Rychka, I. A., and Surovyatkina, E. D. (2001). Prebifurcational noise rise in nonlinear systems. *JETP*, 93(6):1323–1329.

[68] Kuckländer, N. (2006). From Fisher's theorem, Price's equation to Fujiyama landscapes. In Blasius, B. and Groß, T., editors, *An interdisciplinary Introduction to Evolution*. Proceedings of the first Stanislaw Lem Conference, Scholars without Borders. Accepted for publication.

[69] Kuramoto, Y. (1984). *Chemical Oscillations, Waves, and Turbulence*. Springer-Verlag, Berlin.

[70] Laakso, J., Kaitala, V., and Ranta, E. (2003). Non-linear biological responses to disturbance: consequences on population dynamics. *Ecol. Model.*, 162:247–258.

[71] Lai, Y.-C. and Grebogi, C. (1993). Synchronization of chaotic trajectories using control. *Phys. Rev. E*, 47(4):2357–2360.

[72] Liebhold, A., Koenig, W. D., and Bjørnstad, O. N. (2004). Spatial synchrony in population dynamics. *Annu. Rev. Ecol. Evol. Syst.*, 35:467–490.

[73] Lindner, B. (2002). *Coherence and Stochastic Resonance in Nonlinear Dynamical Systems*. PhD thesis, HU Berlin.

[74] Lindsey, W. C. (1972). *Synchronization Systems in Communication and Control*. Prentice-Hall, Englewood Cliffs, NJ.

[75] Linz, S. J. and Lücke, M. (1986). Effect of additive noise and multiplicative noise on the first bifurcations of the logistic model. *Phys. Rev. A*, 33(4):2694–2703.

[76] Longtin, A. (1997). Autonomous stochastic resonance in bursting neurons. *Phys. Rev. E*, 55(1):868–876.

[77] May, R. M. (1976). Simple mathematical models with very complicated dynamics. *Nature*, 261:459–467.

[78] Mehta, N. J. and Henderson, R. M. (1991). Controlling chaos to generate aperiodic orbits. *Phys. Rev. A*, 44(8):4861–4865.

[79] Montbrió, E. and Blasius, B. (2003). Using nonisochronicity to control synchronization in ensembles of nonidentical oscillators. *Chaos*, 13(1):291–308.

[80] Moran, P. A. P. (1949). The statistical analysis of the sunspot and lynx cycles. *J. Anim. Ecol.*, 18:115–116.

[81] Moran, P. A. P. (1953a). The statistical analysis of the Canadian lynx cycle: I. structure and prediction. *Aust. J. Zool.*, 1:163–173.

[82] Moran, P. A. P. (1953b). The statistical analysis of the Canadian lynx cycle: Synchronization and meteorology. *Aust. J. Zool.*, 1:291–298.

[83] Mormann, F., Lehnert, K., David, P., and Elger, C. E. (2000). Mean phase coherence as a measure for phase synchronization and its application to the EEG of epilepsy patients. *Physica D*, 144:358–369.

[84] Murray, J. D. (1989). *Mathematical Biology*. Springer, Berlin.

[85] Neiman, A., Saparin, P. I., and Stone, L. (1997). Coherence resonance at noisy precursors of bifurcations in nonlinear dynamical systems. *Phys. Rev. E*, 56(1):270–273.

[86] Ott, E. (1993). *Chaos in dynamical systems*. Cambridge University Press.

[87] Ott, E., Grebogi, C., and Yorke, J. A. (1990). Controlling chaos. *Phys. Rev. Lett.*, 64(11):1196–1199.

[88] Peltonen, M., Liebhold, A. M., Bjørnstad, O. N., and Williams, D. W. (2002). Spatial synchrony in forest insect outbreaks: Roles of regional stochasticity and dispersal. *Ecology*, 83(11):3120–3129.

[89] Petchey, O. L. (2000). Environmental colour affects aspects of single-species population dynamics. *Proc. R. Soc. Lond. B*, 267:747–754.

[90] Petchey, O. L., Gonzalez, A., and Wilson, H. B. (1997). Effects on population persistence:the interaction between environmental noise colour, intraspecific competition and space. *Proc. R. Soc. Lond. B*, 264:1841–1847.

[91] Pikovsky, A. (1992). Statistics of trajectory separation in noisy dynamical systems. *Phys. Lett. A*, 165:33–36.

[92] Pikovsky, A. S. and Kurths, J. (1997). Coherence resonance in a noise-driven excitable system. *Phys. Rev. Lett.*, 78(5):775–778.

[93] Pikovsky, A. S., Rosenblum, M. G., and Kurths, J. (2001). *Synchronization, a Universal Concept in Nonlinear Sciences*. Cambridge University Press, Cambridge.

[94] Pogromsky, A., Santoboni, G., and Nijmeijer, H. (2002). Partial synchronization: from symmetry towards stability. *Physica D*, 172:65–87.

[95] Post, E. and Forchhammer, M. C. (2002). Synchronization of animal population dynamics by large-scale climate. *Nature*, 420:168–171.

[96] Press, W. H., Teukolsky, S. A., Vetterling, W. T., and Flannery, B. P. (1992). *Numerical Recipes in C: The Art of Scientific Computing*. Cambridge University Press, 2nd edition.

[97] Prudnikov, A. P., Brychkov, Y. A., and Marichev, O. I. (1992). *Integrals and Series*, volume 2: Special Functions. Gordon and Breach Science Publishers. USSR Academy of Sciences, Moscow, translated by N. M. Queen.

[98] Pyragas, K. (1992). Continuous control of chaos by self-controlling feedback. *Phys. Lett. A*, 170:421–428.

[99] Rabinovich, M., Volkovskii, A., Lecanda, P., Huerta, R., Abarbanel, H. D. I., and Laurent, G. (2001). Dynamical encoding by networks of competing neuron groups: Winnerless competition. *Phys. Rev. Lett.*, 87(6):068102.

[100] Ranta, E., Kaitala, V., Lindström, J., and Helle, E. (1997). The Moran effect and synchrony in population dynamics. *Oikos*, 78:136–142.

[101] Ranta, E., Lundberg, P., Kaitala, V., and Laakso, J. (2000). Visibility of the environmental noise modulating population dynamics. *Proc. R. Soc. Lond. B*, 267:1851–1856.

[102] Reichl, L. E. (1998). *A Modern Course in Statistical Physics*. Wiley-Interscience.

[103] Ricker, W. E. (1954). Stock and recruitment. *J. Fisheries Res. Board Can.*, 11(5):559–623.

[104] Ripa, J. (2000). Analysing the Moran effect and dispersal: their significance and interaction in synchronous population dynamics. *Oikos*, 89:175–187.

[105] Ripa, J. and Heino, M. (1999). Linear analysis solves two puzzles in population dynamics: the route to extinction in coloured environments. *Ecol. Lett.*, 2:219–222.

[106] Ripa, J. and Ives, A. R. (2003). Food web dynamics in correlated and autocorrelated environments. *Theor. Pop. Biol.*, 64:369–384.

[107] Rosenblum, M. G., Pikovsky, A. S., and Kurths, J. (1996). Phase synchronization of chaotic oscillators. *Phys. Rev. Lett.*, 76(11):1804–1807.

[108] Royama, T. (1992). *Analytical population dynamics*. Chapman & Hall, London.

[109] Royama, T. (2005). Moran effect on nonlinear population processes. *Ecol. Monogr.*, 75(2):277–293.

[110] Satake, A. and Iwasa, Y. (2002). The synchronized and intermittent reproduction of forest trees is mediated by the Moran effect, only in association with pollen coupling. *J. Ecol.*, 90:830–838.

[111] Schuster, H.-G. (1995). *Deterministic Chaos: An Introduction*. VCH, Weinheim, 3rd edition.

[112] Shraiman, B., Wang, C. E., and Martin, P. C. (1981). Scaling theory for noisy period-doubling transitions to chaos. *Phys. Rev. Lett.*, 46(14):935–939.

[113] Silva, A. C. (2005). *Applications of physics to finance and economics: Returns, trading activity and income*. PhD thesis, University of Maryland, College Park.

[114] Srivastava, H. M. and Karlsson, P. W. (1985). *Multiple Gaussian hypergeometric series*. Ellis Horwood Limited.

[115] Steele, J. H. (1985). A comparison of terrestrial and marine ecological systems. *Nature*, 313:355–358.

[116] Stenseth, N. C. and Chan, K.-S. (1998). Nonlinear sheep in a noisy world. *Nature*, 394:621–623.

[117] Stenseth, N. C., Otterson, G., Hurrell, J. W., Mysterud, A., Lima, M., Chan, K.-S., Yoccoz, N. G., and Ådlansvik, B. (2003). Studying climate effects on ecology through the use of climate indices: the North Atlantic Oscillation, El Niño Southern Oscillation and beyond. *Proc. R. Soc. Lond. B*, 270:2087–2096.

[118] Steuer, R., Daub, C. O., Selbig, J., and Kurths, J. (2004). Measuring distances between variables by mutual information. In Baier, D. and Wernecke, K.-D., editors, *Innovations in Classification, Data Science, and Information Systems*, Studies in Classification, Data Analysis, and Knowledge Organization. Proceedings of the 27th Annual Conference of the Gesellschaft für Klassifikation e.V., Springer Berlin.

[119] Strogatz, S. H. (1998). *Nonlinear Dynamics and Chaos: With Applications to Physics, Chemistry and Engineering*. Perseus Books, Cambridge, Massachusetts, 8th edition.

[120] Strogatz, S. H., Abrams, D. M., McRobie, A., Eckhardt, B., and Ott, E. (2005). Crowd synchrony on the millenium bridge. *Nature*, 438(3):43–44.

[121] Tass, P. and Haken, H. (1996). Synchronization in networks of limit cycle oscillators. *Z. Physik B*, 100(2):303–320.

[122] Tavecchia, G., Coulson, T., Morgan, B. J. T., Pemberton, J. M., Pilkington, J. C., Gulland, F. M. D., and Clutton-Brock, T. H. (2005). Predictors of reproductive cost in female Soay sheep. *J. Anim. Ecol.*, 74:201–213.

[123] Tedesco, P. A., Hugueny, B., Paugy, D., and Fermon, Y. (2004). Spatial synchrony in population of West African fishes: a demonstration of an intraspecific and interspecific Moran effect. *J. Anim. Ecol.*, 73:693–705.

[124] Vasseur, D. A. and Yodzis, P. (2004). The color of environmental noise. *Ecology*, 85(4):1146–1152.

[125] Vik, J. O., Stenseth, N. C., Tavecchia, G., Mysterud, A., and Lingjærde, O. C. (2004). Living in synchrony on Greenland coasts? *Nature*, 427:697–698.

[126] Wichmann, M. C., Johst, K., Schwager, M., Blasius, B., and Jeltsch, F. (2005). Extinction risk, coloured noise and the scaling of variance. *Theor. Pop. Biol.*, 68:29–40.

[127] Wiesenfeld, K. (1985a). Noisy precursors of nonlinear instabilities. *J. Stat. Phys.*, 38(5-6):1071–1097.

[128] Wiesenfeld, K. (1985b). Virtual Hopf phenomenon: A new precursor of period-doubling bifurcations. *Phys. Rev. A*, 32(3):1744–1751.

[129] Wiesenfeld, K., Bracikowski, C., James, G., and Roy, R. (1990). Observation of antiphase states in a multimode laser. *Phys. Rev. Lett.*, 65(14):1749–1752.

[130] Winfree, A. T. (1967). Biological rhythms and the behavior of populations of coupled oscillators. *J. Theor. Biol.*, 16:15–42.

[131] Zhou, C., Kurths, J., Kiss, I. Z., and Hudson, J. L. (2002). Noise-enhanced phase synchronization of chaotic oscillators. *Phys. Rev. Lett.*, 89(1):014101.

Acknowledgements

Saying this I would like to thank my supervisor Junior Prof. Dr. Bernd Blasius for the interesting elementary topic, for sharing valuable ideas concerning this work and motivating discussions. The Volkswagen Stiftung financed gratefully my phd-project.

And I enjoyed very much the growing of our theoretical ecology research group.

Moreover I'd like to thank very much Prof. Dr. Jürgen Kurths for his support and everyone in our nonlinear dynamics group for the friendly and helpful atmosphere.

As well I am obliged to Prof. Dr. Vladimir N. Belykh for introducing me to the automatic control idea via phase-locked loops and for our successful collaboration together with Dr. Grigory V. Osipov.

Thanks also to my fellow phd-student Sébastien Clodong for his assistance not only in technical things. I enjoyed fruitful discussions with Carsten Allefeld, Ralf Tönjes, Lars Rudolf, Ralf Steuer, Jörg-Uwe Tessmer, Björn Naundorf, Volker Ahlers and Marc Timme. Very helpful critical readers were Thilo Gross and Andrea Kölzsch. Sincere thanks to E. R. for lending me a helping hand in the beginning.

And finally big thanks to my family and friends for supporting me invaluably through all ups and downs and for believing in me in times when I did not.